Sedimentary processes and Paleoenvironments of the Precambrian - Cambrian (Pc-C) Interval, Southwestern Yangtze Platform, China

Dissertation

Von

Xiaojuan Sun

zur

Erlangung des Doktorgrades der Naturwissenschaften

im Fachbereich Geowissenschaften an der

Freien Universität Berlin

Berlin, den 05.01.2016

Diese Arbeit wurde von dem Promotionsausschuss des Fachbereiches Geowissenschaften der Freien Universität Berlin am 12. Oktober 2013 genehmigt.

……

Erstgutachter : Prof. Dr. Christoph Heubeck

Freie Universität Berlin

Zweitgutachter: Prof. Dr. Gerhard Franz

Technische Universität Berlin

Die Disputation erfolgte am: 12. February 2016

Erklärung

Hiermit erkläre ich, Xiaojuan Sun, dass diese Arbeit ausschließlich auf Grundlage der angegebenen Hilfsmittel und Hilfen selbstständig von mir verfasst wurde. Diese Arbeit wurde nicht in einem früheren Promotionsverfahren eingereicht.

Berlin, den 5. Januar 2016

Xiaojuan Sun

Zusammenfassung

Plattentektonische und evolutionäre Ereignisse vor und nach der Präkambrium - Kambrium (Pc-C) Grenze markieren einen globalen Wendepunkt in der Erdgeschichte. Veränderungen des Weltklimas und erhöhte plattentektonische Aktivität führten zu wesentlichen Änderungen in der ozeanischen Zirkulation und in der Verfügbarkeit von Nährstoffen, zur Bildung von ausgedehnten Flachmeeren und, am wichtigsten, zu einer rapiden Evolution der Metazoen, die "Kambrische Radiation". Allerdings wird das Verständnis von Ozeanchemie und Bioradiation während dieses zeitlichen Intervalls durch die unzureichende Kenntnis von Paläogeographie und Paläo-Ablagerungsräumen eingeschränkt.

Schichten der Yangtze-Plattform im östlichen Yunnan, Südchina, enthalten eine nahezu vollständige und diverse stratigraphische Aufzeichnung des frühen Kambriums in China und bilden damit ein ideales Archiv für das Studium frühkambrischer Ablagerungsräume im Kontext von etablierter bio-, chemo- und chronostratigraphischer Information. Die vorliegende Arbeit konzentriert sich auf die frühkambrische Zhujiaqing Formation im östlichen Yunnan. Diese ermöglicht eine detaillierte Rekonstruktion der sedimentären und paläogeographischen Bedingungen dieser kritischen Zeit und beschreibt die Ereignisse am stratigraphischen Kontakt von ediakarischen und kambrischen Schichten. Die Flachwasser-, siliziklastisch-phosphoritisch-karbonatische Sequenz der Zhujiaqing Formation wird in zwölf Lithofazies klassifiziert. Ihre räumlichen und zeitlichen Veränderungen zeigen die prozessorientierte Ablagerungsgeschichte der Region. Die Wassertiefe schwankte während des gesamten Ablagerungszeitraums des Zhujiaqing Formation nur wenig, basierend auf den vorherrschenden peritidalen bis tief-subtidalen Ablagerungsräumen. Unterschiedliche Absenkungsraten auf dem Schelf beeinflussten weitgehend die Mächtigkeiten der einzelnen stratigraphischen Einheiten. Im Gegensatz dazu veränderte sich die Wasserchemie während dieser Zeit drastisch. Sie wird durch drei Endglieder von Ablagerungsmilieus reflektiert: (1) Siliziklastisch-phosphatisches, sand-dominiertes Subtidal, (2) phosphatisch-dolomitisches, schlamm-dominiertes Peritidal, und (3) kalk- und dolomitschlamm-dominiertes Subtidal.

Ein zweiter Schwerpunkt dieser Arbeit liegt auf der detaillierten sedimentären Untersuchung des ediakarisch-kambrischen Kontakts nahe der Meishucun-Sektion im südlichen Yunnan, die als Pc-C *Global Stratigraphic Section and Point* (GSSP)-Kandidat diskutiert wurde. Der Kontakt ist in mehreren aktiven Steinbrüchen nahebei aufgeschlossen. Detaillierte Faziesanalyse sowie diagenetische und geochemische Untersuchung der Schichten ober- und unterhalb des verkarsteten Kontaktes zeigen, dass der spätediakarische globale Meeresspiegelrückgang umfangreiche Karbonat-Wattflächen freilegte, was zur Verkarstung führte. Als der Meeresspiegel wieder stieg, lieferte Upwelling große Mengen an Phosphor in tidale Ablagerungsräume, so dass mikrobiell vermittelte frühdiagenetische Phosphatierung in mächtigen basal-kambrischen Phosphoriten erfolgen konnte. Die zeitliche Abfolge der dokumentierbaren diagenetischen Prozesse in den Gesteinen legt nahe, dass eine lokale Verkieselung

der Karbonatplattform bereits während der frühen Versenkung auftrat und möglicherweise auf die Mischungszone von Frisch- und Meerwasser zurückzuführen ist, während Dolomitisierung wahrscheinlich durch Frischwassereinfluss und Versenkung erfolgte.

Das hier untersuchte zeitliche Pc-C Intervall zeigt überall Verkarstung am Top der spätediakarischen Dengying Formation, gefolgt von einer bedeutenden Transgression in der frühkambrischen Zhujiaqing Formation, wiederum gefolgt von einer relativ stabilen Sedimentationsrate in einem flachmarinen Ablagerungsraum mit relativ konstanter Wassertiefe. Während die sedimentären Bedingungen während des frühen Kambrium auf diesem flachen Schelf nur wenig variierten, veränderte sich die Wasserchemie und somit auch die Mineralogie dieser Ablagerungen drastisch. Die Auswirkungen dieser Prozesse sollten in zukünftigen evolutionsbiologischen Studien der metazoischen Epifauna berücksichtigt werden, um Umweltveränderungen in dieser kritischen Zeitspanne besser zu verstehen.

Abstract

Plate-tectonic and evolutionary events prior to and across the Precambrian - Cambrian (Pc-C) boundary globally mark a major turning point in Earth's history. Changes in global climate and increased plate tectonic activity resulted in major changes of ocean circulation and nutrient availability, the formation of extensive shallow seas, and, most importantly, a prominent start in the evolution of metazoans: the "Cambrian radiation events". However, progress in understanding ocean chemistry and bioradiation during this Pc-C interval has been hindered by the lack of a profound knowledge of paleogeography and paleo-depositional environments.

Strata of the Yangtze platform in eastern Yunnan, South China, preserve the most complete and diverse stratigraphic record of the early Cambrian in China, and thus are an ideal archive for studying early Cambrian depositional environment in the context of established bio-, chemo- and chronostratigraphic information. The present dissertation focuses on the earliest Cambrian Zhujiaqing Formation in eastern Yunnan. It provides a detailed reconstruction of its sedimentary and paleogeographic framework as well as describes the nature of the Ediacaran to Cambrian contact. The shallow-water siliceous-phosphoritic-carbonate sequence of the Zhujiaqing Formation is classified in twelve lithofacies; their integrated spatial and temporal changes show the process-oriented depositional history of the area. Apparently, water depth did not change much throughout the deposition of the Zhujiaqing Formation, indicated by its dominant peritidal to shallow-subtidal setting. Differential subsidence rate may have largely controlled stratigraphic thicknesses of individual members in the different sections. In contrast, water chemistry changed intensely through time which is reflected by three depositional environment end members: (1) Siliceous-phosphatic sand-dominated subtidal, (2) phosphatic-dolomitic mud-dominated peritidal, and (3) dolomitic to calcareous mud-dominated subtidal.

A second focus of this thesis lies on the nature of the Ediacaran to Cambrian contact which is well exposed in several active quarries near a former Pc-C Global Stratotype Section and Point (GSSP) candidate, the Meishucun section. Detailed facies, diagenetic and geochemical characterization of the strata above and below the contact shows that the latest Ediacaran global sea level-lowering event exposed extensive carbonate tidal flat surfaces, resulting in karstification. As sea level rose again, transgression-related upwelling supplied large amounts of phosphorus to lower-intertidal to subtidal environments, allowing microbially mediated syndepositional and early diagenetic phosphatization, represented by the thick basal Cambrian phosphorite of the Zhujiaqing Formation. The sequence of multiple diagenetic events suggests that carbonate platform silicification occurred during early burial and was possibly related to the phreatic mixing-zone environment, while dolomitization was likely influenced by meteoric and burial diagenesis.

The Pc-C interval studied here shows karstification at the top of the Ediacaran Dengying Formation followed by a major transgression represented by the Cambrian Zhujiaqing Formation in a relatively

stable low-sedimentation epicontinental depositional environment with relatively constant water depth. While the sedimentological conditions changed within the scope of a shallow continental shelf and platform environment during the Early Cambrian, water chemistry changed dramatically during this time and greatly affected the mineralogy of these deposits. These processes need to be considered in future studies which strive to better understand environmental change during this critical time interval.

Acknowledgements

For the financial support of my work and living in Germany, I would like to thank the following people and organizations: Prof. Christoph Heubeck (Project financed by The German Research Foundation) for financing my field work and travel expenses and for approval letters during my application for Grands; Prof. Zhu Maoyan (Project financed by National Basic Research Program of China) for financing the accommodation and travel expenses during the field work; The China Scholarship Council (CSC) for financing my living expenses in Germany; German Academic Exchange Service (DAAD) for providing Study Completion Grants, and "Frauenbeauftragte" of Freie Universität Berlin for supporting my conference fees.

I thank my advisor Prof. Dr. Christoph Heubeck for his support in various aspects, for his instructions during many field excursions in China and Germany. I am also thankful to his motivation and advice, especially in the writing process of this dissertation.

I would like to thank the Members of FOR 736 for the discussions in seminars and fields, especially Dr. Michael Steiner for providing insights from paleontological aspects as well as helping during field works, Dr. Bernd Weber for his paleoecological feedbacks, Dr. Simon Hohl for geochemical discussions and the patience in helping with lab work and Dr. Ben Yang for the discussions about small shelly fossils.

Prof. Zhang Junming, Dr. Zhao Fangchen from Nanjing Institute of Geology and Palaeontology, Chinese Academy of Sciences and Mr. Zhang Shishan from Kunming of China are thanked for their great field guidance in the rugged but interesting Yunnan and Guizhou areas.

Furthermore, I am grateful to Anna Giribaldi for assistance with thin section preparation, Jan Evers for assistance with the SEM, Kirsten Born for assistance with CL, Martina Grundman for IT support. Thanks for the accompanying of my officemates: Silvia Favaro, Martin Homman, Andreas Scharf, Sami Nabhan and Philip Groß. Eline Le Breton and Alessandro Airo, it is so good to have you around. Mark Handy, Jörg Giese, Jan Pleuger and Jörg Maletz thanks for the nice conversations during the years of my stay in this department.

Last but not least, I would like to thank my great friends in China, Berlin and Manchester as well as my beloved parents for their constant support and letting me keep going in my way!

Structure of this thesis

This thesis is embedded within Subproject 1 of the DFG-Forschergruppe 736 "*The Precambrian-Cambrian Ecosphere (R)evolution: Insights from Chinese Microcontinents*" which generated multi-proxy datasets across the Precambrian-Cambrian stratigraphic interval of South China, Mongolia and Kazakhstan.

This thesis investigates the sedimentary record of the Precambrian - Cambrian (Pc-C) transition on the southwestern Yangtze microcontinent. The study area is located in eastern Yunnan Province where some of the most complete lower Cambrian strata of this microcontinent are preserved. We investigated sections to study the spatial and temporal changes in sedimentary processes and environments during this critical time in Earth history.

The thesis consists of five chapters and two appendixes. Chapter I reviews the Precambrian - Cambrian interval and lists the objectives of this thesis. Chapter II provides details of study methods. Chapters III and IV comprise individual manuscripts in advanced stages of preparation for submission to peer-reviewed scientific journals. Chapter V summarizes the main research results and offers an outlook of possible future studies.

A brief outline of the chapters and manuscripts is given below.

Chapter I: The Ediacaran – Cambrian transition: A critical time in Earth history

This chapter introduces the uniqueness and significance of the Pc-C boundary, reviews the relevant literature and derives the objectives of the thesis. It also includes a geological introduction of the Yangtze microcontinent during the Pc-C interval.

Chapter II: Methods

This chapter describes the guiding theories, data collection and the approach and methods used to analyses samples.

Chapter III: Stratigraphy and paleogeography of the earliest Cambrian Zhujiaqing Formation, South China: An inner-platform environment for the diversification of small shelly fossils

Xiaojuan Sun, Christoph Heubeck

This chapter focuses on the lithology, facies distribution and evolution of the siliceous-phosphatic-calcareous rocks of the earliest Cambrian Zhujiaqing Formation in order to understand the paleoenvironment of the basal-Cambrian bioradiation. High-resolution stratigraphic sections were measured and samples were collected and analyzed. This chapter includes detailed descriptions of representative stratigraphic sections, classification of lithofacies and a description of the temporal and spatial distribution of lithofacies associations. Based on these, a paleoenvironmental reconstruction and

stratigraphic basin evolution is deduced. The results can be used as comparison to Pc-C sections worldwide.

The tasks in preparation of the manuscript were distributed as follows: The authors carried out fieldwork in Yunnan. Xiaojuan Sun wrote the manuscript and drafted the figures. Christoph Heubeck contributed to the discussion and helped greatly in revisions of the manuscript and figures. Field work was organized by Prof. Dr. Maoyan Zhu from Chinese Academy of Sciences-State Key Laboratory of Paleobiology and Stratigraphy, Nanjing.

Chapter IV: The nature of the Ediacaran-Cambrian contact at Meishucun, Yunnan Province, China

Xiaojuan Sun, Christoph Heubeck, Dorothee Hippler, Simon Hohl

This chapter describes the application of multiple sedimentary proxies to examine in detail the Pc-C boundary at one of the most important Pc-C stratigraphic sections worldwide, the Meishucun section of southern Yunnan. It provides a detailed description of microfacies, a reconstruction of the complex diagenetic history and geochemical analyses of phosphatic sedimentary rocks at the Ediacaran-Cambrian transition. The results are important for understanding the evolution, depositional environments and taphonomic conditions of Small Shelly Fauna.

The tasks in preparation of the manuscript were distributed as follows: Xiaojuan Sun, Christoph Heubeck and Dorothee Hippler contributed to field work. Xiaojuan Sun and Christoph Heubeck collected samples. Xiaojuan Sun prepared thin sections and carried out the analyses. Simon Hohl conducted trace element and Rare Earth Element (REE+Y) measurements and drafted part of Figure 12. Xiaojuan Sun wrote the manuscript, Christoph Heubeck, Simon Hohl and Dorothee Hippler contributed to the manuscript through reviews. Xiaojuan Sun drafted figures and tables, which were refined by comments from all co-authors.

Chapter V: Conclusions and outlook

This chapter summarizes the main research results into four conclusions and provides an outlook.

Sample suites were in part also analyzed for biostratigraphic purposes by Ben Yang and Michael Steiner (Freie Universität Berlin, subproject 3) and for geochemistry by Simon Hohl and Harry Becker (Freie Universität Berlin, subproject 4).

Table of Contents

CHAPTER I

The Ediacaran-Cambrian transition:

A critical time in Earth history

1.1. The Precambrian to Cambrian transition

Despite abundant evidence for life back to at least 3.5 Ga, Precambrian fossils mostly record the evolution of bacteria and microbial eukaryotes. Eukaryotes appear to have slowly and gradually increased in diversity up to the first Neoproterozoic glaciation (Sturtian, ~ 700 Ma). Toward the end of the second glaciation (Marinoan, ~ 625 Ma), their diversity increased rapidly. Following the third glaciation (Gaskiers, ~ 580 Ma), Ediacaran biota appeared (Narbonne and Gehling, 2003). However, the origin of many if not most animal phyla can be traced to only within ca. 20 Ma following the Pc-C boundary (ca. 542 Ma) which marks the most important evolutionary radiation in the history of life (Marshall, 2006; Smith and Harper, 2013). On a broader scale, the "boring billion" was either ended by biological evolution (e.g., genetic innovation, development of an arms race), tectonic events (e.g., the Rodinia breakup providing shelf space, the Transantarctic Mountains orogeny feeding nutrients to the shelves), geochemical changes (e.g., a general trend of increasing $^{87}Sr/^{86}Sr$ and $\delta^{13}C_{carb}$ in sea water, changes in the Ca-concentration, availability of Cr or Ni as an essential trace element for photosynthesis making a rapid increase in oxygen possible) or climatic-oceanographic overturns (e.g., the end of glaciations washed nutrients into the sea) at or near the Pc-C transition (Fig. 1).

1.2. The Ediacaran to Cambrian bioradiation

The base of the Ediacaran period (ca. 635 - ca. 542 Ma) is defined by the base of cap carbonate strata of the Nuccaleena Formation in the Enorama Creek section of South Australia (Knoll et al., 2006). Cap carbonates were deposited worldwide after the end-Cryogenian global `Marinoan` glaciation (so-called "Snowball Earth"; Hoffman et al., 1998). The subsequent Neoproterozoic glaciations lack convincing globally correlative deposits (e.g., the Gaskiers glaciation, ca. 582 Ma; Halverson et al., 2005; glaciations on the West African Craton, ca. 560 Ma; Vernhet et al., 2012; Deynoux et al., 2006; and a possible glaciation at the Ediacaran-Cambrian boundary, ~542 Ma). Reliable evidence for a Cambrian glaciation has rarely been documented; as an exception, Landing et al. (2010) documented sections in Avalonian New Brunswick and Ireland that possibly preserve tillite. Nevertheless, glaciations had been common from about 720 Ma until the beginning of the Cambrian, superimposed by major biological innovations during the Neoproterozoic-Cambrian transition (Evans, 2003).

Ediacaran-type biota represent the emergence of large and architecturally complex organisms (Narbonne, 2005) compared to former organisms. They were first recognized by Billings (1872). Numerous studies of the past two decades suggest the Ediacaran organisms were composed of soft, flexible tissue with large surface area and immobile animals or animal-grade organisms (for a review, see Narbonne, 2005). Further biological and ecological innovations during Ediacaran include calcification (e.g., *Cloudina*; Hofmann and Mountjoy, 2001) and predation (Hua, 2003). The Ediacaran biota disappeared around the Pc-C boundary which is currently defined by the first appearance of the trace fossil *Treptichnus pedum* at the base of Member 2 of the Chapel Island Formation, Fortune Head,

southeast Newfoundland (Brasier et al., 1994). Within the next 20 Ma or so, some of Earth's most significant evolutionary chain reactions, the "Cambrian radiation", took place (Marshall, 2006), documented by a spectacular increase in animal disparity and diversity in a relatively short time.

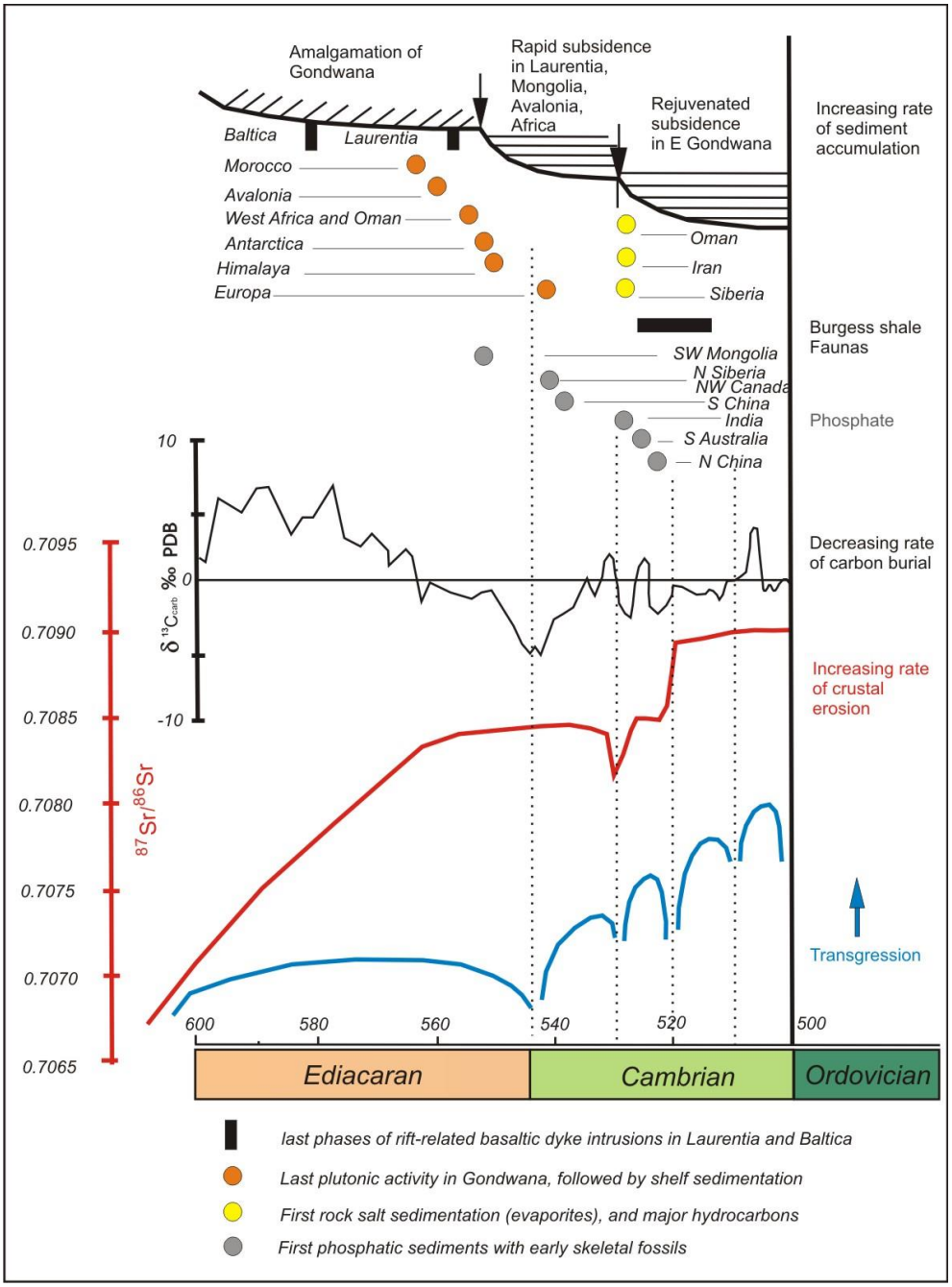

Fig. 1. *Compilation of global tectonic events, sea level changes, isotopic trends and changes in taphonomy during the Ediacaran-Cambrian interval. Modified after Brasier et al., 2001.*

Generally, three successive stages of the Cambrian bioradiation correspond broadly to the lowest three stages of the Cambrian: the diversification of coelomates that produced complex burrows (at the base of the Cambrian, ca. 541 Ma), the diversification of metazoans with mineralized skeletons (at base of Stage 2, ca. 532 Ma), and the appearance of trilobites and diverse lingulate brachiopods (at base of

Stage 3, ca. 520.5 Ma; Landing et al., 2013) (Fig. 2). Unfortunately, in contrast to the other Phanerozoic time periods which almost all have established Global Boundary Stratotype Sections and Points (GSSPs) for chronostratigraphic divisions, Cambrian stages and series have not yet been formally named and defined. The main reasons for this deficiency are (1) a widespread discontinuity at the Pc-C boundary because of exposure (e.g. karstification, denudation) and stratigraphic condensation (phosphorite, glauconite, black shale deposition and hardground formation); (2) a strong biotic provincialism and facies control causing difficulties in correlation between different lithologies and continents; and (3) a paucity of suitable marker beds for a global or even regional correlation.

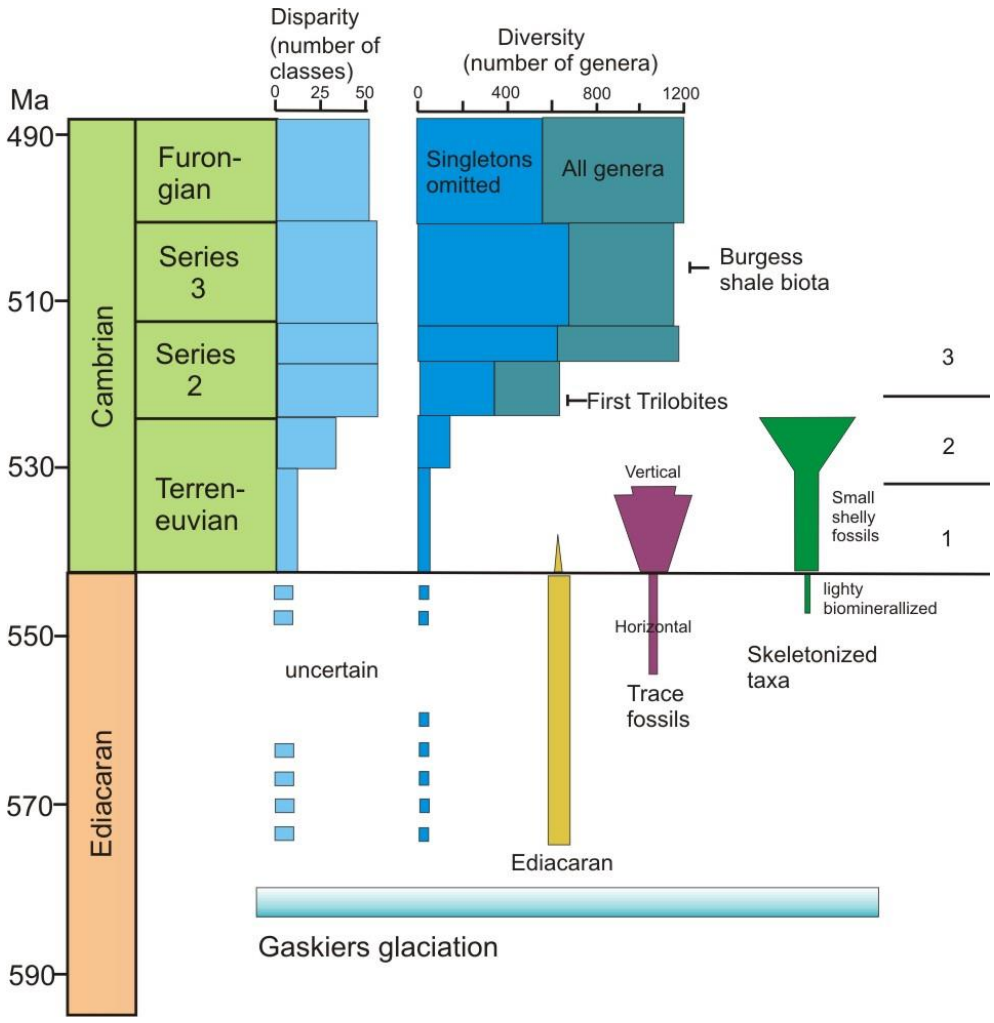

Fig. 2*. Cambrian bioradiation events, illustrating a general increase in disparity and diversity and the three main Cambrian bioradiation stages (Marshall 2006).*

A wide range of stratigraphic methods has been applied to the study of the Precambrian-to-Cambrian transition, most importantly bio-, sequence-, chrono- and chemostratigraphic techniques. Their methods and findings will be briefly outlined below.

Biostratigraphy: The first occurrence of *Treptichnus pedum* indicates the base of the Cambrian. Prior to the appearance of this comparatively complex trace pattern, trace fossil diversity was relatively low

and was dominated by horizontal and simple trails (Jensen, 2003; Porada et al., 2008). An important group of organisms, Small Shelly Fossils (SSFs), appeared just prior to the Pc-C boundary. They were first used by Matthews and Missarzhevsky (1975) and widely applied to the identification and classification of small, usually phosphatized "problematica" in pre-trilobitic, Lower Cambrian strata. SSFs represent a polyphyletic category of mineralized fossil remains, probably related to a specific taphonomic window in the latest Neoproterozoic to early Palaeozoic (Steiner et al., 2007). Few other fossils near the PC-C boundary, most significantly *Cloudina* and *Namacalathus*, also contribute to the paleoenvironmental and biostratigraphic resolution of the Precambrian-Cambrian transition (Grant, 1990). The principal problem of applying the biostratigraphic method to the Pc-C boundary is that SSFs and trace fossils are strongly facies-controlled (Lindsay et al., 1996), endemic, and represent comparatively long stratigraphic ranges (Seilacher et al., 2005).

Sequence stratigraphy: As mentioned above, Pc-C boundary sections worldwide are replete with hiati, unconformities, hardgrounds, and exposure surfaces. Stratigraphically more-or-less continuous sections are rare. The Precambrian-Cambrian-boundary stratotype section, the Chapel Island Formation of southeast Newfoundland, was investigated with regard to its depositional history and sequence stratigraphy (Myrow and Hiscott, 1993). Lithological change from peritidal sandstone and shale to subtidal thinly laminated siltstone at the FAO of *Treptichnus pedum*, the Pc-C boundary suggest a (minor?) flooding surface. The Pc-C interval in the White-Inyo Mountains and the Death Valley region of California basically shows shallowing-upward cycles in which with shallow-subtidal siliciclastic rocks at the base grade into shallow-marine carbonates (Corsetti and Hagadorn, 2003). In the White-Inyo Mountains region, the tops of most carbonate cycles show minor karstification. Lindsay et al. (1996) studied two sections in Zavkhan Basin of southwestern Mongolia which comprise large-scale alternations of siliciclastic- and carbonate-dominated units, aiming at facies and sequence controls on the appearance of the Cambrian biota and concluded that basin analysis would be needed before the Pc-C boundary could be meaningfully defined. Overall, numerous studies worldwide indicate that the Pc-C boundary nearly always conincides with one or several sequential sea-level lowstands and associated sequence boundaries.

Chemostratigraphy: Many geochemical studies have been conducted at the Pc-C transition, including carbon, sulfur and strontium isotopes and redox-sensitive elements, mostly for the purpose of understanding the causal link and interaction between biogeochemical events, earth surface environments, and the dynamics of the solid Earth with biotic evolution (Shields et al., 2004; Sawaki et al., 2010; Li et al., 2013). Carbonate carbon isotope geochemistry, in particular, is a classical proxy to interpret environment changes, thus $\delta^{13}C_{carb}$ values are widely used as important criteria for chemostratigraphic correlations among continents, e.g. South China, Oman, Namibia, Siberia and Canada (Li et al., 2013; Amthor et al., 2003) and have proven useful for identifying the Pc-C boundary where sedimentary environments or lithologies did not allow the preservation of *Treptichnus pedum*.

The Siberian Platform was first to be surveyed for stable-isotope ratios at the Precambrian-Cambrian boundary (Magaritz et al., 1986). Stable-isotope studies on the Pc-C boundary from other parts of the world followed (e.g., Brasier et al., 1996; Kimura et al., 1997; Ishikawa et al., 2008; Li et al., 2009; Jiang et al., 2010).

In South China, the carbonate carbon isotope values from late Ediacaran to the early Cambrian show a generally increasing trend but in detail reveal a noisy transition with extreme $\delta^{13}C$ oscillations until about 520 Ma (Fig. 3), after which a modern marine ecosystem became firmly established (Shields-Zhou et al., 2013).

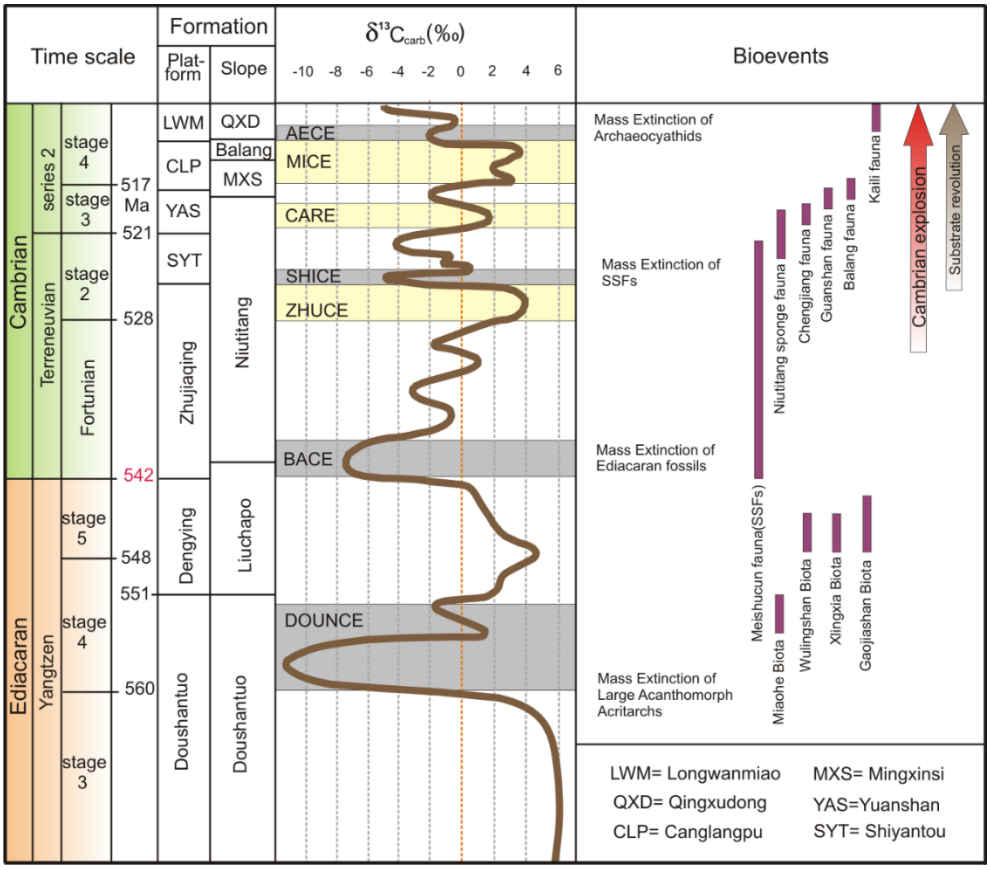

Fig. 3. *Integrated stratigraphic record of the late Ediacaran and early Cambrian showing the chronostratigraphic framework of South China with time–equivalent biozones, bioevents and the "substrate revolution". $\delta^{13}C$ data are after Zhu et al. (2006). The DOUNCE and BACE $\delta^{13}C_{carb}$ negative anomalies represent the South China equivalents to the global "Shuram-Wonoka anomaly" and "Pc-C boundary anomaly", respectively. The large positive ZHUCE excursion coincides with the third major assemblage of Small Shelly Fossils on the South China platform.*

In numerous mixed carbonate-siliciclastic systems, the first appearance of Treptichnus pedum occurs just above a pronounced negative 13C excursion (Maloof et al., 2010) of unknown cause. In contrast to older Neoproterozoic negative $\delta^{13}C$ excursions, this excursion is anomalous and appears not to be associated with a global glaciation.

In recent years, organic carbon, sulfur and strontium isotopes and redox-sensitive elements were increasingly studied to understand the causal link(s) between biogeochemical events and biotic evolution, and also to support stratigraphic correlation through chemostratigraphy. Even though conclusions of chemostratigraphic studies are generally less definitive compared to paleontological studies, chemostratigraphy has shown to be a powerful method where multiple elements and isotopic systems were applied, in particular where these were combined with paleontological and sedimentological investigations. This thesis contributes to the latter by providing a comprehensive sedimentological framework in a key region of this time interval (ca. 542-520 Ma).

Chronostratigraphy: U–Pb ages of zircons from tuff beds or other volcanic detrital units are pivotal in "learning to tell Neoproterozoic time" (Knoll, 2000). A U-Pb zircon age (542.0 ± 0.3 Ma; Amthor et al. 2003) from the Ara Group of Oman defines the abrupt disappearance of the late Ediacaran fossils *Cloudina and Namacalathus*, coinciding with a large-magnitude but short-lived negative excursion in the carbon isotope composition of seawater. Because the boundary in Oman is defined by the abrupt disappearance of *Cloudina* (there is no *Treptichnus pedum* documented in the cores and well cuttings) its biostratigraphic correlation with siliciclastic regions where *Treptichnus pedum* can be common remains problematic. In Newfoundland, where the biostratigraphic and sedimentological control is best, U-Pb radiometric ages of volcanic zircons yielded ages of 530.7±0.7 Ma (Isachen et al. 1994) within a siliciclastically dominated sequence, but this bed unit containing volcanic zircons is ca. 800m above the biostratigraphic Pc-C boundary. The location of the Precambrian-Cambrian boundary in Siberia was interpreted to be constrained by a weighted mean $^{206}Pb/^{238}U$ ID-TIMS zircon date of 542±1.3 Ma from a reworked volcaniclastic breccia near the base of the Nemakit-Daldynian at Knorbusuonka (Maloof et al. 2010). In South China, U-Pb dating of a tuff in Bed 5 of the Meishucun section records a depositional age of 536.5±2.5 Ma (Sawaki, et al. 2008) and 535.2±1.7 Ma (Zhu et al. 2009); however, the Meishucun section overlies an unconformity and the dated bed is well within the Cambrian section.

Thus, all methods applied to-date show problems. It is likely that a fine-scale time framework of the Precambrian-to-Cambrian transition could be established if multiple stratigraphic methods were consistently applied on different scales in the same area. Further detailed studies followed by stratigraphic integration will clearly continue to improve our understanding of the tectonic, climatic, evolutionary and biogeochemical processes of this critical time interval.

1.3. The Latest Ediacaran to earliest Cambrian of the Yangtze platform, South China

The South China or Yangtze block is one of the best candidates worldwide to investigate the Pc-C boundary and early Cambrian events (Fig. 4). It preserves unmetamorphosed, relatively complete, regionally coherent and widespread marine-dominated carbonate-siliciclastic sequences of Ediacaran to Cambrian age, including numerous well-studied fossil *lagerstätten*. Its bio-, litho- chemo- and chronostratigraphic aspects have been intensively investigated for decades.

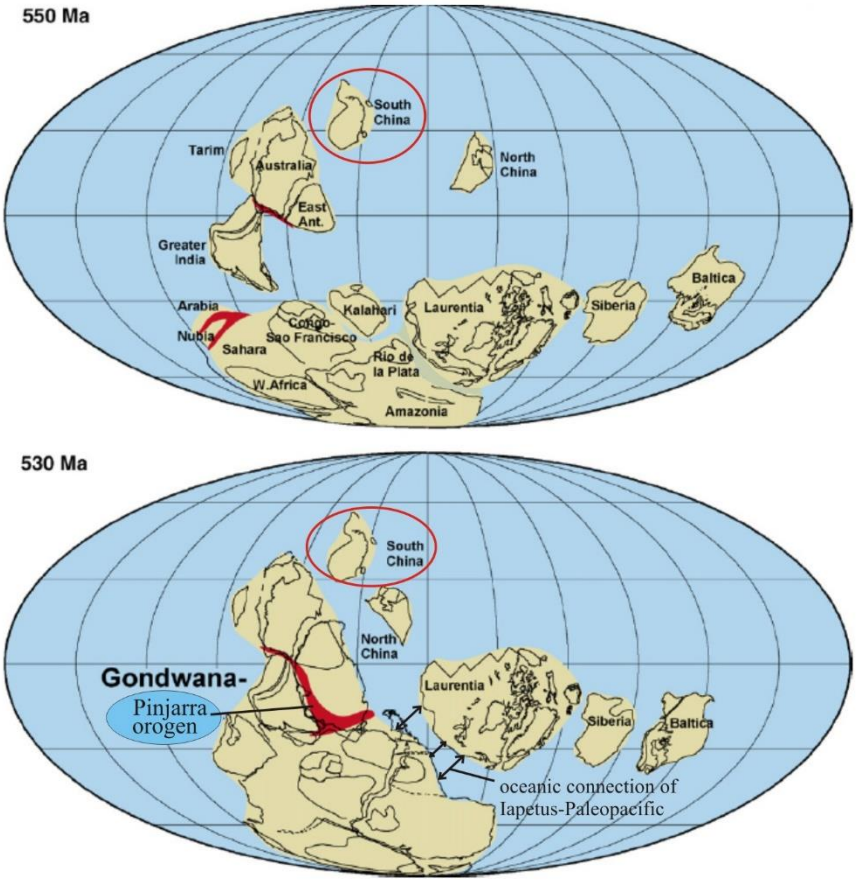

Fig. 4. *Paleogeographic reconstructions during the late Ediacaran (top) and early Cambrian (below), modified after Li et al. (2008). The position of South China is reconstructed in an outer-Gondwana passive margin setting in moderate to low northern latitudes.*

The South China Block consists of the Yangtze and Cathaysia blocks, which were amalgamated during the early Neoproterozoic Sibao-Jining Orogeny at ca. 1000 Ma to >900 Ma (Wang and Li, 2003; Li et al., 2005). Two major rift basins, resulting from the breakup of Rodinia (Meert and Lieberman, 2008), existed along its southeastern and western margins (Wang and Li, 2003): The Kangdian Basin at the block´s western margin and the north-south trending Nanhua Basin (with several sub-basins) at its southeastern margin. The distribution and development of overlying Neoproterozoic strata was influenced by this rifting and consists of four major sequence sets, 820 to 635 Ma old (Wang and Li, 2003). Although the timing of the rift-to-post-rift transition is unresolved, overlying Ediacaran strata (635-542 Ma) are believed to have been deposited in a passive-continental-margin setting during the post-rift period and developed a variety of facies associations from shallow to deep basin (Zhu et al., 2003; Jiang et al., 2003, 2011). Outcrops of Ediacaran to Cambrian shallow- and deep-water facies are well exposed on the Yangtze block but are rare on the Cathaysia block because of strong tectonic deformation and magmatism during the Ordovician-Silurian and Indosinian orogenies there (Li et al., 2003). Post-Marinoan (Ediacaran) marine carbonates and shales are assigned to the Doushantuo Formation and Dengying Formations (both in the shallow-platform facies) or to the Doushantuo and Liuchapo Formations (both representing the deep-basin facies), respectively. The distribution of early

Cambrian shallow-water and deeper-shelf deposits is largely controlled by the architecture of the underlying latest-Ediacaran Dengying Formation carbonate platform strata, which experienced several regressions and karstifications.

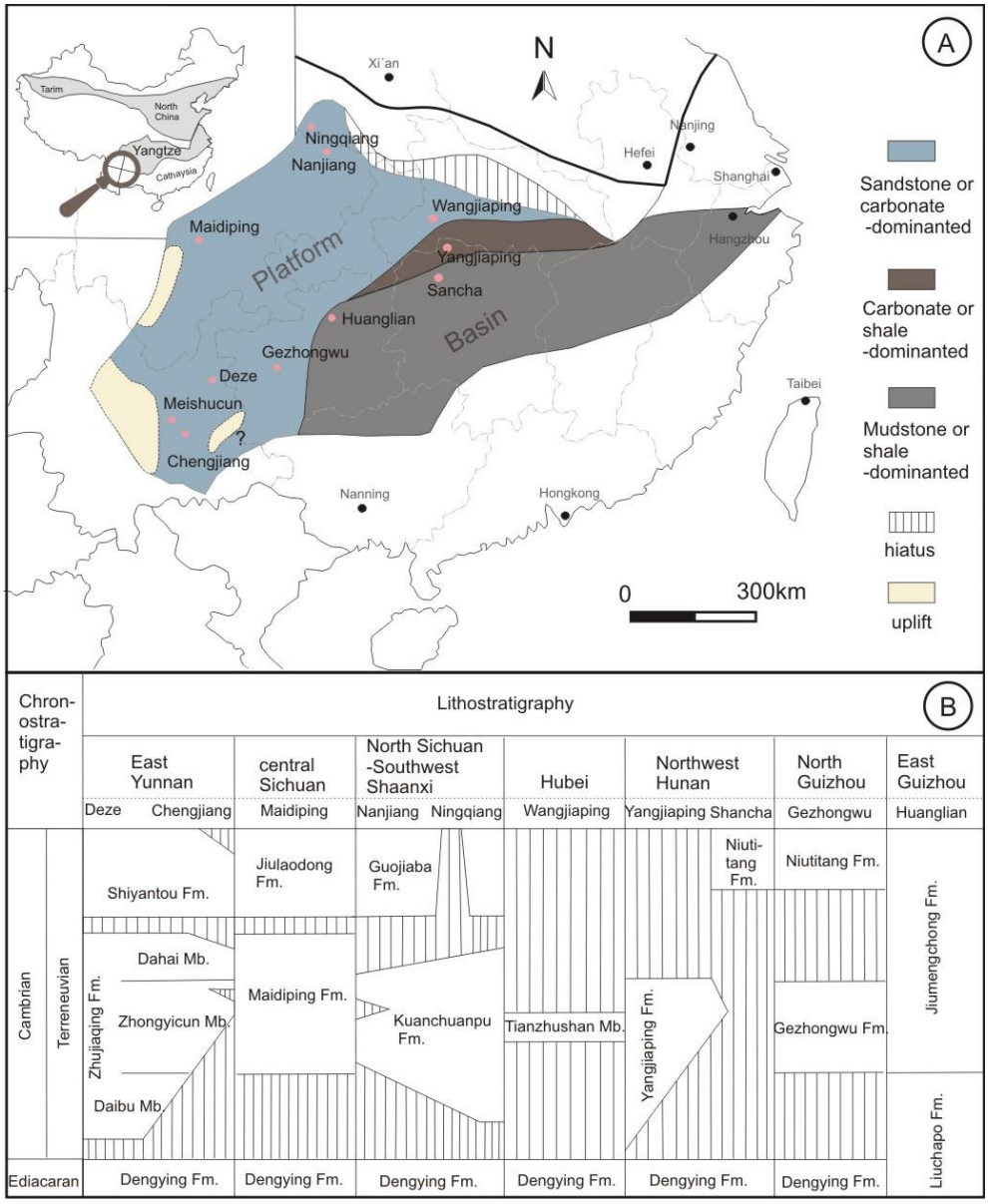

Fig. 5. *(A) Tectonic outline and a generalized paleogeographic reconstruction of the Yangtze platform during the early Cambrian (Terreneuvian). (B) Lithostratigraphic correlation of basal Cambrian strata of the Yangtze platform (Steiner et al., 2007). Locations mentioned in the table are marked by pink point in Figure A.*

The thickness of the Early Cambrian strata decreases from the shallow platform towards the basin (Zhu et al., 2003) (Fig. 5). Because Treptichnus pedum does not occur in carbonates, the base of Early Cambrian strata on the shallow carbonate platform of the Yangtze Platform is taken as the first appearance of skeletal fossils in Earth history, the polygenetic Small Shelly Fossils (SSFs) (Steiner et

al., 2007) while in the deeper part of the basin, due to the lack of fossils there, it is represented by an apparently correlative negative δ13C excursion (Zhu et al., 2006).

Within the South China (or Yangtze) platform, eastern Yunnan preserves the most complete and lithologically varied basal Cambrian strata. This region is therefore one of the best archives worldwide to understand this time interval.

1.4. Main questions and objectives

This study is part of the project "*Ecological and environmental change recorded through stratigraphy and sedimentology at selected Ediacaran-Cambrian boundary sections in East and Central Asia*" that is embedded in the DFG-Forschergruppe 736 "*The Precambrian-Cambrian Ecosphere (R)evolution: Insights from Chinese Microcontinents*". Its aim was to investigate the relationships between the Cambrian bioradiation and the associated paleoenvironmental changes through a multidisciplinary approach including sedimentology, palaeontology, and geochemistry.

Questions in this context and also arising from previous studies include:

- How do shallow platform lithofacies and stratigraphic thicknesses change laterally?
- What is the range of sedimentological and paleogeographic variation over the stratigraphic interval and under which environmental conditions did they form?
- What is the outcrop record of stratigraphic gaps and which bio- and chemostratigraphic changes occur there?
- Under which conditions did widespread early Cambrian phosphorites form? Did this facies form at the same time?

Research presented in this study thus aims to characterize and interpret the sedimentary context and evolution of the southwest Yangtze platform during the Pc-C interval by documenting in detail the stratigraphic succession, classifying the lithofacies in association with their depositional environment, using chemostratigraphic proxies, and determining the degree of multiple generations of diagenesis.

References

Amthor, J.E., Grotzinger, J.P., Schröder, S., Bowring, S.A., Ramezani, J., Martin, M.W. & Matter, A. 2003. Extinction of Cloudina and Namacalathus at the Precambrian-Cambrian boundary in Oman, *Geology* 31, 431-434.

Billings, E. 1872. On some fossils from the Primordial rocks of Newfoundland. *Canadian Naturalist* 6, 465–479.

Brasier, M., Cowie, J. & Taylor, M. 1994. Decision on the Precambrian–Cambrian boundary stratotype. *Journal of International Geoscience* 17, 3–8.

Brasier, M.D., Shields, G., Kuleshov, V.N., & Zhegallo, E.A. 1996. Integrated chemo- and biostratigraphic calibration of early animal evolution: Neoproterozoic–early Cambrian of southwest Mongolia. *Geological Magazine* 133, 445-485.

Brasier, M.D. & Lindsay, J.F., 2001. Did supercontinental amalgamation trigger the "Cambrian Explosion", in: Zhuralev, A.Y., Riding, R. (Eds.), The ecology of the Cambrian radiation. New York, Columbia University Press, pp. 69-89.

Corsetti, F.A., & Hagadorn, J. W. 2003. The Precambrian-Cambrian Transition in the Southern Great Basin, USA. *The sedimentary record* 5, 4-8.

Deynoux, M., Affaton, P., Trompette, R. & Villeneuve, M. 2006. Pan-African tectonic evolution and glacial events registered in Neoproterozoic to Cambrian cratonic and foreland basions of West Africa. *Journal of African Earth Sciences,* 46, 397-426.

Evans, D.A.D. 2003. A fundamental Precambrian–Phanerozoic shift in Earth's glacial style? *Tectonophysics* 375, 353–385.

Fairchild, I.J. & Kennedy, M.J. 2007. Neoproterozoic glaciation in the Earth system. *Journal of the Geological Society* 164, 895–921.

Grant, S.W.F., 1990. Shell structure and distribution of Cloudina, a potential index fossil for the Terminal Proterozoic. *American Journal of Science* 290, 261–294.

Halverson, G. 2006. A Neoproterozoic chronology. In: Xiao, Shuhai, Kaufman, Alan J. (Eds) *Neoproterozoic Geobiology and Paleobiology*, Springer Netherlands, 231–271.

Halverson, G.P., Hoffman, P.F., Schrag, D.P., Maloof, A.C. & Rice, A.H.N. 2005. Toward a Neoproterozoic composite carbon-isotope record. *Geological Society of America Bulletin* 117, 1181–1207.

Hoffman, P. F., Kaufman, A. J., Halverson, G. P. & Schrag, D. P. 1998. A Neoproterozoic snowball earth. *Science* 281, 1342-1346.

Hofmann, H.J. & Mountjoy, E.W. 2001. Namacalathus-Cloudina assemblage in Neoproterozoic Miette Group (Byng Formation), British Columbia: Canada's oldest shelly fossils. *Geology*, 29, 1091-1094.

Hua, H., Pratt, B.R. & Zhang, Y.L. 2003. Borings in Cloudina shells: complex predator-prey dynamics in the terminal Neoproterozoic. *Palaios* 18, 454–459.

Isachen, C.E., Bowring, S.A., Landing, E. & Samson, S.D. 1994. New constraint on the division of Cambrian time. *Geology* 22, 496-498

Ishikawa, T., Ueno,Y.,Komiya, T., Sawaki,Y.,Han, J., Shu,D., Li,Y.,Maruyama, S. & Yoshida, N. 2008. Carbonisotope chemostratigraphy of a Precambrian/Cambrian boundary section in the Three Gorge area, South China: prominent global-scale isotope excursions just before the Cambrian Explosion. *Gondwana Research* 14, 193–208.

Jensen, S. 2003. The Proterozoic and Earliest Cambrian Trace Fossil Record; Patterns, Problems and Perspectives. *Integrative and Comparative Biology*, 43, 219-228.

Jiang, G., Sohl, L.E. & Christie-Blick, N. 2003. Neoproterozoic stratigraphic comparison of the Lesser Himalaya (India) and Yangtze Block (South China): paleogeographic implications. *Geology*, 31, 917–920.

Jiang, G.Q., Shi, X.Y., Zhang, S.H., Wang, Y. & Xiao, S.H. 2011. Stratigraphy and paleogeography of the Ediacaran Doushantuo Formation (ca. 635-551 Ma) in South China. *Gondwana Research*, 19, 831-849.

Jiang, G.,Wang,X.,Shi,X.,Zhang, S.,Xiao,S.,Dong, J.,2010.Organic carbonisotope constraints on the dissolved organic carbon (DOC) reservoir at the Cryogenian–Ediacaran transition. *Earth Planetary Science Letters* 299, 159–168.

Kimura, H., Matsumoto, R., Kakuwa, Y., Hamdi, B. & Zibaseresht, H. 1997. The Vendian-Cambrian $\delta^{13}C$ record, North Iran: evidenve for overturning of the ocean before the Cambrian explosion. *Earth Planetary Science letter*s 147, 1-7.

Knoll, A.H. 2000. Learning to tell Neoproterozoic time. *Precambrian Research* 100, 3–20

Knoll, A. H., Walter, M. R., Narbonne, G. M. & Christie-Blick, N. 2006. The Ediacaran Period: a new addition to the geologic time scale. *Lethaia* 39, 13-30.

Landing, E. & MacGabhann, B.A. 2010. First evidence for Cambrian glaciation provided by sections in Avalonian New Brunswick and Ireland: Additional data for Avalon-Gondwana separation by the earliest Palaeozoic. *Palaeogeography, Palaeoclimatology, Palaeoecology* 285, 174-185.

Landing, E., Geyer, G., Brasier, M.D. & Bowring, S.A., 2013. Cambrian Evolutionary Radiation: Context, correlation, and chronostratigraphy - Overcoming deficiencies of the first appearance datum (FAD) concept. *Earth-Science Reviews* 123, 133-172.

Li, D., Ling, H.F., Jiang, S.Y., Pan, J.Y., Chen, Y.Q., Cai, Y.F. & Feng, H.Z. 2009. New Carbon isotope stratigraphy of the Ediacaran-Cambrian boundary interval from SW China: implication for global correlation. *Geological Magazine* 146, 465-484.

Li, D., Ling, H.F., Shields-Zhou, G.A., Chen, X., Cremonese, L., Och, L., Thirlwall, M. & Manning, C.J. 2013. Carbon and strontium isotope evolution of seawater across the Ediacaran-Cambrian transition: Evidence from the Xiaotan section, NE Yunnan, South China. *Precambrian Research* 225, 128-147.

Lindsay, J.F., Brasier, M.D., Dorjnamjaa, D., Goldring, R., Kruse, P.D. & Wood, R.A. 1996. Facies and sequence controls on the appearance of the Cambrian biota in southwestern Mongolia: implication for the Precambrian – Cambrian boundary. *Geological Magazine* 133, 417-428.

Li, W., Li, X. & Li, Z. 2005. Neoproterozoic bimodal magmatism in the Cathaysia Block of South China and its tectonic significance. *Precambrian Research* 136, 51–66.

Li, Z.H., Wang, J., Li, X.H. & Zhang, S.H. 2003. *From Sibao Orogenesis to Nanhua Rifting: Late Precambrian Tectonic History of Eastern South China. An Overview and Field Guide.* Geological Publishing House, Beijing.

Li, Z. X., Bogdanova, S. V., Collins, A. S., Davidson, A., De Waele, B., Ernst, R. E., Vernikovsky, V. 2008. Assembly, configuration, and break-up history of Rodinia: A synthesis. *Precambrian Research* 160, 179–210.

Magaritz, M., Holser, W.T. & Kirschvink, J.L. 1986. Carbon isotope events across the Precambrian-Cambrian boundary on the Siberian Platform. *Nature* 320, 258-259.

Maloof, A.C., Porter, S.M., Moore, J.L., Dudas, F.O., Bowring, S.A., Higgins, J.A., Fike, D.A. & Eddy, M.P., 2010. The earliest Cambrian record of animals and ocean geochemical change. *Bulletin of the Geological Society of America* 122, 1731-1774.

Marshall, C.R. 2006. Explaining the Cambrian "Explosion" of Animals. *Annual Review of Earth and Planetary Sciences* 34, 355-384.

Matthews, S.C. & Missarzhevsky, V.V., 1975. Small shelly fossils of late Precambrian and Early Cambrian age: a review of recent work. *Journal of the Geological Society London* 131, 289 – 304.

Meert, J.G. & Lieberman, B.S. 2008. The Neoproterozoic assembly of Gondwana and its relationship to the Ediacaran-Cambrian radiation. *Gondwana Research* 14, 5-21.

Myrow, P.M., & Hiscott, R.N. 1993. Depositional history and sequence stratigraphy of the Precambrian-Cambrian boundary stratotype section, Chapel Island Formation, southeast Newfoundland. *Palaeogeography, Palaeoclimatology, Palaeoecology,* 104, 13-35.

Narbonne, G.M., Gehling, J.G., 2003. Life after snowball: the oldest complex Ediacaran fossils. *Geology* 31 (1), 27–30.

Narbonne, G.M., 2005. The Ediacara Biota: Neoproterozoic origin of animals and their ecosystems. *Annual Review of Earth and Planetary Sciences* 33, 421–442.

Porada, H. & Bouougri, E. 2008. Neoproterozoic trace fossils VS. Microbial mat structures: Examples from the Tandilia Belt of Argentina. *Gonwana Research* 13, 480-487.

Sawaki, Y., Nishizawa, M., Suo, T., Komiya, T., Hirata, T., Takahata, N., Sano, Y., Han, J., Kon, Y. & Maruyama, S. 2008. Internal structures and U-Pb ages of zircons from a tuff layer in the Meishucunian formation, Yunnan Province, South China. *Gondwana Research* 14, 148-158.

Sawaki, Y., et al., 2010. The Ediacaran radiogenic Sr isotope excursion in the Doushantuo Formation in the Three Gorges area, South China. *Precambrian Research*, 176, 46–64.

Seilacher, A., Buatois, L.A., Mangano, M.G. 2005. Trace fossil in the Ediacaran-Cambrian transition: Behavioral diversification, ecological turnover and environmental shift. *Palaeogeography, Palaeoclimatology, Palaeoecology* 227, 323-356.

Shields, G., Kimura,H., Yang,J. & Gammon, P. 2004. Sulphur isotopic evolution of Neoproterozoic-Cambrian seawater: new francolite-bound sulphate $\delta^{34}S$ data and a critical appraisal of the existing record. *Chemical Geology* 204, 163–182.

Shields-Zhou, G & Zhu, M. 2013. Biogeochemical changes across the Ediacaran-Cambrian transition in South China. *Precambrian Research* 225, 1-6.

Smith, M. P. & Harper, D. A. T. 2013. Causes of the Cambrian Explosion. *Science* 341, 1355-1356.

Steiner, M., Li, G.X., Qian, Y., Zhu, M.Y. & Erdtmann, B.D. 2007. Neoproterozoic to early Cambrian small shelly fossil assemblages and a revised biostratigraphic correlation of the Yangtze Platform (China). *Palaeogeography, Palaeoclimatology, Palaeoecology* 254, 67-99.

Vernhet, E., Youbi, N., Chellai, E.H., Villeneuve, M. & Archi, A.E. 2012. The Bou-Azzer glaciation: Evidence for an Ediacaran glaciation on the west African Craton (Anti-Atlas, Morocco). *Precambrian Research* 196-197, 106-112.

Wang, J., Li, Z.X. 2003. History of Neoproterozoic rift basins in South China: implications for Rodinia break-up. *Precambrian Research* 122, 141-158.

Zhu, M., Zhang, J., Steiner, M., Yang, A., Li, G. & Erdtmann, B. 2003. Sinian- Cambrian stratigraphic framework for shallow to deep-water environment of the Yangtze Platform: an integrated approach. *Progress in natural science* 13, 951-960.

Zhu, M.Y., Babcock, L.E. & Peng, S.C. 2006. Advances in Cambrian Stratigraphy and paleontology: integrating correlation techniques, palaeobiology, taphonomy and paleoenvironmental reconstruction. *Palaeoworld* 15, 217–222.

Zhu, M.Y., Babcock, L.E. & Peng, S.C. 2006. Advances in Cambrian stratigraphy and paleontology: Integrating correlation techniques, paleobiology, tophonomy and paleoenvrionmental reconstruction. *Palaeoworld* 15, 217-222.

Zhu, R.X., Li, X.H., Hou, X.G., Pan, Y.X., Deng, C.L. & He, H.Y., 2009. SIMS U-Pb zircon age of a tuff layer in the Meishucun section, Yunnan, southwest China: Constraint on the age of the Precambrian-Cambrian boundary. *Science in China Series D: Earth Sciences* 52, 1385-1392.

CHAPTER II

Methods

2.1. Field investigations and sampling

Yunnan has intense precipitation during the wet season, which is normally from July to October. Furthermore, the vegetation is dense and almost impenetrable making it difficult to access the outcrops. Thus all fieldwork was undertaken in May 2011 and June 2012. We focused on two areas in southeast Yunnan and northeast Yunnan and measured a total of eleven sections, five of which were logged and sampled at meter- to centimetre-scale with emphasis on sedimentary structures, textures, lithology and stratigraphic architecture. A 108 m thick stratigraphic window at Laolin section and the areal exposed PC-C boundary in the active Kunyang quarries at Meishucun were covered at very high resolution. The aggregate thickness of all recorded sections is about 238 m.

Petrographic investigations were provided by outcrop observations, polished slabs and about 200 thin sections of limestone, dolostone, phosphorite and sandstone. Phosphorite nomenclature follows Trappe (1998), derived from the limestone classification of Dunham (1962).

2.2. Laboratory analyses

2.2.1. Thin section preparation and staining

Samples were cut into two slices for slab polishing and for thin section preparation. Nearly all the thin sections are 5 cm x 3 cm in size. The sample slice was first cut into a rectangle of standard size (5 x 3 x 0.5 cm), then mounted on a glass slide with epoxy resin. After heating in the oven overnight at 50 °C temperature the sample was cut by machine and subsequently polishing down to 30 µm final thickness using progressively finer grades of abrasive material (carborundum).

Alizarin Red-S dye was used for calcite staining. The recipe is a mixture of 100 ml 0.15 to 0.2% HCl with 0.2 g Alizarin Red-S. Thin sections have to be clean, dry and oil-free. The thin section is then immersed for 12 to 20 sec in the Alizarin Red solution and carefully washed with demineralised water.

2.2.2. Cathodoluminescence microscopy and polarized microscopy

Thin sections were investigated with a transmitted-light microscope equipped with polarizer and analyzer stages (Leica DM EP) at Freie Universität Berlin. Cathodoluminescence investigations were carried out with the hot-cathode CL microscope (type HC3-LM, Lumic Spezialmikroskope, Dortmund) at the Museum für Naturkunde Berlin, Germany. The system was operated at 14 kV with a filament current of 0.1 to 0.3 mA. Thin sections were polished and carbon-coated at Freie Universität Berlin. The coating was done at standard conditions to a thickness of about 15 nm to avoid variations in CL-intensity.

2.2.3. Back-scatter electron microscopy and EDX analysis

EDX analyses on thin sections and polished rock samples were undertaken for spot analyses and elemental mapping. These were performed on a ZEISS SUPRA™ 40 VP Ultra SEM equipped with Oxford Instruments EDX-System and INCA-analysis software at Freie Universität Berlin.

2.2.4. Trace and rare earth elements and Sr isotope analyses

We selected five samples near the PC-C contact for trace and rare earth elements and Sr isotope analysis. We used acetic acid leaching to analyze geochemical signatures solely of the soluble carbonate fraction. About 20 mg of bulk sample powder was treated with 1 ml 3 M acetic acid for 12 hours, following the methods described by Huang et al. (2009). Insoluble residues were separated by centrifugation and filtration through 0.45 µm cellulose acetate syringe filters. To remove the acetic acid, the supernatant was dried down and re-dissolved in 0.5 ml 3 M HNO_3. Afterwards, the solution was equilibrated in 1 ml 0.28 M HNO_3, weighed and diluted with 0.28 M HNO_3 to 1: 20.000 for trace element and to 1: 40.000 for major element analysis.

All trace and rare earth element analyses on carbonate leachates were performed on a Thermo-Finnigan Element XR sector-field ICP mass spectrometer at the Freie Universität Berlin using a Scott type quartz spray chamber and a 100 µl/min nebulizer. Sample time was 120 s with 20 samples/peak and 60 total scans. With this analytical setup, tuning generally yielded low oxide rates of 2-5 % CeO^+ and less than 1% BaO^+. We determined element concentrations by external calibration to the matrix-matching CAL-S carbonate standard (Yeghicheyan et al., 2003). For drift correction, the diluted samples were doped with solutions of 2 ppb In and 1 ppb Tl for elements analyzed in low-resolution mode (REE+Y), and 12.5 ppb Co for elements analyzed in medium-resolution mode (Ba, Mn, Sr). Background corrections were performed by subtraction of the raw intensities of aspirated 0.28 M HNO_3. The analytical precision for trace and rare earth elements was usually better than 5% RSD. Detection limits were 25 ppb for Ba and Mn, 200 ppb for Sr, 100-620 ppt for LREE and 16-240 ppt for HREE, respectively. Procedural blanks on trace elements and REE were negligible, being generally below the acid-background-signal intensities. We calculated Ce/Ce* and Eu/Eu* according to Bau and Dulski (1996), with normalization of concentrations against the standard values of Post-Archean Australian Shale (= PAAS; McLennan, 1989).

Aliquots of the acetic acid carbonate leachates were used for Sr isotopic composition measurements. Approximately 1 µg Sr was loaded on 1 ml AG 50W-X8 (200-400 mesh) cation-exchange resin with 2.5 M HCl for separation of Sr from the matrix. Thereafter, the Sr isotopic composition was determined using a Thermo-Finnigan Triton TIMS at Freie Universität Berlin. Repeated measurements of the reference material NIST SRM 987 yielded $^{87}Sr/^{86}Sr = 0.710266$ (± 15, n = 6). Mass fractionation was corrected assuming a $^{87}Sr/^{86}Sr$ ratio = 0.1194 (Nier, 1938) and the exponential law. Minor interferences of ^{87}Rb on ^{87}Sr were corrected using $^{85}Rb/^{87}Rb = 2.59265$. Initial $^{87}Sr/^{86}Sr$-ratios were calculated assuming depositional ages of 600 Ma, $^{87}Rb/^{86}Sr$ ratios calculated from ICP-MS data, and a half-life of

^{87}Rb of $4.88*10^{10}$ years. Corrections of the potential radiogenic ingrowth of Rb are approx. 2 ‰. In general, corrections are minor and do not change the interpretation of the carbonate data.

References:

Dunham, R.J., 1962. Classification of carbonate rocks according to depositional texture. In: Ham,W.E. (Ed.), Classification of Carbonate Rocks.AmericanAssociation of Petroleum Geologists Memoir 1, pp. 108–121.

Huang, J., Chu, X., Chang, H & Feng, L. 2009. Trace element and rare earth element of cap carbonate in Eidacaran Doushantuo Formation in Yangtze Gorges. *Chin. Sci. Bull* 54, 3295-3302.

McLennan, S.M. 1989. Rare earth elements in sedimentary rocks: Influence of provenance and sedimentary processes. Geochemistry and Mineralogy of Rare Earth Elements, 21, 169-200.

Trappe, J. 1998. Phanerozoic Phosphorite Depositional Systems. Springer, Berlin; Heidelberg. p. 46

Yeghicheyan, D., Carignan, J., Valladon, M., Bouhnik Le Coz, M., Samuel, J., BenBakkar, M., Bruguier, O.,Keller, F., Pin, C., Pour- tales, S., Hénin, O., Macé, J., Morin, N., Guilmette, C., & Marin, L. 2003. The new carbonate reference material Cal–S: prelim- inary results, Abs. Geoanal., p. 146

CHAPTER III

Stratigraphy and paleogeography of the earliest Cambrian Zhujiaqing Formation, South China: An inner-platform environment for the diversification of small shelly fossils

Stratigraphy and paleogeography of the earliest Cambrian Zhujiaqing Formation, South China: An inner-platform environment for the diversification of small shelly fossils

Xiaojuan Sun[a], Christoph Heubeck[b]

[a] *Institute of Geological Sciences, Freie Universität Berlin, Malteserstraße 74-100, 12249 Berlin, Germany*

[b] *Department of Geosciences, Universität Jena, Burgweg 11, 07749 Jena, Germany*

3.1. Abstract

The Early Cambrian record of small shelly fossil bioradiation and associated biogeochemical changes is well preserved in the Terreneuvian (earliest Cambrian; 542-521 Ma) strata of the Zhujiaqing Formation (eastern Yunnan Province, South China), a shallow-water, siliceous-phosphorite-carbonate sequence. Although these deposits represent an excellent archive for understanding the biogeochemical and palaeobiological changes occurring at that time, their stratigraphic architecture remains poorly understood. We here present a detailed sedimentological study of five stratigraphic sections of an inner-platform setting, classify twelve characteristic lithofacies and define three environmental end members: siliceous-phosphate subtidal, dolomite peritidal, and carbonate subtidal. A thorough knowledge of the changes in water depth and palaeogeography of the Zhujiaqing Formation will improve our understanding of the stratigraphic preservation condition and in deciphering the pattern of early Cambrian bioradiation in South China.

Keywords: Cambrian, Yangtze platform, Yunnan, Carbonate deposits, Small Shelly Fossils, Zhujiaqing Formation

3.2. Introduction

Plate-tectonic and evolutionary events prior to and across the Precambrian - Cambrian (Pc-C) boundary globally mark a major turning point in the Earth's history. These include the break-up of Rodinia and the subsequent assembly of some of its constituent cratons into Gondwana (Li et al., 2008; Meert and Lieberman, 2008), several glaciations (Deynoux et al., 2006; Fairchild and Kennedy, 2007) and the major bioradiation of metazoans (McCall, 2006; Marshall, 2006), the latter in a relatively short geological time (about 40 Ma). However, the geological record of the Pc-C transition worldwide is incomplete because the critical shallow-marine depositional settings nearly all record one or several regressive cycles. These caused rapid and widespread lithological changes and the formation of prominent stratigraphic hiati, both of which hinder the extraction of time-stratigraphic information.

Because this incompletely represented time period records the beginning of major metazoan diversification events, best represented by the near-global small shelly fossils (SSFs) record, a calibrated time scale for the "Early Cambrian" is a prerequisite for the understanding of the Cambrian bio-radiation. Lindsay et al. (1996), among many others, pointed out that basin analysis will be a necessary prerequisite to meaningfully define the Pc-C boundary because there is no convincing evidence for global synchroneity of events and because the first appearance of Cambrian fauna, as currently defined, is strongly facies-dependent (see also Maloof, 2010; Landing et al., 2013). For example, Weber et al. (2007) showed that the first appearance datum (FAD) of *Trichophycus pedum (T. pedum)*, the index fossil of the Pc-C boundary, appears in carbonate settings to lie in slightly younger strata than in siliciclastica due to facies restriction. Maloof et al. (2010) questioned the reliability of SSF biostratigraphy in lower Cambrian strata because the FAD of SSFs scatters over a considerable time interval (ca. 10 Ma) and because numerous sedimentary hiati in shallow-water-facies strata diminish their utility. Chemostratigraphy, usually using carbonate carbon isotopes, is partially compromised due to disconformities, condensed intervals and regional signals which mask global trends (Jiang et al., 2012). In addition, the role of carbonate diagenesis in interpreting Ediacaran carbonate carbon isotope variability is disputed (Knoll et al., 1996; Derry, 2010). Solutions to these problems and their consequences must be tested in the stratigraphic record.

Strata in eastern Yunnan, in the southwestern part of the Yangtze platform, preserve the most complete and diverse stratigraphic record of the early Cambrian in China aside from the Three Gorges region of central China. Recent geochemical data (Shields-Zhou et al., 2013) indicate that the Pc-C interval (ca. 560-520 Ma) represents a "noisy" transition from the late Precambrian Dengying Formation to the early Cambrian Zhujiaqing Formation, showing generally increasing values of $\delta^{13}C_{carb}$ with several prominent excursions of unknown origin (Zhu et al., 2006, 2007). In eastern Yunnan, studies to date focused on biostratigraphy and on regional and global correlation (Luo et al., 1982; Qian, 1989; Qian et al., 2002; Li et al., 2004; Steiner et al., 2007), and some early Cambrian sections in eastern Yunnan have also been sampled for geochemistry, notably the Xiaotan and Laolin sections. These studies largely aimed at reconstructing oceanic redox conditions (Och et al., 2013; Xu et al., 2014), biogeochemical interactions (Cremonese et al., 2011, 2013) and past sea water chemistry (Li et al., 2009, 2013; Shields et al., 2001). All these works markedly contributed to improving the biostratigraphic and geochemical record of the Pc-C transition. Consequently, Landing et al. (2013) proposed the Laolin section of northeastern Yunnan as a new Global Boundary Stratotype Section and Point (GSSP) candidate for the upper Terreneuvian series (Stage 2), tentatively named "Laolinian Stage".

However, no detailed sedimentological framework has been established in eastern Yunnan, especially near the Laolin section area but such a comprehensive sedimentological and paleogeographic framework is required to support and interprete geochemical and paleobiological information. Lithostratigraphic and paleogeographic publications of eastern Yunnan mainly date from the 1980s and

1990s, which focused on the mineralogy of the widespread stratiform phosphorites, their concentration mechanisms and the general depositional environment (Ge et al., 1983; Lei et al., 1986; Chen et al., 1987; Zeng et al., 1987; Huang et al., 1990) without placing sections in a regional process-oriented context with detailed facies analysis. The present study thus aims to investigate the depositional setting and stratigraphic architecture of the Lower Cambrian Zhujiaqing Formation in eastern Yunnan. We studied five profiles at outcrop-scale and through thin-section petrography, defined the spatial and temporal distribution of twelve lithofacies, derived a sedimentological interpretation and placed our findings in a basinwide context.

3.3. Geological background

3.3.1. General paleogeography of the Yangtze platform across the Pc-C transition

The Yangtze platform developed during the late Neoproterozoic to early Cambrian on the southeastern margin of the Yangtze micro-continent at low latitude. Its paleogeographic and tectonic framework had a major influence on its stratigraphic architecture. The platform was internally structured by numerous fault-bounded shelf basins; along its margins, slope and basinal-facies sediments were deposited (Fig. 1A; Zhu et al., 2003; Vernhet and Reijmer, 2010; Jiang et al., 2012).

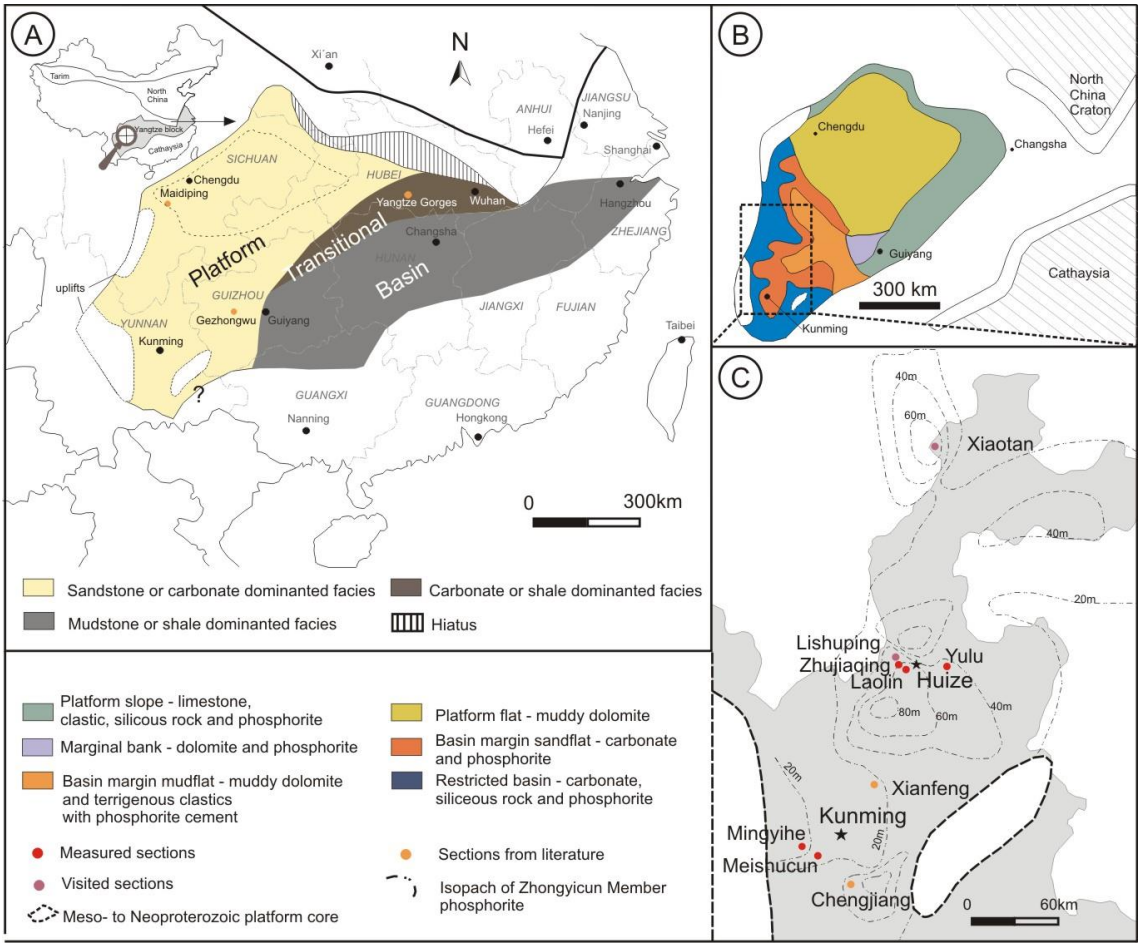

Fig. 1. *A) Generalized paleogeographic reconstruction of the Yangtze microcontinent during the early Cambrian. B) Sedimentary facies and palaeogeography of the Yangtze micro-continent during the Zhongyicun Member of the Zhujianjing Fm. (see Fig. 2 for stratigraphic sequence). C) The extent of Zhongyicun Member Phosphorite deposition in eastern Yunnan, and the locations of the sites discussed in the text (Luo et al., 1982; Li, 1986).*

In the western part of the Yangtze shelf platform, sedimentation was controlled by the north-south-trending Kangdian rift basin since the Neoproterozoic; the rifting continued until the early Ediacaran (Wang and Li, 2003) and then passed into the phase of thermal subsidence. The youngest Ediacaran unit in shallow-water facies of the Yangtze platform is the Dengying Formation (ca. 551-542 Ma; Zhu et al., 2007); it has a highly varying thickness between 90 and 800 m and is dominated by shallow-marine carbonates. Rare siliciclastic intervals represent regressive events, and paleokarst surfaces across the platform indicate occasional widespread exposure (Xue et al., 1992; Siegmund and Erdtmann, 1994). The contact of the Dengying Formation to overlying Cambrian strata is a widespread unconformity almost everywhere on the Yangtze platform (Zhu et al., 2003). Thickness of early Cambrian strata increases from the deeper-water setting (e.g., in southern Hunan) towards the shallow-platform facies (e.g., in eastern Yunnan, northwestern Guizhou and southern Sichuan). Aside from the exposures in the Three Gorges region, strata in eastern Yunnan, especially in the north, preserve the most complete stratigraphic record of the Ediacaran-Cambrian transition and the early Cambrian in China.

3.3.2. Earliest Cambrian stratigraphy in Eastern Yunnan

Internationally, the Cambrian is divided into four series. The current concept divides the lowest series, the "Terreneuvian" (Landing et al., 2007) into the Fortunian Stage and the overlying, not yet named "Cambrian Stage 2". The top of the Terreneuvian Series (and the top of Cambrian Stage 2) has not been defined yet, but is expected to be close to the FAD of Gondwana trilobites.

At the beginning of the Cambrian, eastern Yunnan likely formed a shallow-water embayment to the east of an island chain on the southwestern side of the inner Yangtze platform (Fig. 1B). The paleogeography may have been varied, and structural compartmentalization by north-south- and east-west-trending faults likely resulted in a number of depositional "sags" (Li et al., 1986; He et al., 1989) which accommodated variable thicknesses of earliest Cambrian strata.

The Ediacaran Dengying Formation consists of dolomitized shallow-water carbonate and quartzose siltstone and reaches a maximum thickness of about 600 m in Yunnan (Zhu et al., 2003). The overlying Cambrian Zhujiaqing Formation of eastern Yunnan overlies the Dengying Formation unconformably and ranges from a few tens of m to more than 200 m in thickness (Fig. 1C); a well-developed paleokarst surface occurs at its base in southeast Yunnan. Litho- and biostratigraphy of the Zhujiajing Fm. was established from sections near Dahai and Yulu in Huize County (Fig. 2; Luo et al., 1982; Qian et al.,

1999; Luo et al., 1991; Qian et al., 1996, 2002; Zhu et al., 2001). Three members are recognized: The basal Daibu Member (approx. 0 to 60 m thick) comprises uniform, thin- to medium-bedded dark grey chert, and siliceous / argillaceous dolostone with interbedded siltstone. It grades upwards into the Zhongyicun Member (approx. 10 to 80 m thick), which is lithologically differentiated but widely contains several mineable phosphorites beds: In the southern sections, e.g., near Meishucun, the Zhongyicun Member consists mainly of medium- to thick-bedded granular phosphorite. In the Laolin section of northern Yunnan, this member is thicker and consists of carbonate, siltstone and phosphorite. SSFs of Zone I (*Anabarites trisulcatus - Protohertzina anabarica*) and Zone II (*Siphogonuchites triangularis - Paragloborilus subglobosus*) in this member show an upward-increasing diversity. The uppermost unit of the Zhujiaqing Formation, the calcareous Dahai Member, is lithologically uniform in eastern Yunnan but its thickness ranges from only 1m in the Meishucun section in the south to ~36 m at Laolin and 60 m at Xiaotan section in the north (Li et al., 2013; Cremonese et al., 2013).

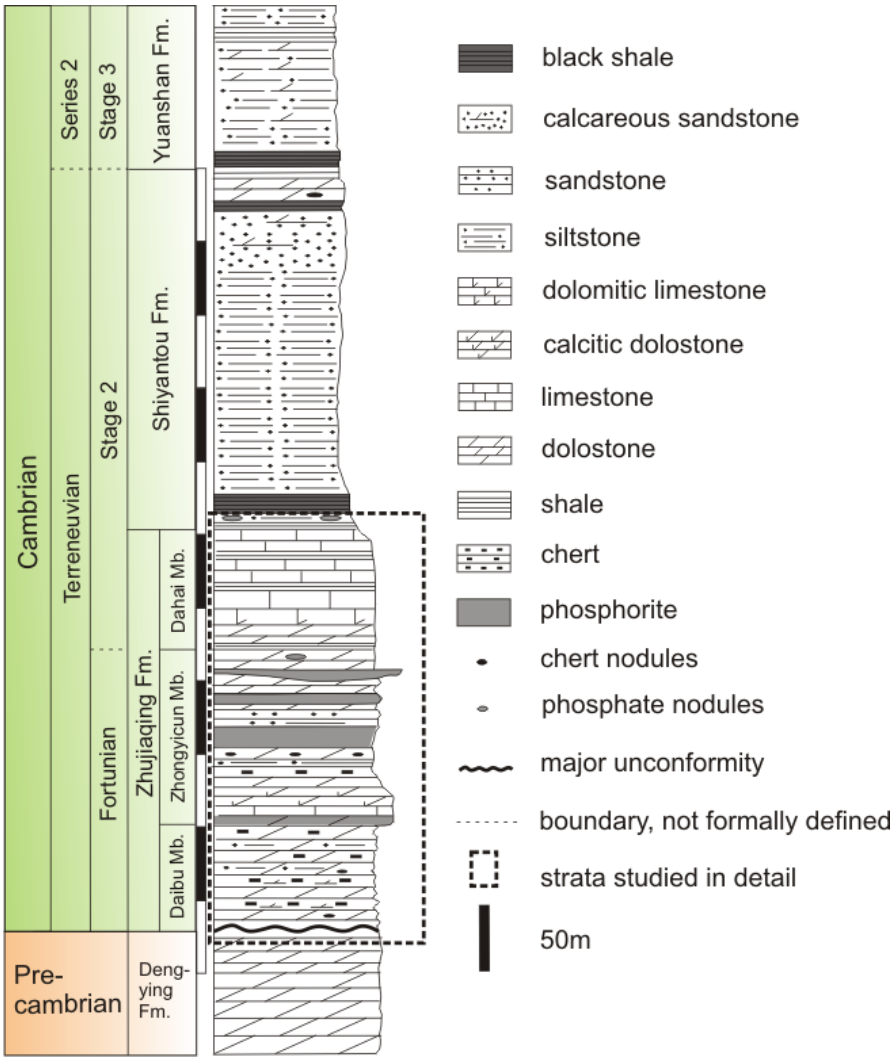

Fig. 2. *Generalized stratigraphic column of Early Cambrian strata in eastern Yunnan.*

Its lower part comprises whitish, medium- to thick-bedded dolostone and calcitic dolostone; the upper part comprises grey, thin- to thick-bedded dolomitic limestone with abundant SSFs of Zone III (’*Heraulithipegma yunnanensis*’’ - *Watsonella crosbyii*). The overlying Shiyantou Formation reaches up to 250 m in Xiaotan section and consists of quartzose silty mudstone. Its base usually consists of thin beds of black or grey glauconitic, phosphatic sandstone. The *Sinosachites-Tannuolina* SSFs of Zone IV occur in thin-bedded and lenticular limestones in its upper part. The overlying Yuanshan Formation is a black shale and carbonaceous siltstone. Its lower part contains the earliest record of trilobites in China (Steiner, 2001).

3.4. Methods and materials

We measured three representative and well-exposed stratigraphic sections (Laolin, Yulu and Zhujiaqing) from northern Yunnan and two sections (Meishucun and Mingyihe) from southern Yunnan, with particular emphasis on lithological description, sedimentary textures and stratigraphic surfaces. Subsequently, we conducted lithofacies analysis by integrating our field data with literature data and thin section petrography, summarized the spatial and temporal distribution of lithofacies and developed the paleogeography. SEM analyses provided detailed information on element distribution and mineral morphology. Selected polished thin sections were carbon-coated and examined by hot cathodoluminescence (CL) at the Museum für Naturkunde Berlin. The acceleration voltage of the electron beam was 14 keV and the beam current ranged between 0.1 and 0.3 mA.

3.5. Results and analyses

3.5.1. Representative sections

3.5.1.1. Laolin

The Laolin section is located along a roadcut (N26°16´44.1" E103°13´25.1") near Laolin village in Huize County (Figs. 3, 4A), about 2 km due east of a deeply incised tributary to the Yangtze River and ca. 16 km from the county seat Huize. It is one of the best sites in northeastern Yunnan to study the Pc-C transition in a shelf environment. The carbon and oxygen chemostratigraphy of this section has been documented by Shen et al. (2001), Zhu et al. (2001) and Li et al. (2009). We measured a continuous profile 108 m in stratigraphic thickness, including the uppermost part of the Dengying Formation, part of the Daibu Member, the Zhongyicun Member and the Dahai Member.

The exposed two meters of the uppermost Dengying Formation are composed of light grey, massive, coarsely recrystallized dolostone. Overlying strata, about 55 m thick, presumably including a large part of the Daibu Member, are covered. The remaining exposed five m of the Daibu Member consist of thin- and parallel-bedded, planar to wavy, dark grey siliceous dolostone and dolomitic chert. A fault zone affects the bedsets, and numerous joints and calcite-filled veins permeate the strata. The lower part of the Zhongyicun Member (5 to 24 m of the measured profile) consists of rhythmically bedded

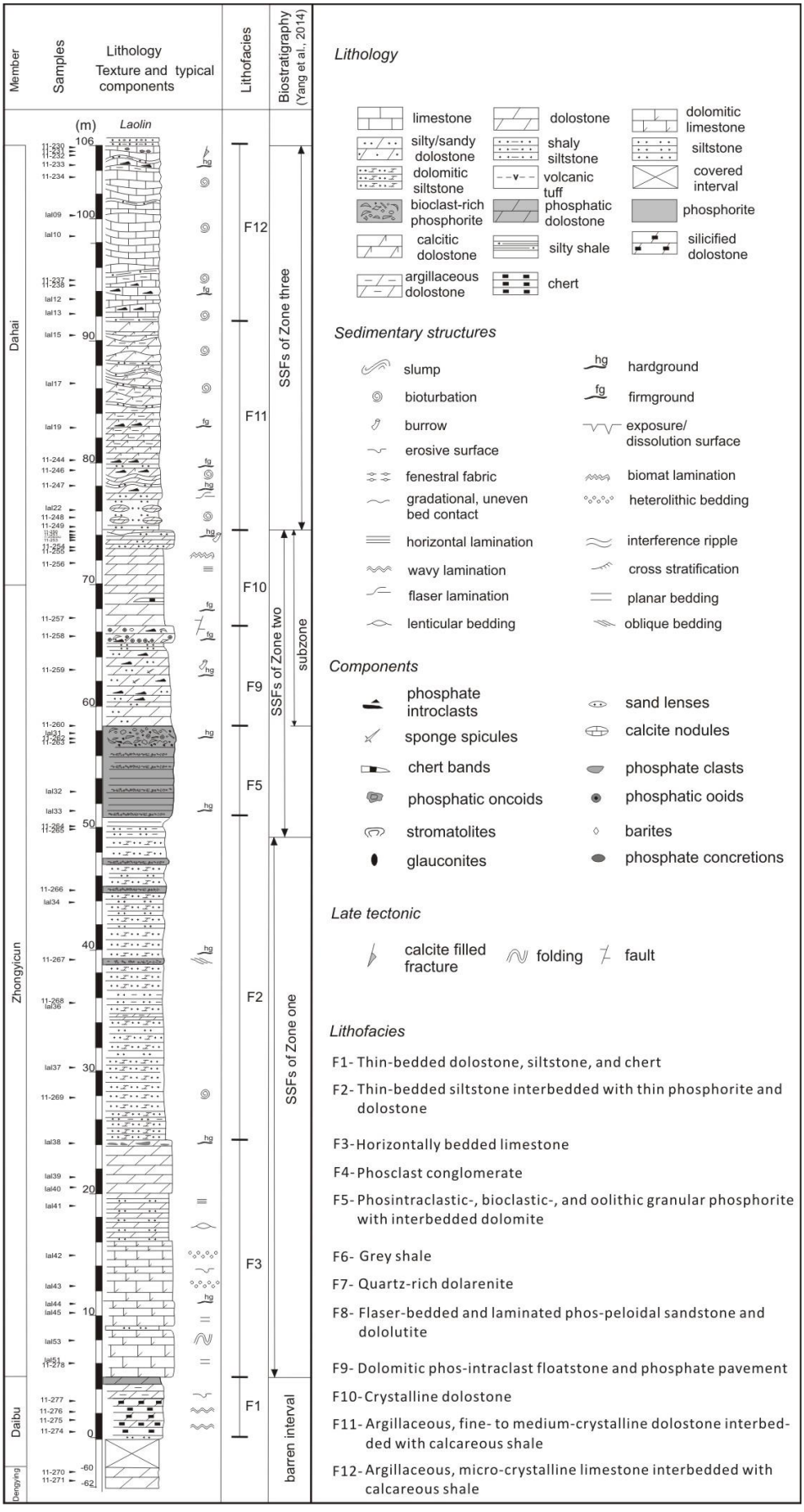

Fig. 3. *Stratigraphic column of the Laolin section and the corresponding lithofacies.*

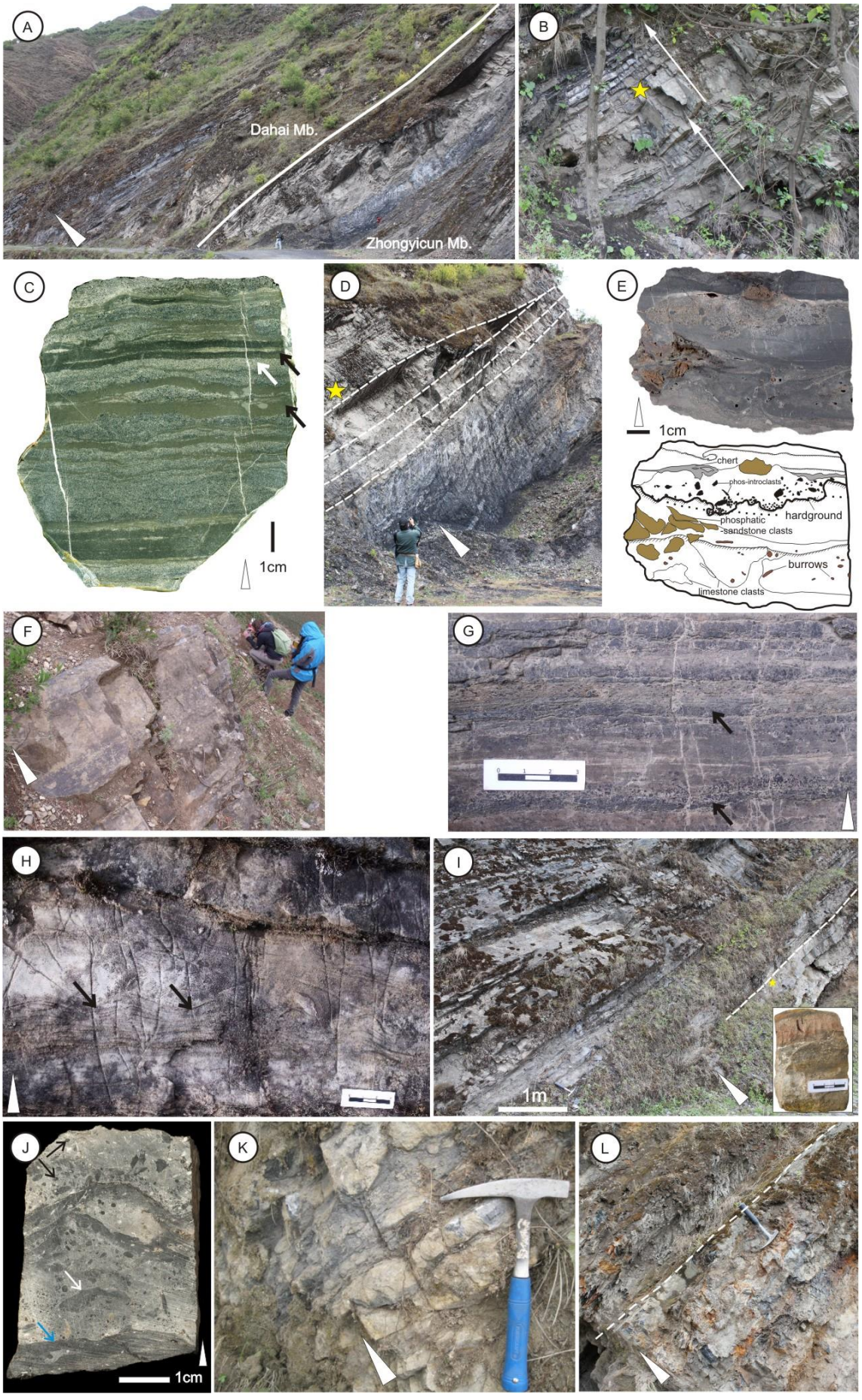
A
Dahai Mb.
Zhongyicun Mb.
B
C
1cm
D
E
1cm
chert
phos-introclasts
phosphatic
hardground
sandstone clasts
burrows
limestone clasts
F
G
H
I
1m
J
1cm
K
L

Fig. 4. *Outcrop lithologies and sedimentary textures of Laolin section. White triangles point to stratigraphic-up. A) Roadcut showing the contact of the Zhongyicun Member to the overlying Dahai Member. B) Lower Zhongyicun Member dolomitic limestone showing thinning-upward cycles (arrows). The yellow star indicates the location of the sample shown in (C). C) Wavy to lenticular lamination in dolomitic limestone. The light grey lamina (e.g., white arrow) is packstone, the brownish and dark grey laminae (e.g., black arrows) are argillaceous dolomitic mudstone. D) Organic-rich granular phosphorite (below the dashed lines) overlain by tabular phosphatic dolostone. The yellow star indicate the location of the sample shown in (E). E) Upper image: polished hand sample of phosphatic dolostone. Note several generations of hardgrounds, burrows and lithoclasts. Lower image: Line drawing of the hand sample above. F) Medium- to thick-bedded phosphatic dolostone. G) Close-up view of laminated, poorly sorted black phosintraclasts (e.g., arrows). H) Laterally linked stromatolitic hemispheroids (arrows) in thick- to medium-bedded dolostone. I) Thick-bedded sparitic dolostone (below the dashed line) overlain by grey argillaceous dolostone. The yellow star indicate the location of the sample at lower right. Burrows shown in the sample are in a reddish phosphatic-sandstone lens in sparitic dolostone. J) Phosphate intraclasts (e.g., white arrow), firmgrounds (e.g., blue arrow) and phosphatic small shelly fossils (e.g., black arrows) in grey argillaceous dolostone in Dahai Member. K) Nodular limestone in Upper Dahai Member. L) Parallel contact (dashed line) of basal silty shale of Shiyantou Formation to underlying nodular limestone of Dahai Member.*

Medium- to thick-bedded dolomitic limestone (Fig. 4B). Lenticular and wavy laminae appear in thin beds (Fig. 4C); flaser bedding is common in thick beds. Dark grey, thin-bedded dolomitic siltstone follows up-section (24 m to 50 m) and is increasingly interbedded with thin-bedded, horizontally stratified, dolomitic phosphorite (40 – 50 m of the measured section). This unit is overlain by black, organic-rich, thin- to medium-bedded granular phosphorite (50 - 58m) (Fig. 4D), followed by thick- to medium-bedded phosphatic dolostone (58 – 67 m) with hardgrounds (Fig. 4D, 4E) and abundant phos-intraclasts aligned in strings 1 to 5cm thick with erosive bases (Fig. 4F, 4G).

The overlying Dahai Member is on average 39 m thick (from 67 m to 106 m). Its lowermost 6 m consist of thick-bedded, whitish to light grey dolostone. The unit is slightly cherty at the base whereas microbial laminae occur in its upper part (Fig. 4H). The overlying 1.5 m (73 - 74.5 m) consist of abundantly burrowed, medium- to thick-bedded silty sparitic dolostone followed by thin- to medium-bedded, abundantly bioturbated, slightly nodular argillaceous dolostone (74.5 – 92 m) (Fig. 4I). Phos-intraclasts and SSFs are common in some beds, commonly with firmgrounds (Fig. 4J). The section ends with an approx. 14 m thick, partly dolomitized, slightly nodular-limestone (Fig. 4K) (92 m and higher) with a clast composition and texture similar to that of the underlying dolostone. The uppermost part of the section, a 20 to 25 cm thick bed near the top of the Dahai Member contains lenses of phosphate conglomerate and is conformably overlain by shaly laminated siltstone of the basal Shiyantou Formation (Fig. 4L).

3.5.1.2. Yulu

Our investigation of the Yulu section, measured at Hongyangou village near Yulu town, was limited to about 10 m of the top of the Zhongyicun Member and the overlying 16 m of the lower Dahai Member

due to vegetation cover (Fig. 5). The base of the section consists of 3 m of black, organic-rich shaly siltstone with dolomite lenses (Fig. 6A). Small-scale slump folds occur within black siltstone (Fig. 6B). The siltstone is overlain by medium-bedded phosphatic dolostone, interbedded with slightly bioturbated, thin-bedded shaly siltstone (Figs. 6C, D) (3 - 7 m). An overlying, about four-meter-thick section consists of thick-bedded organic-rich phosphatic dolostone. Above an approx. 1 m-thick unexposed interval, a medium- to thick-bedded wavy dolostone about two m thick is overlain by quartz- and phosphate-sandy dolostone (13 to 21m). Weathering of this unit is intense, so that the more resistant dolomite-cemented beds crop out prominently (Fig. 6F). The overlying 7 m of the section are composed of thick-bedded gray dolostone (3 m thick) with common phosphatic firmgrounds (Fig. 6F) and medium-bedded nodular dolostone rich in organic flakes. The nodules consist of calcitic, phosphatic SSF-bearing dolostone embedded in calcareous silty shale (Fig. 6G).

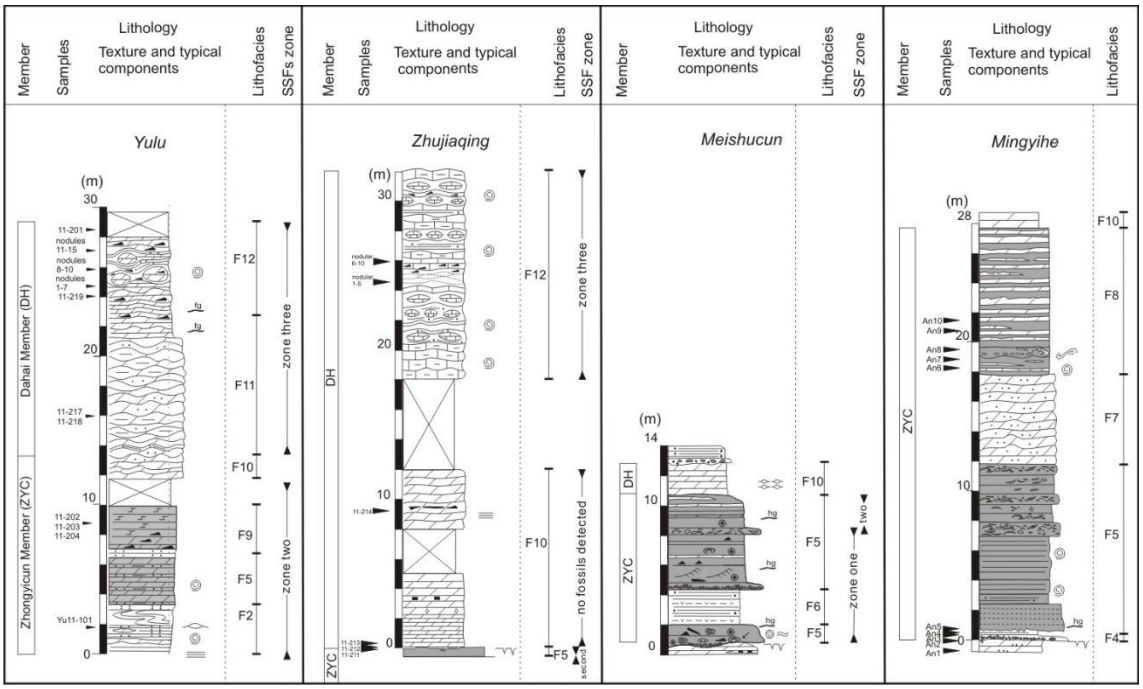

Fig. 5. Representative stratigraphic sections of the basal Cambrian Zhujiaqing Formation in Yunnan.

3.5.1.3. Zhujiaqing

Our investigation of the Zhujiaqing section focused on the Dahai Member of the Zhujiaqing Formation (Fig. 5). Its basal contact to the underlying Zhongyicun Member is an uneven, possibly paleokarst surface (Fig. 7A), overlain by a whitish, thin-bedded dolostone (0 - 1.8 m), in turn overlain by a thick-bedded dolostone (1.8 – 5 m). Above a 3 m-thick covered interval, thick- and wavy-bedded dolomudstone to wackestone make up the section between 8 and 12 m. In some beds, millimeter-scale rhythmic laminations of alternating white dolomite and grey phosphorite laminae occur; we counted 46 laminas bundled into a bed only about 3 cm thick. The alternating white and grey horizontal lamination is overlain by a very thin, discontinuous phos-intraclast wackestone only about 3 cm thick (Fig. 7B).

The following, approx. 6 m thick interval, is covered. Medium- to thick-bedded, horizontally bedded, wavy and flaser-bedded nodular limestone with interbedded organic rich silty shale occurs from 18 to 32 m. Within this unit, at 26 m, a less nodular, ca. 0.5 m thick limestone contains abundant black phos- intraclasts and small shelly fossils.

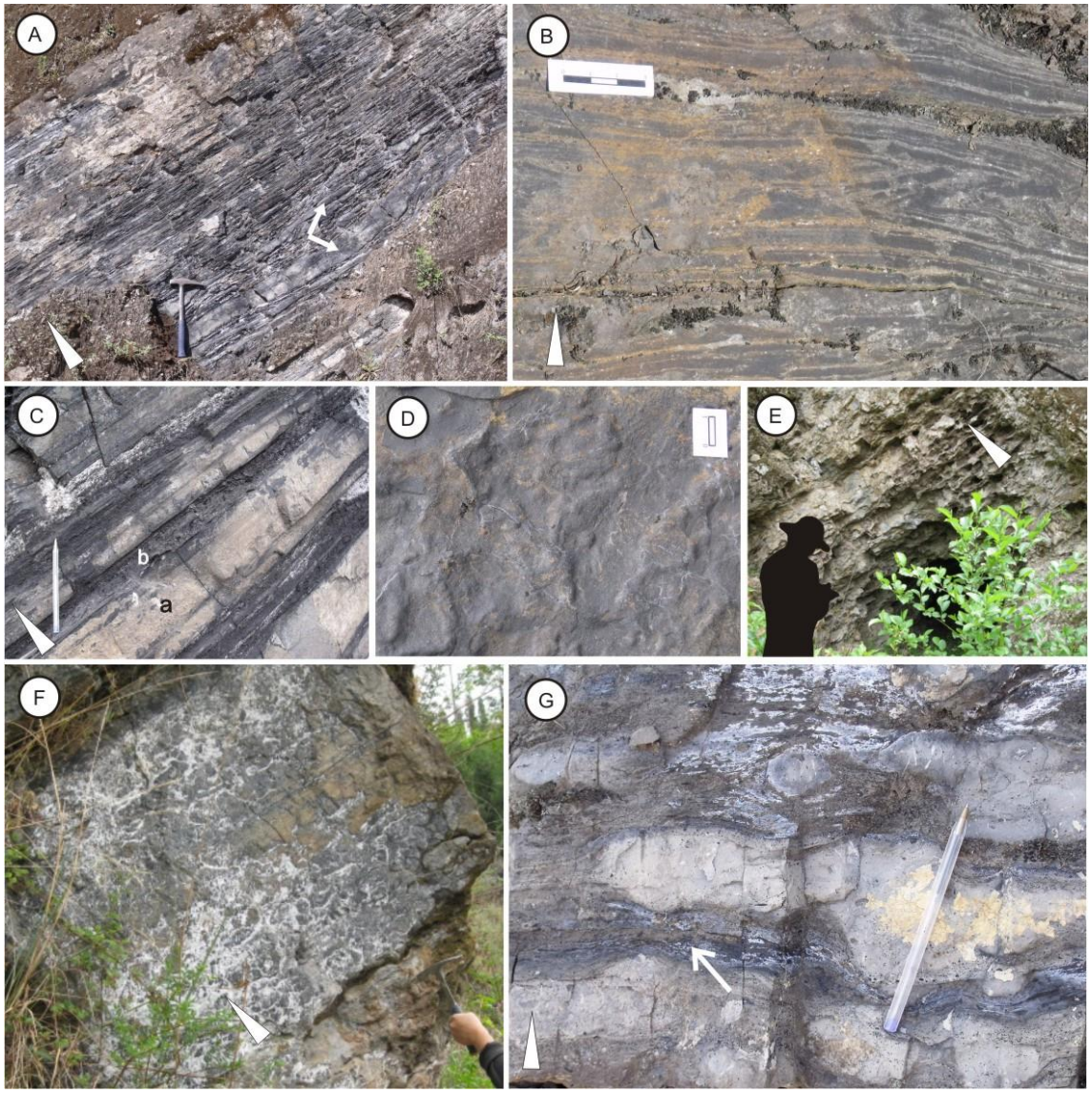

Fig. 6. *Outcrop lithologies and sedimentary structures of the Zhongyicun and Dahai Members at Yulu section. White triangles point to stratigraphic-up direction. A, B) Black shaly siltstone with dolomite lenses in (A) (e.g., white arrows) and slump folds in (B). C) Phosphatic dolostone (a) interbedded with black shaly siltstone (b). D) Moderately bioturbated shaly siltstone. Top-down view; the scale bar is 1cm in length. E) Sandy dolostone of the lower Dahai Member. F) Thick grey dolostone. Several phosphatic firmgrounds form the nodular texture. G) Nodular dolostone in Dahai Member. Note the uneven contact of light-grey, early diagenetic dolomite nodules and surrounding dark-grey, organic-rich calcareous shale (e.g., white arrow).*

3.5.1.4. Meishucun

The Meishucun section is located approx. 2 km southwest of Dianchi Lake in Jining County, approx. 50 km SSW of Kunming, capital of Yunnan Province. Except for some data from the protected former GSSP-candidate section at the margin of the quarry, our stratigraphic profiles were recorded within the adjacent large active phosphate open-pit mine and reaches 14 m in thickness. The base of the profile includes the uppermost (ca. 1 m) beds of the Dengying Formation which are mainly composed of thick-bedded, recrystallized sandy dolostone or calcareous sandstone. Abundant parallel stratification and common herringbone cross-bedding suggest a shallow-marine, likely (sub-) tidal environment. The top of the Dengying Formation is a well exposed, regional, uneven karsted surface with deep, sediment-filled fractures and cavities (Fig. 7C). It is overlain by the Zhongyicun Member of the Zhujiajing Formation, beginning with a prominent, several-m-thick (0-2 m) grey phos-rudstone and granular phosphorite (Fig. 7D) composed of phoslithoclasts, phosphatized ooids, phosphatic aggregate grains, phosphatized small shelly fossils and stromatolite fragments. Interference ripples and bioturbation are common in the granular phosphorite. The middle part of the Zhongyicun Member (2 - 4.5 m) is a pale grey, thinly bedded laminated silty shale containing pyrite, glauconite and phosphatic silt- and sandstone (Fig. 7E). Much of this unit consists of a slightly aquatically reworked and diagenetically altered volcanic tuff with a depositional age of approx. 536 Ma (Jenkins et al., 2002; Compston et al., 2008; Sawaki et al., 2008; Zhu et al., 2009). The upper part of the Zhongyicun Member (4.5 – 11 m) is again composed of thin- to thick-bedded granular phosphorite with interbedded dolomite and two phosrudstones. The granular phosphorite shows numerous scour structures, indicating intensive reworking. The contact of the Zhongyicun Member to the overlying Dahai Member, a grey to yellow, thin- to medium-bedded dolostone that also contains minor quartz and phosphate of silt and sand size, is a surface of distinct lithological change. Fenestral fabrics are common. The top of the Dahai Member is overlain by thin-bedded, black, glauconite-bearing, phosphate–clast- and nodule-bearing silty shale of the Shiyantou Formation.

3.5.1.5. Mingyihe

The Mingyihe section is located ca. 4 km southwest of Mingyihe in an abandoned phosphate mine. Exposed strata consist of the uppermost, only ~20 cm thick dolostone of the Dengying Formation, overlying ~28 m phosphorite and dolostone of the Zhongyicun Member and ~0.1 m white dolostone of the basal Dahai Member.

The Dengying Formation at Mingyihe is composed of yellowish, coarse-sparitic dolostone, containing fine-sand-grained phosphate strings and a few chert nodules. Its top is micro-karsted. The overlying Zhongyicun Member begins with a very thin bed (2-5 cm) of well rounded, poorly sorted phosphate rudstone. The overlying up to 0.4 m of the section consists of thin-bedded shaly siltstone and phosphate. Overlying thick- to medium-bedded units (0.4 – 12 m) consist of horizontally bedded,

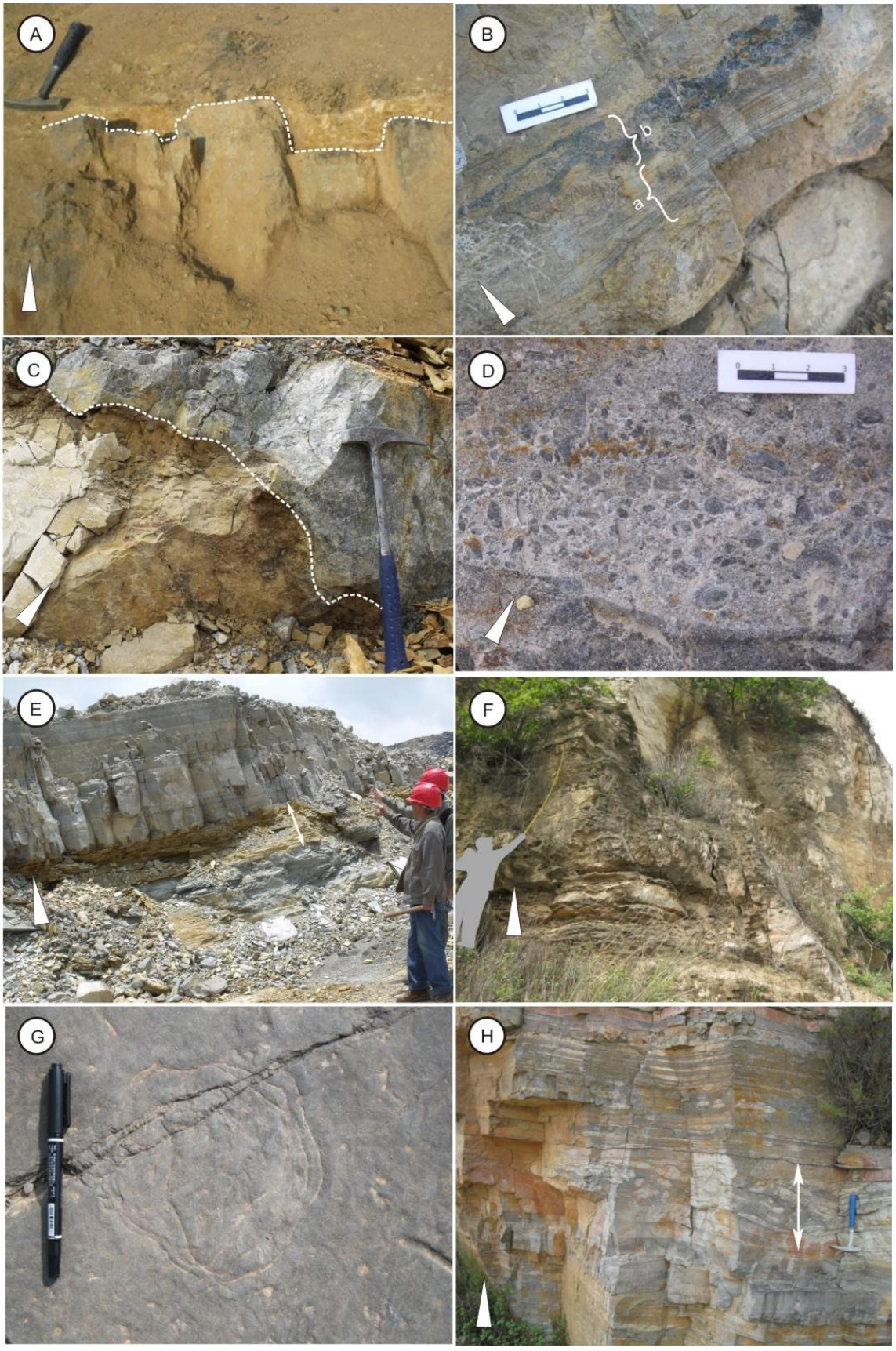

Fig. 7. *Outcrop lithologies and sedimentary textures at Zhujiaqing, Meishucun and Mingyihe sections. A) Uneven contact (dashed line) between phosphorite of the upper Zhongyicun Member and dolostone*

of the basal Dahai Member at Zhujiaqing section. B) Bundles of alternating dolomite and phosphorite laminae (a) overlain by phos-intraclast wackestone (b) in thick-bedded dolostone of Dahai Member at Zhujiaqing section. C) Paleokarst surface (dashed line) between yellowish calcareous sandstone of the Dengying Formation, overlying SSF-bearing grey phosphorite of the Zhujiaqing Formation. D) Granular phosphorite at Meishucun section. E) Silty shale (actually a bentonitic tuff; between arrows) and framing grey planar-bedded phosphorite at Meishucun section. F) Calcareous sandstone at Mingyihe section. G) Horizontal traces, probably shallow-marine ichnofacies Aulichnites *or* Archaeonassa *(Seilacher et al., 2005) on a bedding plane at Mingyihe section. H) Grey phosphorite with whitish-orange dolomite lenses in Mingyihe section. Note convolute bedding in the center.*

intraclast-bearing and bioturbated grey dolomitic phosphorite; SSFs are concentrated in its upper part (7 - 12 m). The middle part of the Zhongyicun Member is composed of a weathered calcareous sandstone (Fig. 7F) (12 – 18 m) showing flaser bedding, crossbedding and herringbone cross-bedding. Grey, thick-bedded phosphorite with white dolomite flasers and thin beds or laminas from 18 to 27.9 m follows up-section. Horizontal bioturbation by annelids on bedding planes is abundant at 18 m (Fig. 7G). A ca. 45 cm-thick phosphorite interbedded with dolomite (19.25-19.7 m) show convolute bedding; the slumping direction is NNE (Fig. 7H). Upsection, the dolomite component increases gradually. The Zhongyicun Member is overlain by medium-bedded, brittle, white dolostone of the Dahai Member of which, however, only the basal 10 cm are well exposed.

3.5.2. Lithofacies assemblages and their lateral distribution

Lithofacies are classified and described based on their sedimentary structures, textures and specific lithological associations. This study goes beyond the compilation of mere lithologies columns but also integrates the sections with published biostratigraphic and chemostratigraphic data. As a result, depositional models proposed here not only correlate lithologic units but time slices and thus provide better information than former studies on paleogeography and basin evolution.

3.5.2.1. Lithofacies assemblages

Thin-bedded dolostone, siltstone, and chert (F1)

Dolostone, chert and siltstone occur in rhythmically thin-interbedded units (Fig. 8A). Generally, dolomite content increases upsection whereas the proportion of siliciclastics decreases. In the grey, fully recrystallized argillaceous dolostones, few very-fine-grained detrital quartz grains and phosclasts occur (Fig. 9A). Wavy, oblique and horizontal laminations commonly exist. The yellowish siltstone consists mainly of quartz. Chert beds are dark grey and show planar bedding.

Lithofacies interpretation

Judging from the wavy and oblique laminations, current or wave energy was low. The lack of features indicative of tidal or wave reworking suggests a low-energy subtidal or deeper environment. The high degree of recrystallization of the dolostone shows a strong diagenetic influence; however, the thin-

bedded nature is likely primary, because bedding planes separating the lithologies are strictly parallel and do not form concretions or lozenges; if so, laminations may be controlled by environmental or climatic fluctuations (Tucker, 2003; Salad Hersi, et al., 2015).

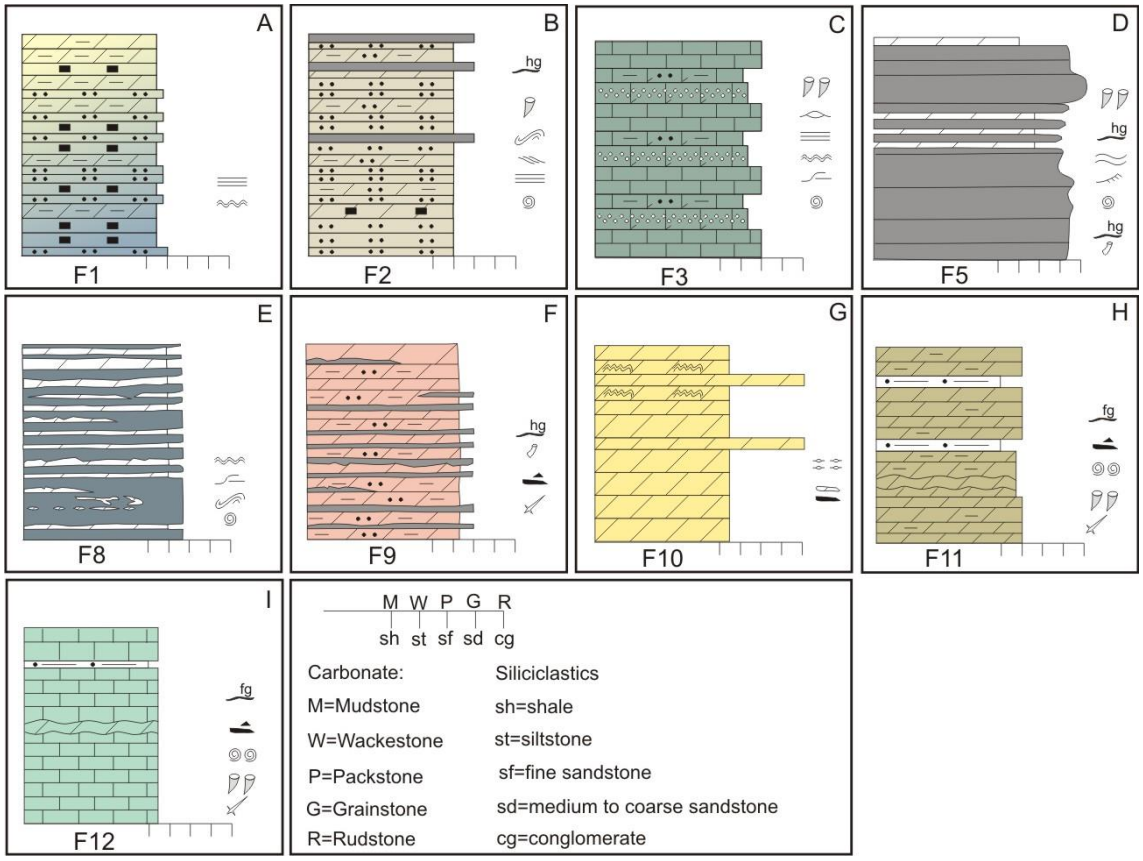

Fig. 8. *Logs of recognized lithofacies associations in the studied sections of the Zhujiaqing Formation. See Figure 3 for a more detailed legend.*

Thin-bedded siltstone interbedded with thin phosphorite and dolostone (F2)

In the northern sections (Laolin, Zhujiaqing and Yulu), thin-bedded grey to dark grey siltstone interbedded with a few thin dolomitic phosphorite and dolostone beds is widespread in the Zhongyicun Member (Figs. 8B, 6B). The proportion of siltstone, phosphorite and dolostone varies among sections, but phosphorite content generally increases up-section. The grain composition in the siltstone beds is of high textural and mineralogical maturity. Well-sorted quartz silt is common whereas mica, phos-peloids and organic material are subordinate. The siltstone cement is calcareous, phosphoritic, siliceous or argillaceous. Bioturbation appears widespread in the calcareous siltstone, but its intensity is insufficient

to erase the original lamination. Dolomitic phosphorite beds are 5 to 10 cm thick and consist of bedding-parallel, elongate channel fills and lenses of phosclast rudstone, phosclasts lack features indicative of

corrosion or amalgamation (Fig. 9B). The rudstone is embedded in faintly laminated sandstone and siltstone which consist dominantly of quartz, phos-peloids and dolomite.

Lithofacies interpretation

This lithofacies indicates a variable energy setting well above wave base with abundant detrital supply. This is supported by the abundant presence of the sand to silt-sized detritus, the wide development of small oblique lamination in siltstone and the phosclast rudstone lenses in the phosphorite beds. The poorly sorted phosclast rudstone in the thin phosphorite beds likely represents occasional and short-term high-energy deposition from storm or strong subtidal currents. Such type of event concentration of granular phosphorite was documented, e.g., in the mid-Permian Phosphoria Formation (Trappe, 1998).

Horizontally bedded limestone (F3)

Horizontally bedded limestone is organized in repetitive units which grade from thick- to thin-bedded (Fig. 8C). In the thin beds, heterolithic facies are represented by very thin (0.5 to 2 cm thick) grey packstone interlaminated with dark brownish argillaceous dolomitic wackestone (Fig. 4C). Bioturbation is not intense in this lithofacies so that the original lamination is largely preserved. Grain types in the packstone include well-rounded, fine-grained phoslithoclasts, cortoids, dolostone clasts, reworked dolomite crystals and carbon-rich opaque clasts (Fig. 9C). The dominant facies in thick beds is homogenous packstone of the same grain composition as in thin beds. Meniscus cementation occurs in some thick beds (Fig. 9D).

Lithofacies interpretation

The fine-grained, heterolithic wackestone to packstone in the thin beds indicates variable current velocity, which is common in tidal environments (Tucker and Wright, 1990; Gomez and Astini, 2015). Good sorting and homogenous texture of the allochems in the thick packstone bed indicate accumulation in moderately agitated water, possibly in current-washed sand shoals. The lack of evidence for exposure or bird's-eye structures rules out an intertidal depositional setting. The thin beds may represent a low-energy restricted back shoal setting, in which silt settling out of suspension during low-energy conditions episodically alternated with reworked packstone derived from the peripheral sand shoals. The common occurrence of cortoids also indicates a restricted environment (Flügel, 2004).

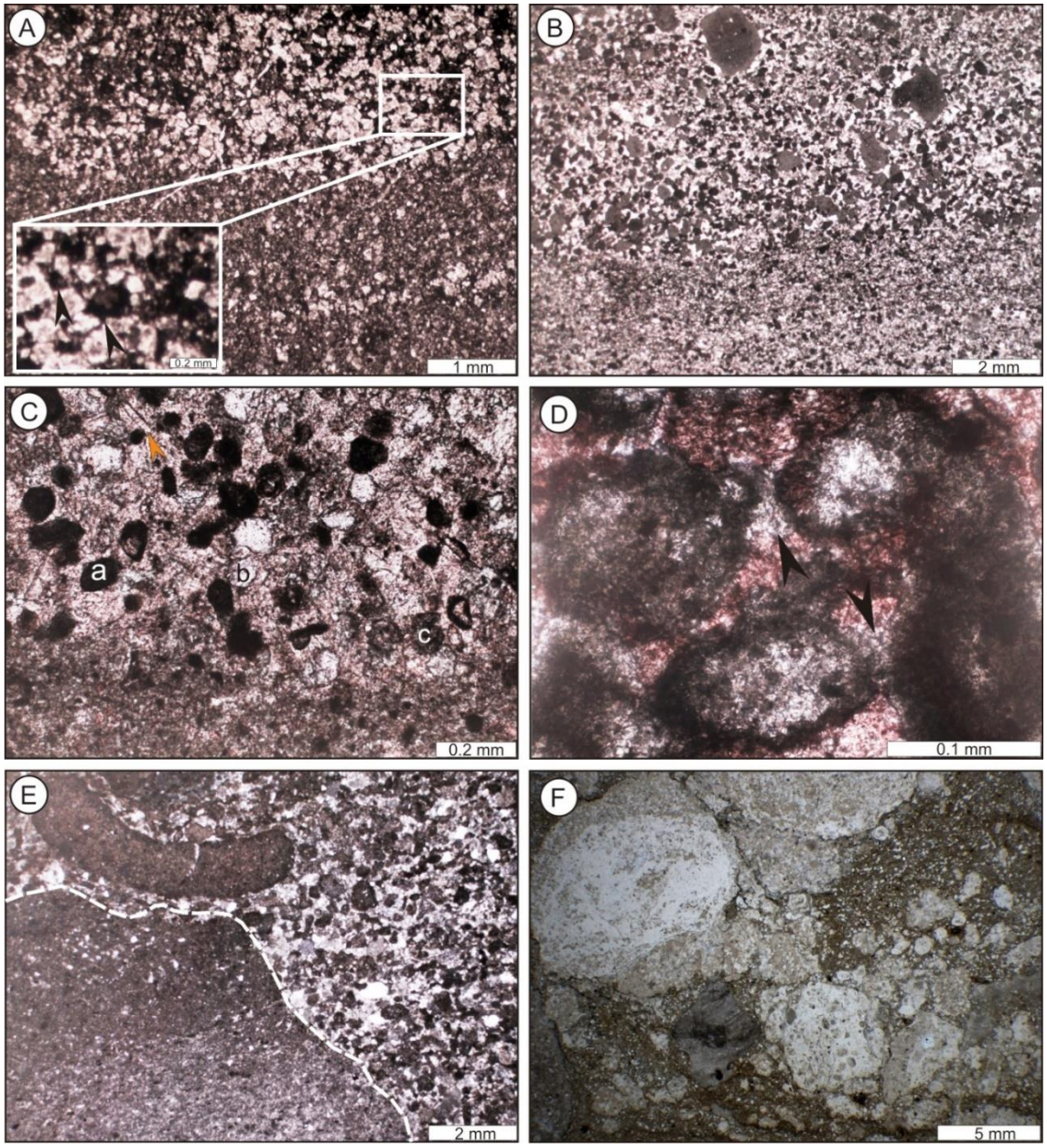

Fig. 9. *Thin-section photomicrographs of representative microfacies of Lithofacies F1 to F4. A) Argillaceous dolostone in F1. The vertical increase of dolomite crystal size may indicate an original texture change from mudstone to packstone. Note the fine-grained phosclasts (arrows) in the packstone lamina. The opaque rims around phosclasts consist of carbon-rich matter (sample 11-275 from Laolin section). B) Dolomitic phosclast rudstone in F2. Phosclasts (black) consists of phosphatic mudstone (sample 11-267 from Laolin section). C) Packstone in the thin beds of F3. Calcite appears red due to Alizarin Red staining. Framework grains include carbon-rich opaque clasts (e.g., a), phoslithoclasts (e.g., b), dolostone (e.g., c) and cortoids (e.g., arrow) (sample lal 42 from Laolin section). D) Packstone in the thick beds of F3. Calcite appears reddish due to staining. Meniscus cement occurs at grain contacts (e.g., arrows) (sample lal53 from Laolin section). E) Phosclast conglomerate of F4 overlying a micro-karsted surface (white dashed line) (sample An1 from Mingyihe section). F) Phosclast conglomerate of F4. The matrix consists of quartzose silt and dolomite silt (sample 2012-4 from Meishucun section).*

Phosclast conglomerate (F4)

Phosclast conglomerate overlies karsted surfaces or other stratigraphic discontinuities at Meishucun and Mingyihe sections (Figs. 5, 7C). The lateral extent of this lithofacies is highly discontinuous, occasionally limited only to a few meters. The conglomerate thickness does not exceed a few to tens of centimeters. Various sub-angular to rounded phosclasts cover a composite grain spectrum. The groundmass mainly consists of dololutite and quartz sand or silt (Figs. 9E, 9F).

Lithofacies interpretation

This lithofacies likely relates to an upper intertidal to supratidal environment. Phosclasts were eroded from underlying strata and then concentrated by reworking. Similar lithofacies occur on top of the Middle Cambrian Thorntonia limestone in northeast Georgina Basin, Australia (Southgate, 1988) where they also overlie a disconformity in an emergent environment.

Phosclastic-, bioclastic- and oolithic granular phosphorite with interbedded dolomite (F5)

Widespread phosclast, bioclast and oolithic granular phosphorite with interbedded dolomite (Fig. 8D) predominantes in the lower Zhongyicun Member of southern sections (Meishucun and Mingyihe) and the upper Zhongyicun Member of the northern sections. Sedimentary structures include planar and oblique bedding (Figs. 4D, 7E). In the southern sections, the phosphorite is mainly thick-bedded; in the northern sections, dominantly thin-bedded. Variable grain types include phosphatic superficial and compound ooids, phosphatic oncolites, phosphatic shell fragments, phoslithoclasts and a few interspersed quartz and dolomite clasts. Phosphatic SSFs always occur in shell concentrated beds (Fig. 10A). Phosphatic coated grains predominate in the southern sections, where phosphatized microbial mats and stromatolites are observed (Fig. 10B). In contrast, the northern sections display a higher proportion of phoslithoclasts. The cement of the phosphorite consists of dolospar and crystalline apatite. The variable cement mineralogy is likely due to micro-geochemical conditions in the soft sediment, in turn in part a function of basin paleobathymetry, and the complex diagenetic history of the phosphorite deposition.

Lithofacies interpretation

This lithofacies occurs widely in the study area. Sedimentary structures suggest variable energy caused by tides, waves, currents or minor water level changes. The common microbial mats in the southern sections might have provided a favorable microenvironment for phosphogenesis as in the case of the Ediacaran Doushantuo phosphorite (She et al., 2013) and formed thick stratiform economic phosphate deposits. In the northern sections, grains are mainly reworked and concentrated. Consequently, we interpret the depositional environment of this lithofacies as inter- to shallow subtidal, consistent with adjacent facies types.

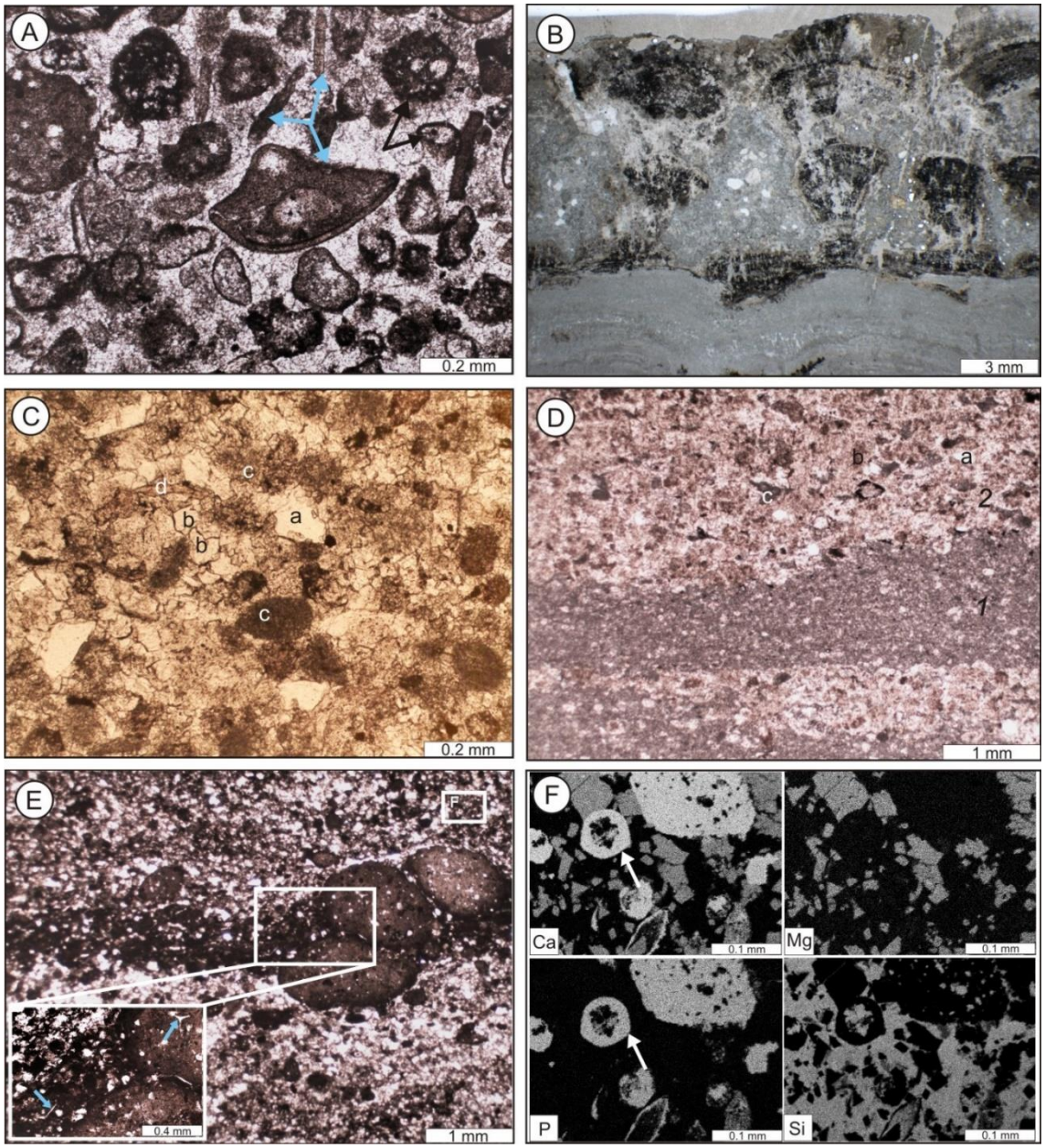

Fig. 10. *Thin-section photomicrographs of representative microfacies of Lithofacies F5 to F9. A) Bioclast-rich phosphorite of F5. Small shelly fossils show higher and lower degrees of phosphatization (e.g., blue arrows). The doloclasts are marginally microbored and filled by dark carbon-rich material (e.g., black arrows). The rock is cemented by dolospar (sample 11-262 from Laolin section). B) Phosphatic stromatolite in F5 (sample 11-721 from Meishucun section). C) Dolarenite of F7. Grains include fine-grained quartz (e.g., a), doloclasts (e.g., c) and phosclasts (e.g., d). Note the recrystallization of the rock and the neomorphic dolospars (e.g., b) (sample 11-135 from Meishucun section). D) Laminated phos-peloidal sandstone (2) and dololutite (1) of F8. The sandstone consists of very fine-grained quartz (a), phos-peloids (b) and minor doloclasts (c). Note the slightly erosive contact at the base of sandstone lamina. (sample An 10 from Mingyihe section). E) Phos-intraclast floatstone in F9. Sponge spicules distributed in the matrix and phos-intraclasts (e.g., arrows). The matrix is dolomitized and phosphatized. Rectangle at upper right indicates the area shown in Fig. F (sample 11-259 from Laolin section). F) SEM-backscattered electron (BSE) element maps of Ca, Mg, P and Si in*

the matrix of a phos-intraclast floatstone showing a phosphate concretion (arrow) grown around a siliceous nucleus.

Grey shale (F6)

A local distinct lithofacies in the Meishucun section is here named grey shale. The rock consist of flaky laminated argillaceous shale containing abundant silt- or sand-sized glauconite, phosphorite, barite and pyrite grains. Its color is pale grey at fresh outcrops and yellowish where weathered (Fig. 7E).

Lithofacies interpretation

Due to its limited distribution and the very fine grain size, this lithofacies may have been deposited in a restricted shallow subtidal environment. Siegmund (1995) interpreted much of this lithofacies as having been derived, at least in part, from reworked volcanic tuffs based on the presence of volcanic minerals and textural evidence suggesting diagenesis of volcanic glass.

Quartz-rich dolarenite (F7)

The quartz-rich dolarenite lithofacies shows bimodal cross bedding, wavy bedding and flaser bedding (Fig. 7F). The dolarenite is typically recrystallized to a coarse interlocking fabric (Fig. 10C). Well rounded, fine- to medium-grained quartz is unevenly distributed.

Lithofacies interpretation

The sedimentary structures indicate a well-agitated shallow-water environment, such as a tidal sand flat environment. Quartz grains are plausibly derived from coastal dune belts and transported by offshore-directed wind or tidal currents onto the tidal sand flat.

Flaser-bedded or laminated, phos-peloidal sandstone and dololutite (F8)

Flaser-bedded or laminated, phos-peloidal sandstone and dololutite (Fig. 8E) are widely developed in the upper Zhongyicun Member of the Mingyihe section. Convolute bedding occasionally occurs (Fig. 7H). The sandstone alternates with offwhite, recrystallized laminated dololutite (Fig. 10D). The bases of the dark grey sandstone beds are slightly erosive. The grains are densely packed and mainly consist of very-fine-grained phos-peloids. The thickness of individual dololutite lamina is commonly ~ 0.1-5 mm although some reach up to 10 mm. Infaunal activity is indicated by *Cordia* and *Aulichinites*-like trace fossils, both of which indicate a shallow-water oxygenized sea floor.

Lithofacies interpretation

Features in this lithofacies point to an intertidal environment. Tidal influence is indicated by the rhythmical alternation of laminated fine-grained phos-peloidal sandstone with offwhite dolostone.

Microbial activity on intertidal flats readily traps air and liquids, thus easily forming convolute bedding. Horizontal traces may have formed during slack-water periods in small and shallow tidal pools.

Dolomitic phos-intraclast floatstone and phosphate pavement (F9)

Dolomitic phos-intraclast floatstone is organized in medium- to thick-bedded, horizontally stratified beds (Fig. 8F), which show abundant micro-scours and phosphatic pebble strings (Fig. 4G). Abundant siliceous sponge spicules also occur in this lithofacies. Phosphatic pebbles range from 1 mm to 5 mm in diameter and are embedded in a silt- to sand-sized carbonate and quartz matrix (Fig. 10E) with phosphorite micro-concretions (Fig. 10F). Where the concretions are stratiform and grow large, they coalesce to form dark phosphatized beds or phosphatic pavements 1 to 3 cm thick.

Lithofacies interpretation

The depositional environment of this lithofacies is likely shallow-subtidal. The numerous phosphatic pavements and erosional features suggest favorable conditions for phosphatization, including low net sedimentation rate, and a high degree of reworking. Storms or highly variable tidal currents may be responsible for the poor sorting, the lack of orientation of reworked phosintraclasts and the lack of tidal structures. The original silty, quartzose and fine-grained calcareous groundmass was dolomitized. A similar in-situ phosphate precipitation in a middle Cambrian shallow submergent marine environment was described by Southgate (1986).

Crystalline dolostone (F10)

In the crystalline dolostone lithofacies, light grey to whitish-yellowish coarse-grained (sucrose) dolostone alternates with whitish, microbially laminated dolostone (Figs. 4H, 8G). The microbial laminae are preferentially silicified and outline hemispheroids formed by stromatolitic cyanobacteria. Interbedded flat-pebble conglomerate beds are commonly only a few centimeter thick and composed of microbial dolostone or phosphatic intraclasts (Figs. 7B, 11A). In-situ breccia and fenestral porosity also occur.

Lithofacie Interpretation

This lithofacies likely represents m-scale shallowing-upward, peritidal cycles. Microbial laminae probably developed within a lower-intertidal algal marsh; the grey coarse-grained sucrose dolomite may represent a saline, lower intertidal to shallow subtidal environment with a minor to moderate evaporitic component, responsible for the formation of the collapse breccia. Dolomitization likely occurred during early diagenesis in the shallow subsurface.

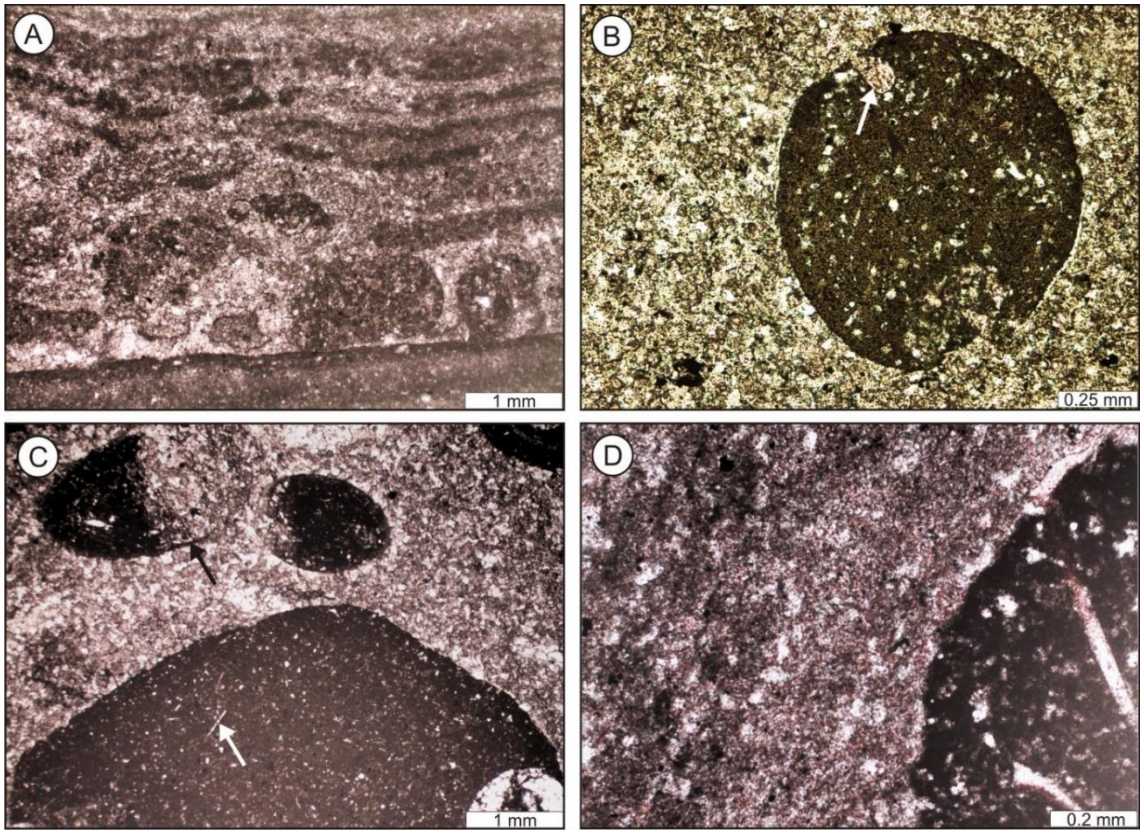

Fig. 11. *Thin-section photomicrographs of representative microfacies of lithofacies F10 to F12. A) Conglomerate composed of flat-pebble microbial dolostone of F10 (sample 11-255 from Laolin section). B) Phosphatized small shelly fossil of F11. The mud infill of the shell was also phosphatized, then bored (arrow) and the cavity subsequently filled by carbonate mud which was later dolomitized (sample 11-201 from Yulu section). C) Phosintraclast and phosphatized small shelly fossils of F11. Phosintraclast (lower part) shows the same composition as the fossil infill. Abundant sponge spicules exist in the phosphatized mud (e.g., white arrow). Phosphatized small shelly fossils were later affected by dolomitization (e.g., black arrow) (sample 11-244 from Laolin section). D) Partly dolomitized sparitic limestone, a common microfacies of F12. Sparitic calcite is stained red while dolomite remains colorless. The black grain to the right is a phosphatized small shelly fossil (sample lal12 from Laolin section).*

Argillaceous, fine- to medium-crystalline dolostone interbedded with calcareous shale (F11)

The argillaceous dolostone is medium- to thin-bedded (Figs. 4K, 8H) and contains minor (<10%) proportions of phosphatic small shelly fossils and angular phosintraclasts (Figs. 11B, C). Bioturbation is prevalent and may explain the random distribution and orientation of phosclasts and phosphatic fossils. Black phosphatic hardgrounds occur in thick- to medium-bedded dolostone, but their lateral continuity does not exceed a few decimeters. The interstratified calcareous shale shows foliations (Fig. 6G).

Lithofacies interpretation

The depositional environment of this lithofacies may have been a sheltered low-energy subtidal setting. This is supported by the mud-dominated texture of the argillaceous dolostone. The low proportion of clastic grains and the high degree of bioturbation indicate slow rates of sedimentation. The phosphatic small shelly fossils appear redeposited. They may have experienced little transportation because many SSFs occur in the dolostone with phosintraclasts and near firmgrounds. These initial stages of hardground formation can be easily reworked as cohesive intraclasts. Also, because phosphatization of shelly fragments requires long exposure to or near the sediment-water interface, a low sedimentation rate is called for.

Argillaceous micro-crystalline limestone interbedded with calcareous shale (F12)

This lithofacies is organized in medium- to thin-bedded, wavy to slightly nodular beds (Fig. 8I). It grades vertically from Facies F11. The limestone consists of microspar (Fig. 11D), phosphatic small shelly fossils and angular phos-intraclasts. Phosphatized small shelly fossils are mainly 0.5 to 3 mm in length, occur in clusters and are partly replaced by dolomite crystals. Bioturbation is abundant.

Lithofaces interpretation

Sedimentary textures and main grain components are identical to F11, but the terrestrial input is reduced. The depositional environment may have been shallow subtidal. A comparable facies was outlined by Brasier et al. (1979) as "shelly limestone facies", the product of low sedimentation rate and many phases of re-deposition and diagenetic alteration.

3.5.2.2. Lithofacies distribution in eastern Yunnan

Fig. 12 shows the lithofacies distribution of the Zhujiaqing Formation across the southwest Yangtze platform, including information from sections studied by Yang et al. (2014), Li et al. (2009), Zhu et al. (2001), He et al. (1989), Ge et al. (1989), Lei (1986), and Luo et al. (1982). The twelve lithofacies described above collectively record depositional environments that range from peritidal to shallow subtidal.

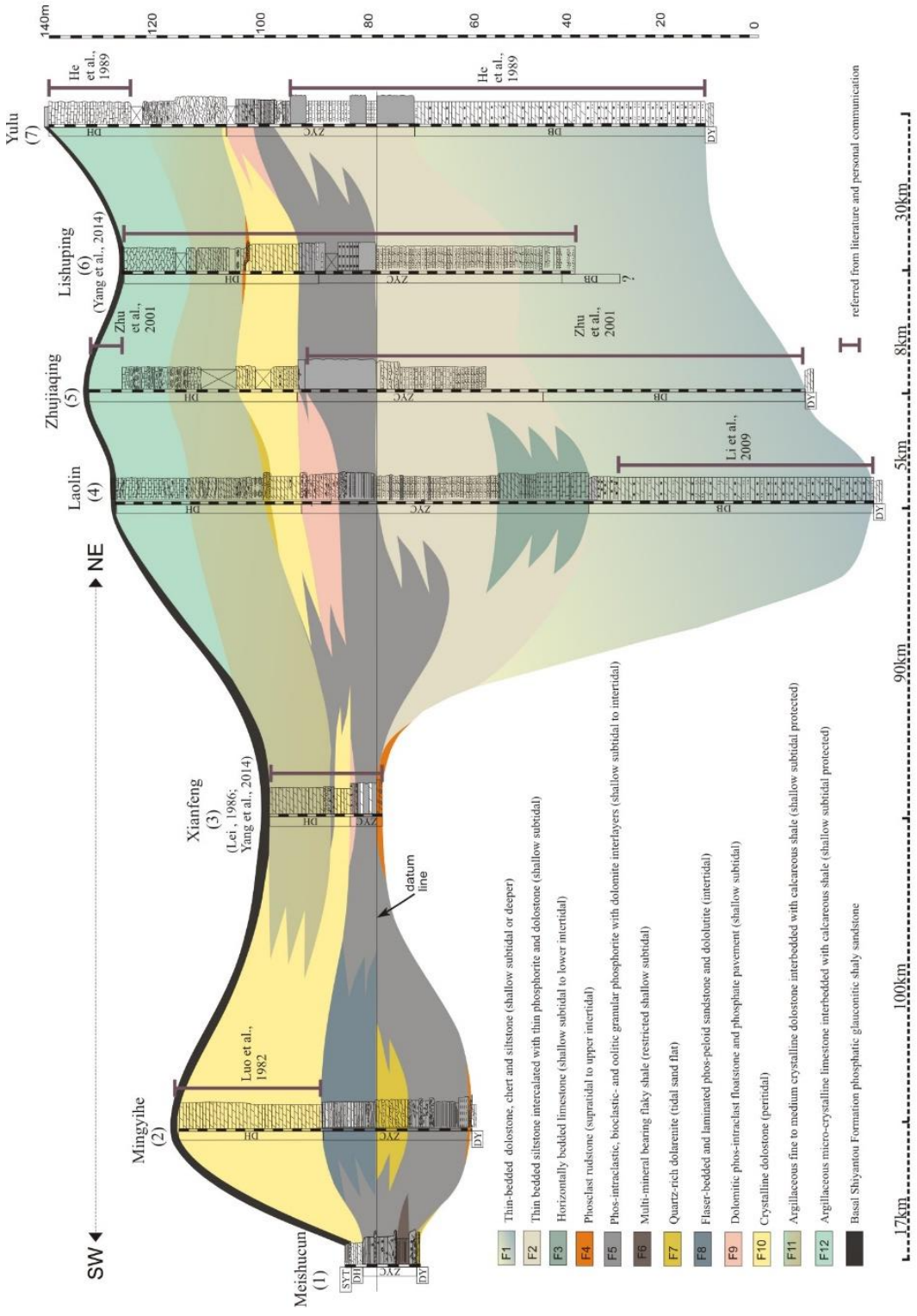

Fig. 12. *Lithofacies distribution of the Zhujiaqing Formation in Yunnan. See Fig. 1C for locations of each section.*

In the northern area, a major unconformity includes an abrupt lithofacies change above the crystalline dolostone of Dengying Formation; the correlative surface in the Meishucun and Mingyihe sections is karsted. Subtidal thin-bedded dolostone, chert and siltstone (F1) followed by thin-bedded siltstone

interbedded with thin phosphorite and dolostone (F2) were subsequently deposited in Laolin, Zhujiaqing, Lishuping and Yulu areas.

F1 and F2 of Yulu section may have been deposited from relatively deeper environments compared to the Laolin section because of the higher proportion of interbedded silty shale in F2. In the Laolin section, horizontally bedded subtidal limestone (F3) forms a local facies. The termination of F2 towards Xianfeng section (Yang et al., 2014) is inferred to intersect with phos-intraclastic, bioclastic and oolithic phosphorite (F5) because phosphorites reach their greatest thickness between Laolin and Xianfeng in the Zhongyicun Member (Fig. 1B) while in the Xianfeng section, only 1m conglomeratic dolostone was deposited during the same time period (Yang et al., 2014). This lithology can be attributed to phosclast conglomerate (F4). Further south, in the Mingyihe and Meishucun sections, F5 represents the main lithofacies. Above the stratigraphic datum (the top of SSF Zone I), major phosphorite (F5) was deposited across the entire area. In the Mingyihe section, this lithofacies grades into intertidal flaser-bedded or laminated phos-peloidal sandstone and dololutite (F8). In the Yulu section, F5 changes to F2, but still contains two phosphorite beds. Shallow subtidal dolomitic phos-intraclast floatstone and phosphate pavement (F9) was deposited above F5 in the Laolin section but ended laterally near the Zhujiaqing section (Qian et al., 1996; Zhu et al., 2001). A 1m thick phosphatic dolostone interval in Xianfeng below the Dahai Member is reported to include abundant phosphatic hardgrounds, ooids and oncoids (Lei, 1986; Yang et al., 2014), and can thus attributed to lithofacies F9. Whitish to light grey coarse crystalline dolostone (F10) occur in all sections. This lithofacies represents a peritidal environment with very little terrestrial input and the least phosphorus content among all lithofacies. F10 reaches 8 to 10 m thickness in the Laolin, Zhujiaqing and Lishuping sections but only about 1 meter in the Yulu section and approx. 3 m in the Xianfeng section. Our field data of the Dahai Member of the Mingyihe section is limited due to poor exposure but the nearby Baideng section, about 5 km northwest of the Mingyihe section, shows identical lithologies in the Zhongyicun Member (Luo et al., 1982), so we infer the same lithologies in the Dahai Member as well (Fig. 12). In the Baideng section, the Dahai member is represented by 30 m thick dolostone, the lower 17.5 m-thick dolostone is composed of thick bedded, whitish fine-crystalline dolostone with wavy laminations and bird-eyes structure, as well as thin chert interlayers. The upper 15.5 m of Dahai Mb. is light grey thick-bedded coarse-crystalline dolostone without any small shelly fossils detected. This 30 m thick dolostone can be summarized as F10 because of its relatively pure dolomite composition and a peritidal depositional environment. The thickness of F10 between the Mingyihe and the Meishucun section decreases from 30 to 3 m which may either be due to non-deposition, facies change or uplift and erosion. In sections further south, such as in Chengjiang (Fig. 1C), its thickness further decreases to only 20 cm (Sato et al., 2014). Overlying F10 in the northern sections, argillaceous fine- to medium-crystalline dolostone interbedded with calcareous shale (F11) and here assigned to a subtidal facies occurs widely from the Yulu to the Xianfeng section. These facies grade stratigraphically upward into argillaceous, micro-crystalline

limestone interbedded with calcareous shale (F12). These two lithofacies, however, are absent in the Mingyihe and Meishucun sections which maybe due to non-deposition or facies change.

3.6. Discussion

Fig. 13 illustrates a process-oriented depositional history of the Zhujiaqing Formation. Dominant carbonate strata representing multiple lithofacies accumulated under shallow-marine to peritidal conditions over an unevenly subsiding early Cambrian shelf which was concurrently infilled by sediment.

The non-uniform thickness and rapid lateral facies change within SSFs of Zone I suggest a pronounced paleobathymetric relief which may have been enhanced by differential subsidence. As a transgression flooded the area, the northeastern part of the study area became dominated by low-energy subtidal, thin-bedded chert, siltstone and dolostone (F1). The coastal environments may have been rich in phosphorus; thus, various types of phosphate grains (F5) accumulated under low sedimentation rates in extensive shallow-subtidal to intertidal environments in the areas to the southwest, whereas in the northeast, the increased terrestrial input allowed deposition of shallow-subtidal siltstone (F2) (Fig. 13B). Thin phosphate beds in F2 may indicate a temporary relative shallowing of the shelf, resulting in increased sediment bypass and winnowing. Limestone (F3) locally developed. Even though the ecological potential for bioturbation is high in lithofacies F1, F2 and F3, these facies show abundant lamination because (especially vertical) metazoan mobility was not well-developed yet. The abundant carbonaceous material, especially in F1, testifies to an organic-rich environment.

After Time 1, the northeastern part of the study area accumulated intertidal to subtidal thin-bedded granular phosphorite (F5). In the Zhujiaqing section, based on the common uneven bedding contacts and the abrupt lithofacies change, karstification may have occurred (Fig. 5); if so, however, it left no record such as karst breccias or other diagnostic features. At the same time, a transitional subtidal lithofacies (F9) overlies the lower lithofacies F5 at the Laolin section. Hardgrounds are common in F9 and F5, implying a low sedimentation rate or a water chemistry that facilitated rapid sea floor lithification and increased bioturbation. Subsequently, the widespread deposition of peritidal dolostone (F10) marks the transition of the basin from a siliceous and phosphatic, sand-dominated shallow-subtidal environment to a muddy, peritidal carbonate platform. However, local high-energy environments developed around Time 2, indicated by medium-bedded dolostone (F7) at Laolin and phosclast conglomerate (F4) at Lishuping. Fig. 13C shows the variable lithofacies distribution at Time 2.

After Time 2, a rise of relative sea level inundated most of eastern Yunnan. In the northeast, mud-dominated argillaceous carbonate interbedded with calcareous shale (F11 and F12) indicate vast-

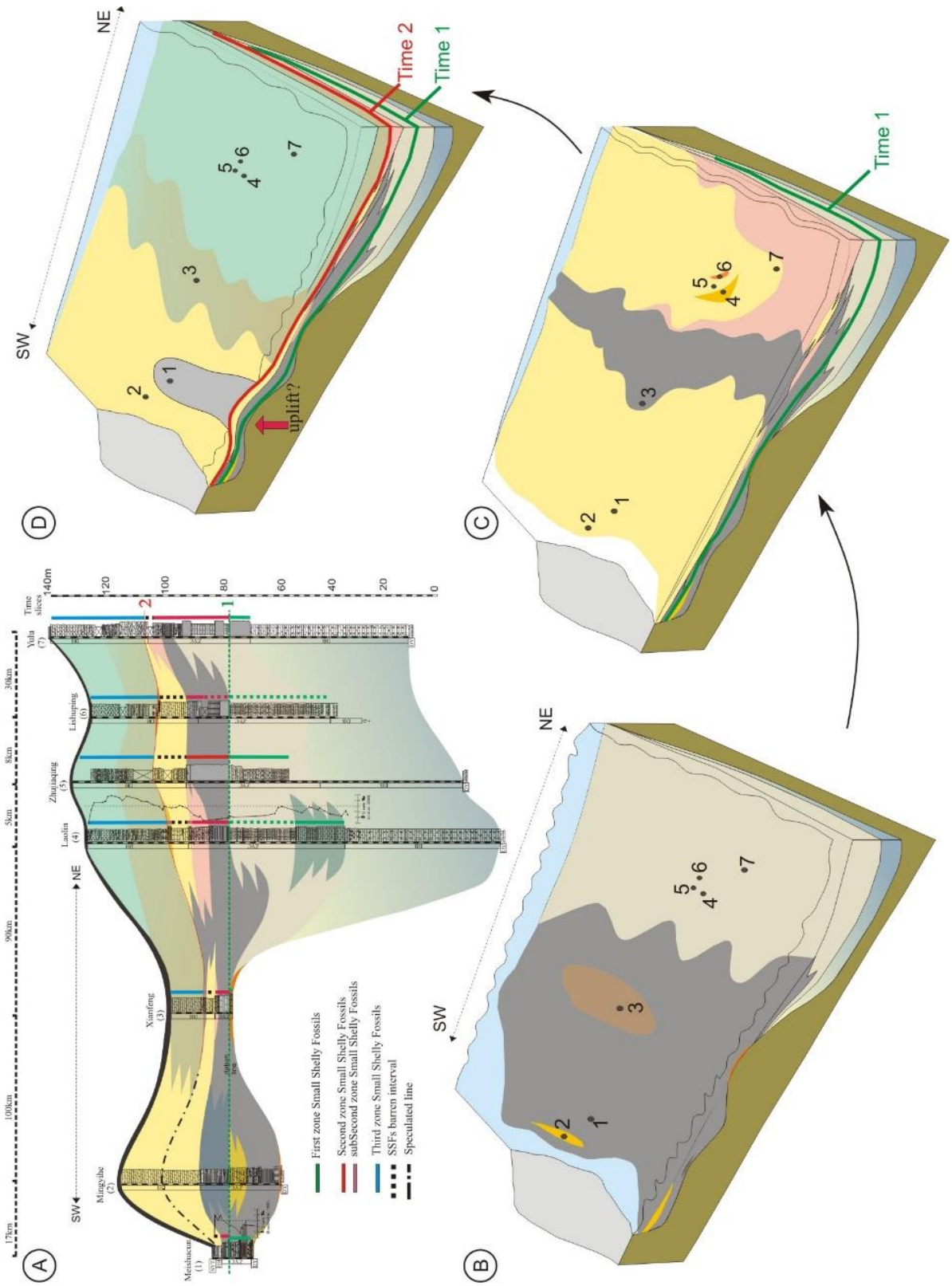

Fig. 13. *Depositional models of the Zhujiaqing Formation. A). Combination of lithofacies distribution, biostratigraphy and chemostratigraphy of Zhujiaqing Formation.* $\delta^{13}C_{carb}$ *data of Meishucun after Brasier et al., 1990;* $\delta^{13}C_{carb}$ *data of Laolin after Li et al., 2009; Biozone data of Meishucun, Laolin and Lishuping after Yang et al., 2014; Biozones data of Zhujiaqing after Qian et al., 1996; Biozone data of Yulu after Qian et al., 1999. B). Siliceous - phosphatic sand-dominated subtidal environment at Time*

1. C) Phosphatic-dolomitic mud-dominated peritidal environment at Time 2. D) Dolomitic-calcareous mud-dominated subtidal environment by the end of Time 2, prior to deposition of the Shiyantou Formation.

protected shallow subtidal environments. Lithofacies towards the southwest changed to subtidal argillaceous dolostone (F11) in Xianfeng and peritidal crystalline dolostone (F10) in Mingyihe and Meishucun which may indicate a shallower bathymetry and probably reduced protection from wave energy (Fig. 13D). The absence of evaporites in peritidal crystalline dolostone, however, excludes hypersaline settings. In the argillaceous dolostone of Xianfeng section, thin beds of phosphatic siltstone (Lei et al., 1986) show that local phosphorus-rich environments persisted locally and temporally.

By the end of Time 2, transgression had led to the deposition of black silty mud and sand all over the Yangtze platform, including eastern Yunnan, although this deposition did not entirely occur at the same time. At the investigated sections, the basal 10 to 30 cm of this silty mud and sand unit all show glauconitic and phosphorite sandstone or conglomerate, suggesting increased reworking, possibly associated with tectonic uplift or sea level regression. Lastly, the platform developed into a shallow siliciclastic shelf.

Perhaps surprisingly, depth of deposition of the Zhujiaqing sediments, mainly a shallow subtidal to peritial setting, did not change much despite of highly variable thicknesses. The environment thus appears to be controlled by differential subsidence. Although the timing of the rift-to-post-rift transition of the Kangdian rift basin (Wang and Li, 2003) is unresolved, Ediacaran strata (635-542 Ma) are believed to have been deposited in a passive-continental-margin setting during the post-rift period (Jiang et al., 2003), causing the highly variable thickness of the Dengying Formation. Our study shows that post-rift subsidence continued to control lithofacies distribution in the early Cambrian Zhujiaqing Formation which may have continued in the overlying siltstones of the Shiyantou Formation whose thickness ranges from 50 to 200 m in eastern Yunnan. The relatively constant shallow water depth and reduced terrestrial input during the deposition of the earliest Cambrian Zhujiaqing Formation thus provided a rather stable setting for the onset of the metazoan bioradiation.

Even though water depth remained relatively constant and the sedimentological settings ranged between shallow continental shelf and platform during the deposition of the Zhujiaqing Formation, water chemistry evidently changed dramatically during this time, greatly affecting sediment composition. We speculate that SSFs evolution may reflect adaptation to these environmental variations.

During the Pc-C interval, there is clear evidence for at least one widespread transgression although the synchroneity and evidence for any single continent-wide transgression is only documented by a coarse framework, largely due to limited geochronological resolution. On the Yangtze platform, the earliest Cambrian interval is represented by the phosphorite- and carbonate- dominated Zhujiaqing Formation in Yunnan, the dolostone-dominated upper Maidiping Formation in western Sichuan, the black shale-

dominated Niutitang Formation in eastern Guizhou and the shaly-limestone-and-black-shale-dominated Yanjiahe Formation in the Yangtze Gorges area. Even though the detailed synchroneity of these formations is far from clear, they all developed on top of the karsted Dengying Formation in the pre-trilobitic Cambrian and thus include one or several transgressions.

3.7. Conclusions

The basal Cambrian (Terreneuvian) Zhujiaqing Fm. of eastern Yunnan, especially in northeastern Yunnan, records numerous vertical and lateral facies changes in shallow subtidal to intertidal settings under variable but generally low sedimentation rates. Lithofacies vary within a siliceous-phosphate subtidal, dolomite peritidal, and carbonate subtidal triangle. Brief subaerial exposure likely occurred in places, but these are mostly local and below regional stratigraphic resolution. Such relatively stable shallow-water environments likely provided near-optimal physical conditions for metazoan evolution but the three lithologic end members identified through regional facies analysis reflect concomitant significant changes in water chemistry and reduced ecological stability. If such relative sedimentary stability during the earliest Cambrian were combined in key locations worldwide with highly variable water chemistry, as demonstrated for the southern Yangtze platform, metazoan and small shelly fossil evolution would have been affected by the necessity to rapidly develop adaptive strategies.

3.8. Acknowledgements

This work was funded by the German Research Foundation (DFG Research Group FOR 736 "*The Precambrian-Cambrian Biosphere (R)evolution: Insights from Chinese Microcontinents*") and by a China Scholarship Council (CSC) scholarship to the first author. We are grateful to Zhang Shishan and Fangchen Zhao for assistance during fieldwork, Anna Giribaldi (FU Berlin) for the help in thin section preparations, Jan Evers (FU Berlin) for technical assistance in using the Scanning Electron Microscope, and all members of FOR 736 for scientific discussions. XS also gratefully acknowledges financial support by a DAAD-Abschlussstipendium.

3.9. References

Brasier, M.D. & Hewitt, R.A. 1979. Environmental setting of fossiliferous rocks from the uppermost Proterozoic- Lower Cambrian of central England. *Palaeogeography, Palaeoclimatology, Palaeoecology* 27, 35-57.

Cremonese, L., Shields-Zhou, G., Struck, U., Ling, H.F., Och, L., Chen, X. & Li, D., 2013. Marine biogeochemical cycling during the early Cambrian constrained by a nitrogen and organic carbon isotope study of the Xiaotan section, South China. *Precambrian Research* 225, 148-165.

Chen, Z.M. & Chen, Q.Y. 1987. Paleogeography of Yangzi Platform and the characteristics of the phosphorite distribution of Early Meishucun Stage, Early Cambrian. *SCIENTIA GEOLOGICA SINICA*, 3, 246-257.

Chen, D., Wang, J., Yan, J. & Wie, H. 2012. Tectono-depositional patterns and palaeogeography in the Middle Yangtze River region during the Early Cambrian. *Chinese Journal of Geology* 4, 1052-1070. (In Chinese with English abstract).

Deynoux, M., Affaton, P., Trompette, R. & Villeneuve, M., 2006. Pan-African tectonic evolution and glacial events registered in Neoproterozoic to Cambrian cratonic and foreland basins of West Africa. *Journal of African Earth Sciences* 46, 397-426.

Derry, L.A., 2010. A burial diagenesis origin for the Ediacaran Shuram-Wonoka carbon isotope anomaly. *Earth and Planetary Science Letters* 294, 152–162.

Fairchild, I.J. & Kennedy, M.J., 2007. Neoproterozoic glaciation in the Earth System. *Journal of the Geological Society* 164, 895–921.

Flügel, E., 2004. Microfacies of Carbonate Rocks: Analysis, Interpretation and Application. Spring-Verlag, Berlin. (118 pp).

Ge, H.R., Luo, C.S. & Li, J. 1983. Phosphorite sedimentary environment of Meishucun age, early Cambrian, and condition of phosphorus accumulation in eastern Yunnan. *Journal of Mineralogy and Petrology* 9, 11-21. (in Chinese with English Abstr.).

Gomez, F. J. & Astini, R.A., 2015, Sedimentology and sequence stratigraphy from a mixed (carbonate–siliciclastic) rift to passive margin transition: The Early to Middle Cambrian of the Argentine Precordillera. *Sedimentary Geology* 316, 39–61.

Huang, D.Y. & Lei, W.L. 1990. The aggregating phosphorus environment and sedimentary pattern of the Dahai phosphorus ore belt between Dongchuan city and Huize County. *Yunnan Geology* 9, 38-49. (in Chinese with English Abstr.)

Jiang, G., Shi, X., Zhang, S., Wang, Y. & Xiao, S., 2011. Stratigraphy and paleogeography of the Ediacaran Doushantuo Formation (ca. 635–551 Ma) in South China. *Gondwana Research* 19 (4), 831–849.

Jiang, G., Wang, X.Q., Shi, X.Y., Xiao, S.H., Zhang, S.H. & Dong, J. 2012. The origin of decoupled carbonate and organic carbon isotope signatures in the early Cambrian (ca. 542-520 Ma) Yangtze platform. *Earth and planetary Science Letters* 317-318, 96-110.

Knoll, A.H., Bambach, R.K., Canfield, D.E. & Grotzinger, J.P., 1996. Comparative Earth history and Late Permian mass extinction. *Science* 273, 452–457.

Landing, E., Peng, S. C., Babcock, L. E., Geyer, G., & Moczydlowska-Vidal, M. 2007. *Global standard names for the lowermost Cambrian series and stage.* Episodes 30, 287-289.

Landing, E., Geyer, G., Brasier, M.D. & Bowring, S.A., 2013. Cambrian Evolutionary Radiation: Context, correlation, and chronostratigraphy - Overcoming deficiencies of the first appearance datum (FAD) concept. *Earth-Science Reviews* 123, 133-172.

Lei, W.L., 1986. On the geological characteristics and mineralization mechanism of early Cambrian phosphorite of Xianfeng, Xundian county. *Yunnan Geology* 5, 209-221. (in Chinese with English Abstr.)

Lindsay, J.F., Brasier, M.D., Dorjnamjaa, D., Goldring, R., Kruse, P.D. & Wood, R.A. 1996. Facies and sequence controls on the appearance of the Cambrian biota in southwestern Mongolia: implication for the Precambrian – Cambrian boundary. *Geological Magazine* 133, 417-428.

Li, Y.Y. 1986. Proterozoic and Cambrian phosphorites – regional review: China. *In:* Cook, P.J. & Shergold, J.H. (ed.) *Phosphate Deposits of the World; Volume 1: Proterozoic and Cambrian Phosphorites*. Cambridge University Press, Cambridge, 42-61.

Li, Z.X., Bogdanova, S.V, Collins, A. S., Davidson, A., De Waele, B., Ernst, R.E., Fitysimons, I.C.W., Fuck, R.A., Gladkochub, D.P., Jacobs, J., Karlstrom, K.E., Lu, S., Natapov, L.M., Pease, V., Pisarevsky, S.A., Thrane, K. & Vernikovsky, V., 2008. Assembly, configuration, and break-up history of Rodinia: A synthesis. *Precambrian Research 160*, 179-210.

Li, G.X. & Xiao, S., 2004. Tannuolina and Micrina (Tannuolinidae) from the Lower Cambrian of eastern Yunnan, South China, and their scleritome reconstruction. *Journal of Paleontology* 78, 900–913.

Li, D., Ling, H.F., Jiang, S.Y., Pan, J.Y., Chen, Y.Q., Cai, Y.F. & Feng, H.Z., 2009. New Carbon isotope stratigraphy of the Ediacaran-Cambrian boundary interval from SW China: implication for global correlation. *Geol. Mag*. 146(4), 465-484.

Li, D., Ling, H.F., Shields-Zhou, G.A., Chen, X., Cremonese, L., Och, L., Thirlwall, M. & Manning, C.J., 2013. Carbon and strontium isotope evolution of seawater across the Ediacaran-Cambrian transition: Evidence from the Xiaotan section, NE Yunnan, South China. *Precambrian Research* 225, 128-147.

Luo, H., Jiang, Z., Wu, X., Song, X. & Ou, Y., 1982. The Sinian-Cambrian Boundary in Eastern Yunnan. Yunnan People's Publishing House, P.R. China. (In Chinese with English Abstr.)

Luo, H., Wu, X. & Ou, L. 1991. Facies changes and transverse correlation of the Sinian-Cambrian boundary strata in eastern Yunnan. *Sedimentary Geology and Tethyan Geology*, 65, 27-35.

Maloof, A.C., Porter, S.M., Moore, J.L., Dudas, F.O., Bowring, S.A., Higgins, J.A., Fike, D.A. & Eddy, M.P., 2010. The earliest Cambrian record of animals and ocean geochemical change. *Bulletin of the Geological Society of America* 122, 1731-1774.

Marshall, C.R., 2006. Explaining the Cambrian "Explosion" of Animals. *Annual Review of Earth and Planetary Sciences* 34, 355-384.

McCall, G.J.H., 2006. The Vendian (Ediacaran) in the geological record: Enigmas in geology´s preclude to the Cambrian explosion. *Earth-Science Reviews* 77, 1-229.

Meert, J.G. & Lieberman, B.S., 2008. The Neoproterozoic assembly of Gondwana and its relationship to the Ediacaran-Cambrian radiation. *Gondwana Research* 14, 5-21.

Och, L.M., Shields-Zhou, G.A., Poulton, S.W., Manning, C., Thirlwall, M.F., Li, D., Ling, H.F., Osborn, T. & Cremonese, L., 2013. Redox changes in Early Cambrian black shales at Xiaotan section, Yunnan Province, South China. *Precambrian Research* 225, 166-189.

Qian, Y., 1989. Early Cambrian Small Shelly Fossils of China with Special Reference to the Precambrian–Cambrian Boundary. Stratigraphy and palaeontology of systemic boundaries in China, Precambrian-Cambrian boundary (2). Nanjing University Publishing House.

Qian, Y., Zhu, M.Y., He, T.G. & Jiang, Z.W. 1996. New investigation of Precambrian-Cambrian boundary sections in eastern Yunnan. *Acta Micropalaeontologica Sinica*, 13, 225-240.

Qian, Y., Zhu, M.Y. & Li, G.X., 2002. A supplemental Precambrian-Cambrian boundary global stratotype section in SW China. *Acta Palaeontologica Sinica* 41 (1), 19-26.

Salad Hersi, O., Abbasi, I. A. & Al-Harthy, A., 2015. Sedimentology, rhythmicity and basin-fill architecture of a carbonate ramp depositional system with intermittent terrigenous influx: The Albian Kharfot Formation of the Jeza-Qamar Basin, Dhofar, Southern Oman. *Sedimentary Geology*, *331*, 114–131

Siegmund, H. & Erdtmann, B.D. 1994. Facies and Diagenesis of Some Upper Proterozoic Dolomites of South China. *Facies*, 31,255-264.

She, Z.B., Strother, P., McMahon, G., Nittler, L.R., Wang, J.H., Zhang, J.H., Sang, L.K., Ma, C.Q. & Papineau, D. 2013. Terminal Proterozoic cyanobacterial blooms and phosphogenesis documented by the Doushantuo granular phosphorites I: In situ micro-analysis of textures and composition. *Precambrian Research*, 235, 20-35.

Shields, G. & Stille, P., 2001. Diagenetic constraints on the use of cerium anomalies as palaeoseawater redox proxies: an isotopic and REE study of Cambrian phosphorites. *Chemical Geology* 175, 29-48.

Shields-Zhou, G & Zhu, M. 2013. Biogeochemical changes across the Ediacaran-Cambrian transition in South China. *Precambrian Research* 225, 1-6.

Steiner, M., Zhu, M., Weber, B. & Geyer, G., 2001. The Lower Cambrian of eastern Yunnan: trilobite-based biostratigraphy and related faunas. *Acta Palaeontologica Sinica*, 40, 63-79.

Steiner, M., Li, G.X., Qian, Y., Zhu, M.Y. & Erdtmann, B.D., 2007. Neoproterozoic to early Cambrian small shelly fossil assemblages and a revised biostratigraphic correlation of the Yangtze Platform (China). *Palaeogeography, Palaeoclimatology, Palaeoecology* 254, 67-99.

Southgate, P.N. 1986. Proterozoic and Cambrian phosphorites-specialist studies: Middle Cambrian phosphatic hardgrouds, phoscrete profiles and stromatolites and their implications for phosphogenesis. *In:* Cook, P.J. & Shergold, J.H. (ed.) *Phosphate Deposits of the World; Volume 1: Proterozoic and Cambrian Phosphorites.* Cambridge University Press, Cambridge, 327-351.

Southgate, P.N. 1988. A model for the development of phosphatic and calcareous lithofacies in the Middle Cambrian Thorntonia limestone, northeast Georgina Basin, Australia. *Australian Journal of Earth Sciences*, 35, 111-130

Trappe, J. 1998. *Phanerozoic Phosphorite Depositional Systems.* Springer, Berlin ; Heidelberg. (173 pp).

Tucker, M.E. 1985. Shallow-marine carbonate facies and facies models. *Geological Society, London. Special Publications* 18, 147-169.

Tucker, M.E., 2003. Mixed clastic-carbonate cycles and sequences: Quaternary of Egypt and Carboniferous of England. *Geologia Croatica* 56 (1), 19-37.

Tucker, M.E. & Wright, V.P., 1990. Carbonate Sedimentology. Blackwell Science, Oxford.

Vernhet, E. & Reijmer, J.J.G., 2010. Sedimentary evolution of the Ediacaran Yangtze platform shelf (Hubei and Hunan provinces, Central China). *Sedimentary Geology*, 225, 99–115.

Wang, J. & Li, Z.X. 2003. History of Neoproterozoic rift basins in South China: implications for Rodinia break-up. *Precambrian Research*, 122, 141-158.

Weber, B., Steiner, M. & Zhu, M.Y. 2007. Precambrian-Cambrian trace fossils from the Yangtze Platform (South China) and the early evolution of bilaterian lifestyles. *Palaeogeography, Palaeoclimatology, Palaeoecology*, 254, 328-349.

Xue, Y.S., Tang, T.F. & Yu, C.L. 1992. Paleokarst Cave phosphorites of the Upper Sinian Dengying Formation in Southern China. *Acta Sedimentologica Sinica*, 10, 145-153.

Xu, L.G., Lehmann, B., Zhang, X.G., Zheng, W. & Meng, Q.T. 2014, Trace element distribution in black shales from the Kunyang phosphorite deposit and its geological significances. *Acta Petrologica Sinica*, 30, 1817-1827. (In Chinese with English Abstr.)

Yang, B., Steiner, M., Li, G.X. & Keupp, H. 2014. Terreneuvian small shelly faunas of east Yunnan (South China) and their biostratigraphic implications. *Palaeogeography, Palaeoclimatology, Palaeoecology*, 398, 28-58.

Zeng, Y.F. & Yang, W.D., 1987. Mechanism of enrichment of Kunyang and Haikou phosphorite deposits, Yunnan China. *Acta Sedimentologica Sinica*, 5, 19-28.

Zhu, M., Li, G. & Zhang, J., 2001. Early Cambrian stratigraphy of east Yunnan, southwestern china: a synthesis. *Acta Palaeontologica Sinica*, 40, 4-39.

Zhu, M., Zhang, J., Steiner, M., Yang, A., Li, G. & Erdtmann, B., 2003. Sinian- Cambrian stratigraphic framework for shallow to deep-water environment of the Yangtze Platform: an integrated approach. *Progress in Natural Science* 13(12), 951-960.

Zhu, M.Y., Babcock, L.E. & Peng, S.C. 2006. Advances in Cambrian stratigraphy and paleontology: Integrating correlation techniques, paleobiology, taphonomy and paleoenvironmental reconstruction. *Palaeoworld*, 15, 217-222.

Zhu, M., Zhang, J. & Yang, A., 2007, Integrated Ediacaran (Sinian) chronostratigraphy of South China. *Palaeogeography, Palaeoclimatology, Palaeoecology* 254, 7-61.

Seilacher, A., Buatois, L. A. & Gabriela Mángano, M., 2005. Trace fossils in the Ediacaran–Cambrian transition: Behavioral diversification, ecological turnover and environmental shift. *Palaeogeography, Palaeoclimatology, Palaeoecology*, 227(4), 323–356.

CHAPTER IV

The nature of the Ediacaran-Cambrian contact at Meishucun, Yunnan Province, China

The nature of the Ediacaran-Cambrian contact at Meishucun, Yunnan Province, China

Xiaojuan Sun[a], Christoph Heubeck[b], Dorothee Hippler [c], & Simon Hohl[a]

[a] *Institute of Geological Sciences, Freie Universität Berlin, Malteserstraße 74-100, 12249 Berlin, Germany*

[b] *Department of Geosciences, Universität Jena, Burgweg 11, 07749 Jena, Germany*

[c] *Institute of Applied Geosciences, Graz University of Technology, Rechbauerstrasse 12, 8010 Graz, Austria*

4.1. Abstract

The extensive, well-exposed Ediacaran-Cambrian boundary interval at Meishucun, Yunnan, south China, offers a unique opportunity to study in detail sedimentary, microbial and diagenetic processes related to one of the world's most significant bioradiation events. We here presented a detailed study of the facies, diagenesis and geochemical characters of the Ediacaran-Cambrian boundary stratigraphic interval at Meishucun. The late Ediacaran global sea level-lowering event exposed extensive carbonate tidal flat surfaces, resulting in karstification. As sea level rose, early-diagenetic phosphatization in a lower-intertidal to subtidal, low to medium-energy marine environment became widespread, represented by the basal Cambrian Zhujiaqing Formation. Deposition of thick phos-onco- and phos-oo-packstones testifies to the important role of microbial activity. Phosphorus was likely derived from transgression-related upwelling rather than directly from terrestrial weathering and was concentrated and fixed by microbial mats. Silicification of the carbonate platform occurred in early burial diagenesis possibly related to phreatic mixing-zone environment, dolomite was likely influenced by meteoric and burial diagenesis. Several depositional gaps of similar character also exist stratigraphically higher in the lower Cambrian of south China. The data presented here are of significance for those concerned with the interpretation of Precambrian to Cambrian environmental change and are instrumental for a more realistic understand about the advent of Cambrian bioradiation.

Key words: Yangtze platform, Diagenesis, Hiatus, Pc-C, Phosphorite

4.2. Introduction

Life underwent a major radiation shortly after the Ediacaran-Cambrian (E-C) boundary, including the first widespread appearance of skeleton-bearing animals, numerous innovative morphologies, extinction of the Ediacaran biota, and a sudden increase in animal diversity (Brasier, 1986; Amthor et al., 2003; Seilacher et al., 2005; Marshall, 2006; Zhu et al., 2006; Zhu et al., 2007; Landing et al., 2013; Na and Kiessling, 2015). However, the E-C transition in most parts of the world coincides with a sea-level lowstand which resulted in erosional unconformities, condensation or exposure surfaces and karstification of shelf sections. The processes associated with this sea-level lowstand eliminated or obscured substantial parts of the critical rock record during the time period between the latest Ediacaran

and the earliest Cambrian (Peters et al., 2012). The incomplete stratigraphic record, combined with the scarcity of reliable index fossils, thus hinders our understanding of ecological causes and events and also makes correlation between E-C boundary sections difficult. A detailed understanding of the magnitude and timing of erosion, as well as the composition of the eroded material between the latest Ediacaran and the lower Cambrian, however, is relevant to understanding event chains, because these erosion products may contribute significantly to the shallow-water nutrient budget (Planavsky et al., 2010, Maruyama et al., 2013). Significantly, one of Earth's major phosphogenic events overlies the unconformable E-C contact in many parts of the world (Central Asia, South China, Australia, India), hinting at a major nutrient-fuelled ecological turnover.

One of the best exposed, least metamorphosed and lithologically varied regions to study the nature of the E-C transition is the Yangtze Platform, South China (Yeh et al., 1986; Liu et al., 1995; Wang et al., 2003; Charvet, 2013, and many others), where shallow-water carbonates of the latest Ediacaran Dengying Formation (ca. 555-543 Ma) reach several hundred meters in thickness. Overlying Cambrian strata are most complete in eastern Yunnan Province (Zhu et al., 2001; Xue et al., 2006; Steiner et al., 2007). They include the classical Sinian-Cambrian boundary section near Meishucun village, which had been proposed as a potential E-C GSSP (Global Stratigraphic Section and Point) stratotype (Cowie and Brasier, 1989; Luo et al., 1980, 1984). The Kunyang phosphorite mine (Fig. 1) in the Meishucun area contains numerous partial sections bridging the E-C boundary interval, in addition to the protected formerly proposed type sections. In the past three decades, much detailed work was done on Meishucun´s paleontology and biostratigraphy (Luo et al., 1984; Qian et al., 1989; Parkhaev, 2010; Yang et al., 2013), stable isotope geochemistry (Brasier et al., 1990; Li et al., 1994; Siegmund, 1995; Shields et al., 1999; Schields and Stille, 2001; Xu et al. 2014) and geochronology (Compston et al., 2008; Zhu et al., 2009). However, the detailed sedimentology of the section, especially the nature of the unconformable contact between the Dengying Formation carbonates and the overlying early Cambrian Zhujiaqing Formation phosphorites has received less attention and is to-date limited to discussions related to the degree of stratal omission and their correlation across eastern Yunnan (Luo et al., 1984; Qian et al., 1996).

The objectives of this contribution are thus 1) to document the detailed stratigraphy, petrography and sedimentary facies of the E-C boundary interval as exposed in the Kunyang quarries at Meishucun, 2) to discuss the local depositional environment at the very beginning of the Cambrian period and 3) to provide details on the diagenetic processes in order to elucidate the nature of the E-C contact and its impact on the Cambrian bioradiation event.

4.3. Regional geology

4.3.1. Structural geology and outcrop conditions

Several active open-pit mines of the Kunyang Phosphorite mine near the village of Meishucun, ca. 60 km southwest of Kunming, capital of Yunnan Province, lie, aligned approximately E-W, on the south-

dipping limb of a major, regional, ESE-WNW trending anticline, which is segmented by several northeast-striking, steeply dipping faults. Because the strata are inclined by only about 20^0 to the south (Fig. 1) and the mined unit, stratiform phosphate deposits of the basal Cambrian, immediately overly the unconformable E-C contact, this contact is widely exposed in freshly quarried or blasted exposures. Plane exposures of the unconformity surface reach tens to hundreds m^2 in size, so that the quarries allow detailed observations in three dimensions over an area of several km^2.

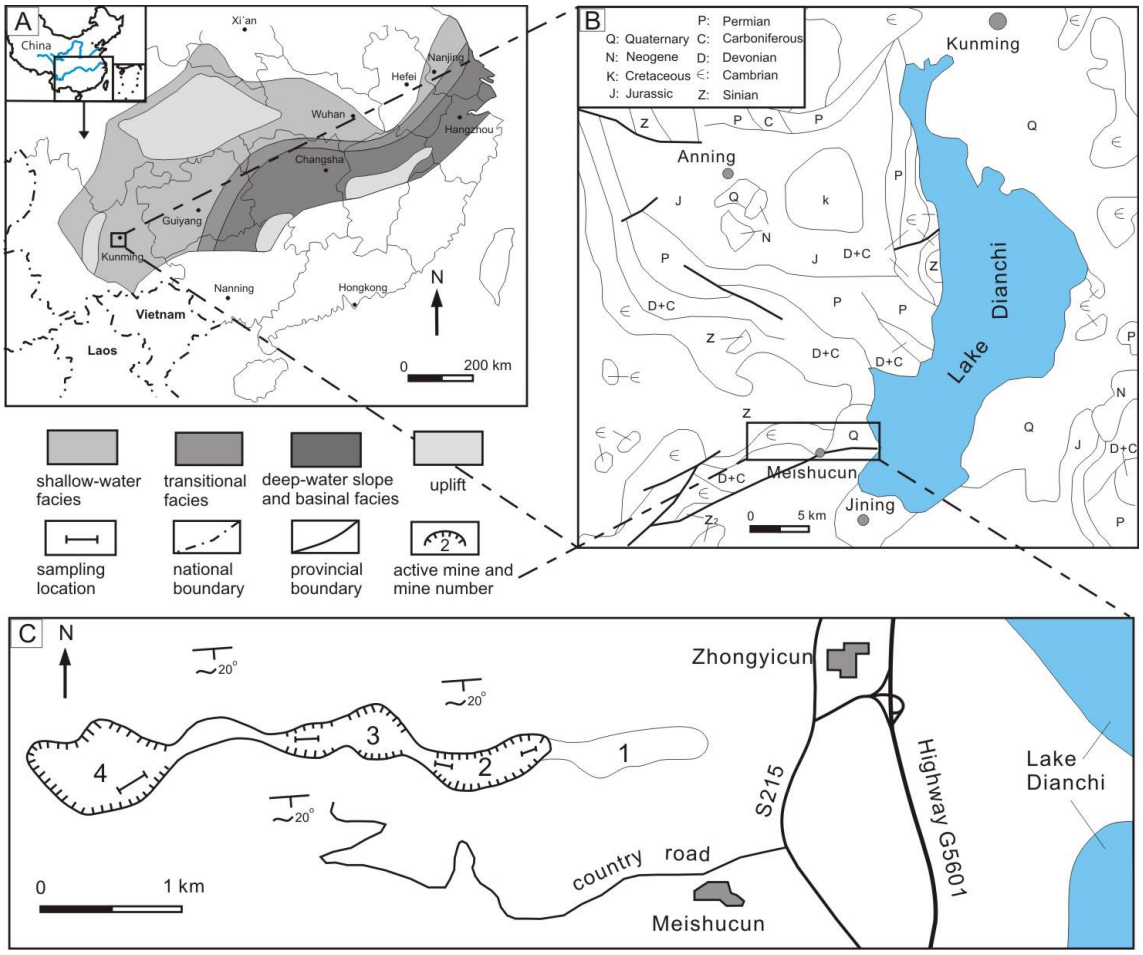

Fig. 1. *Locality map and paleogeographic setting of the studied area. A) Simplified paleogeographic map of the Yangtze Platform during the Ediacaran-Cambrian transition (modified from Steiner et al., 2007). B) Generalized geological map of the area southwest of Kunming, Yunnan Province (modified after Luo et al., 1984). C) Location of Kunyang phosphorite mine near Meishucun on the south-dipping limb of an E-W trending anticline. Numbers (1-4) identify open-pit mines and bars the studied sections (sites A to D in the text from right to left), respectively.*

4.3.2. "Lower Cambrian" lithostratigraphy in northeastern Yunnan

The appropriate stratigraphic subdivision of the E-C transition in northeast Yunnan has long been subject to dispute (Luo et al 1980, 1982, 1990; He, 1989; Qian et al., 1996; Zhang et al., 1997; Zhu et al., 2001) (Fig. 2). The uppermost eight meters of strata below the base of the phosphorites at Meishucun were reported by Luo et al. (1980) to contain some small shelly fossils (his Xiaowaitoushan Member, abbreviated XWTS) which, however, is now considered as an infiltration of basal Cambrian sediment in paleokarst cavities at the top of the Dengying Formation (Qian et al., 1996). Based on observations

near Yulu (Yunnan Province, approx. 250 km northeast of Meishucun), He et al. (1989) defined the Daibu Member (DB), a new basal unit of the Cambrian in southwest China, consisting of interbedded chert and dolomitic limestone between the Baiyanshao Member (BYS) of the Ediacaran Dengying Formation and the basal Cambrian Zhongyicun Member (ZYC) of the Zhujiaqing Formation. He et al. (1989) considered its base to be a parallel unconformity and its top to be gradual to the Zhongyicun Member. Luo et al. (1990), however, considered the Daibu Member as a facies change of the (Ediacaran) Xiaowaitoushan Member in other parts of Yunnan area; Zhang et al. (1997) interpreted the Xiaowaitoushan Member to represent the lower part of the Daibu Member. At Meishucun, Zhu et al. (2001) considered the Daibu member to be absent and recommended to discard the use of the "Xiaowaitoushan Member".

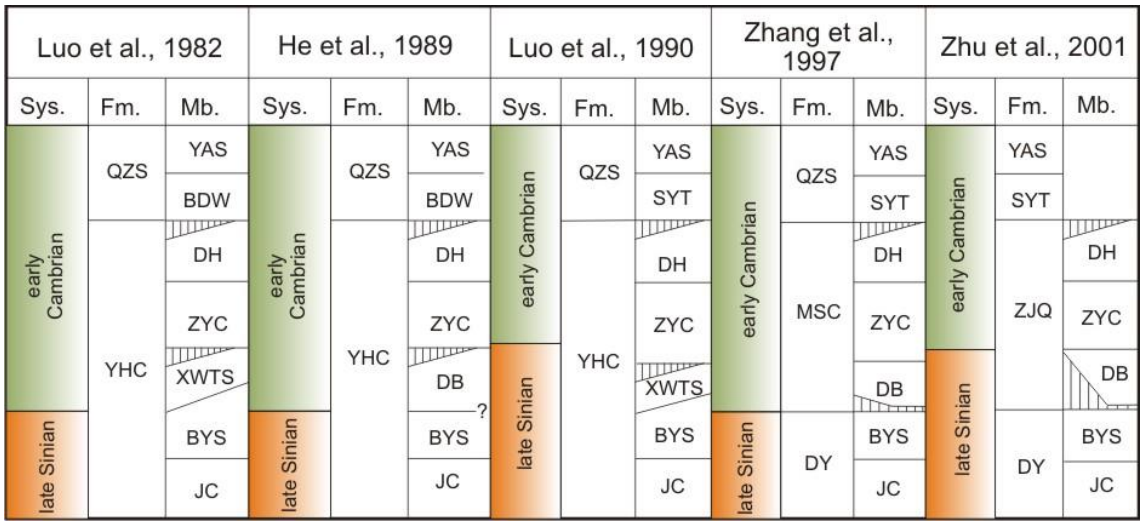

Fig. 2. *Lithostratigraphic correlation diagram across the E-C boundary interval in northeastern Yunnan, south China. Vertical hachures represent depositional hiati. Formation and number names are abbreviated as follows: JC-Jiucheng; BYS-Baiyanshao; XWTS-Xiaowaitoushan; DB-Daibu; ZYC-Zhongyicun; DH-Dahai; YHC-Yuhucun; BDW-Badaowan; SYT-Shiyantou; YAS-Yuanshan; QZS-Qiongzhusi. Note the different positioning of the E-C boundary among publications.*

In eastern Yunnan, the uppermost Dengying Formation consists of dolostone of the Baiyanshao Member. It is overlain by the Zhujiaqing Formation, named after its type section near Zhujiaqing village, Huize County (Zhu et al., 2001), about 200 km north of the Meishucun area. This formation is (from base to top) composed of three lithostratigraphically defined members: (1) the aforementioned, basal, medium-bedded siliceous dolomitic limestone of the Daibu Member, approx. 0 to 60 m thick; (2) granular phosphorite, dolomitic phosphorite and siltstone of the Zhongyicun Member, approximately 5 to 80 m thick; and (3) thick dolostone and marly dolomitic limestone of the Dahai Member, approx. 1 to 70 m thick.

4.3.3. Age and location of the Precambrian-Cambrian boundary at Meishucun

Based on their discovery of SSFs in the uppermost Dengying dolostones, Luo et al. (1980, 1982) placed the Precambrian-Cambrian (Pc-C) boundary at the Meishucun section initially (his Marker A) at the base of the newly defined Xiaowaitoushan Member but moved this position later to Marker B (Luo et

al., 1990), mainly because δ13Ccarb isotope values across marker B showed a major change there, but no recognizable change at the two positions given for Marker A in the literature (in unit 1: Luo et al. 1992; at the base of unit 3: Qian and Bentson, 1989). A negative δ13Ccarb excursion is also present in several other sections of northeastern Yunnan (Zhou et al., 1997; Li et al., 2009, 2012) and was thus taken as an indicator of the E-C boundary (Landing et al., 2013). It subsequently became clear, however, that the absence of a negative δ13Ccarb shift could also well be due to non-deposition or erosion, early diagenetic overprint, late-stage hydrothermal alteration, or a combination of these reasons. In the absence of conclusive chemo-, chrono- and biostratigraphic evidence, and because of the clear evidence for condensation, hiati, and erosion, the issue of the precise location of the Pc-C boundary at Meishucun weakened its strength as a GSSP candidate and was left formally unresolved. Because the lowest member of the Zhujiaqing Formation, the Daibu Member, is apparently absent in Meishucun, the unconformity between the top of the Baiyanshao Member of the Dengying Formation, unconformably overlain by the Zhongyicun Member of the Zhujiaqing Formation, is now largely considered to represent the E-C boundary (Zhu et al., 2001) (Fig. 3).

A prominent, so-called "white clay", a dolomitic and fine-grained clastic unit interbedded with a bentonitic clay (Siegmund, 1995) divides the Zhongyicun Member into a lower and an upper phosphorite unit. This bentonite is widely thought to be an altered volcanic tuff. Zircons extracted from this unit have been dated at least four times: Compston et al. (1992) obtained an age of 525 ± 7 Ma (2 σ; 41 single-grain analyses; SHRIMP); Jenkins et al. (2002) obtained an age of 538.2±1.5 Ma (reprocessing of the former sample plus several additional grains; SHRIMP); Sawaki et al. (2008) measured an age of 536.5 ± 2.5 Ma (U–Pb nano-SIMS; oscillatory rims of 4 grains) and Zhu et al. (2009) obtained an age of 535.2 ± 1.7 Ma (13 concordant grains plus 4 nano-SIMS ages of Sawaki et al. 2008; SIMS). Because errors of uncertainty of the latter three analyses all overlap, it is safe to assume that the bentonitic clay is approximately 536 Ma old, which is unambiguously interpreted as a depositional age. The basal Cambrian index fossil *Treptichnus pedum* is known from the upper part of the lower phosphorite unit of the Zhongyicun Member (Weber and Zhu, 2004; Weber et al. 2007), along with abundant fauna of SSF Zone 1, characterized by the "protoconodonts" *Protohertzina anabarica, Protohertzina uniguliformis* and the symmetrical tubes of *Anabarites trisulcatus* (Steiner et al., 2007). This fossil assemblage is recognizable throughout eastern Yunnan and much of south China. In Meishucun section, the first appearance of this zone is well below the first occurrence of *Treptichnus pedum*, immediately above the unconformity and within the basal beds of the lower phosphorite unit (Crimes and Jiang, 1986); however, Shields et al. (1999) correctly point out that the stratigraphic use of trace fossils in such highly condensed sections as Meishucun is problematic.

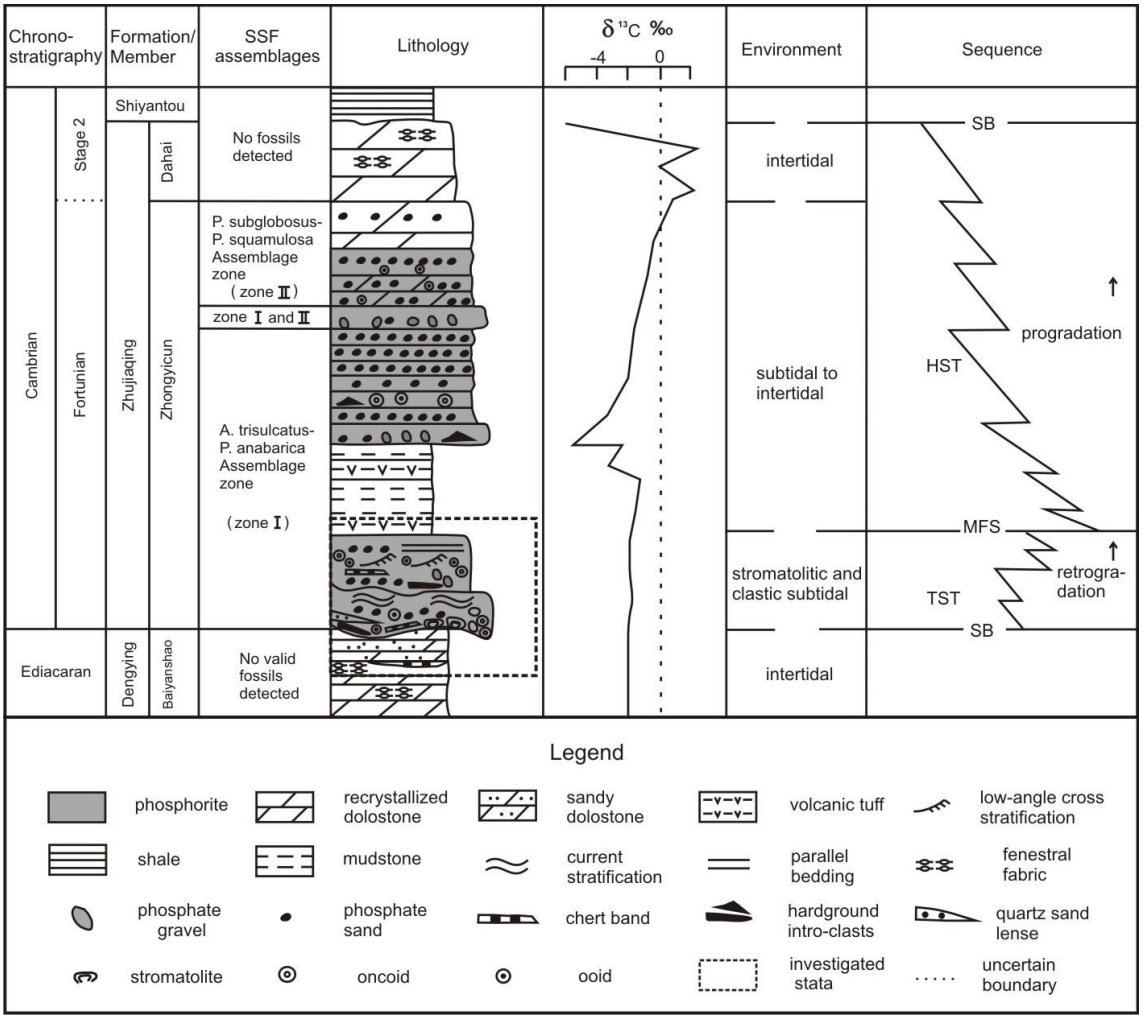

Fig. 3. *Ediacaran-Cambrian stratigraphy of Meishucun section. Carbon isotope data from Brasier et al. (1990a), lithology modified from Siegmund et al. (1995), environmental interpretation from Zeng et al. (1994), depositional sequence adapted from Zeng et al. (1994) and Zhu et al. (2001), and biozones adapted from Yang et al. (2014). Strata discussed in this study are highlighted by the dashed rectangle.*

4.4. Methods

We measured four outcrop sections at fresh exposures, spaced several hundred meters apart in three active quarries of the Kunyang phosphorite mine, and sampled representative lithologies at dm- to cm-scale resolution. Petrographic thin sections were stained with Alizarin Red and examined by standard transmitted-light microscopy at the Freie Universität Berlin. Subsequently, we assigned microfacies following the classifications of Trappe (1998) and Flügel (2009). Polished thin sections were coated with carbon and examined by cathodoluminescence (CL) at the Museum für Naturkunde Berlin. In addition, we assigned five samples near the E-C contact for geochemical (trace and rare earth elements, Sr isotopes) analysis. For this purpose, we used acetic acid leaching in order to analyze geochemical signatures solely of the soluble carbonate fraction. About 20 mg of bulk sample powder was therefore treated with 1ml 3 M acetic acid for 12 hours, following the methods described by Huang et al. (2009). Insoluble residues were separated by centrifugation and filtration through 0.45 µm cellulose acetate syringe filters. To remove the acetic acid, the supernatant was dried down and re-dissolved in 0.5 ml 3

M HNO_3. Afterwards, the solution was equilibrated in 1 ml 0.28 M HNO_3, weighed and diluted with 0.28 M HNO_3 to 1: 20.000 for trace element and to 1: 40.000 for major element analysis.

All trace and rare earth element analyses on carbonate leachates were performed on a Thermo Finnigan Element XR sector-field ICP mass spectrometer at the Freie Universität Berlin using a Scott type quartz spray chamber and a 100 µl/min nebulizer. Sample time was 120 s with 20 samples/peak and 60 total scans. With this analytical setup, tuning generally yielded low oxide rates of 2-5 % CeO^+ and less than 1% BaO^+. We determined element concentrations by external calibration to the matrix-matching CAL-S carbonate standard (Yeghicheyan et al., 2003). For drift correction, the diluted samples were doped with solutions of 2 ppb In and 1 ppb Tl for elements analyzed in low-resolution mode (REE+Y), and 12.5 ppb Co for elements analyzed in medium-resolution mode (Ba, Mn, Sr). Background corrections were performed by subtraction of the raw intensities of aspirated 0.28 M HNO_3. The analytical precision for trace and rare earth elements was usually better than 5% RSD. Detection limits were 25 ppb for Ba and Mn, 200 ppb for Sr, 100-620 ppt for LREE and 16-240 ppt for HREE, respectively. Procedural blanks on trace elements and REE were negligible, being generally below the acid-background-signal intensities. We calculated Ce/Ce* and Eu/Eu* according to Bau and Dulski (1996), with normalization of concentrations against the standard values of Post-Archean Australian Shale (= PAAS; McLennan, 1989).

Aliquots of the acetic acid carbonate leachates were used for Sr isotopic composition measurements. Approximately 1 µg Sr was loaded on 1 ml AG 50W-X8 (200-400 mesh) cation-exchange resin with 2.5 M HCl for separation of Sr from the matrix. Thereafter, the Sr isotopic composition was determined using a Thermo-Finnigan Triton TIMS at Freie Universität Berlin. Repeated measurements of the reference material NIST SRM 987 yielded $^{87}Sr/^{86}Sr$ = 0.710266 (± 15, n = 6). Mass fraction was corrected assuming a $^{87}Sr/^{86}Sr$ ratio = 0.1194 (Nier, 1938) and the exponential law. Minor interferences of ^{87}Rb on ^{87}Sr were corrected using $^{85}Rb/^{87}Rb$ = 2.59265. Initial $^{87}Sr/^{86}Sr$-ratios were calculated assuming depositional ages (600 Ma), $^{87}Rb/^{86}Sr$ ratios (calculated from ICP-MS data) and a half-life of ^{87}Rb of $4.88*10^{10}$ years. Corrections of the potential radiogenic ingrowth of Rb are on the order of 2 ‰. In general, corrections are minor and do not change the interpretation of the carbonate data.

4.5. Results

4.5.1. Lithology and Geometry

Luo et al. (1982) defined eight "Beds" (the formal lithostratigraphic unit next in rank below a Member) between the upper Dengying Formation dolostone to the Dahai Member dolostone at Meishucun section, which is a scheme still in use for Meishucun detailed stratigraphy today. In the following, we will use the term ‘‘Bed’’, combined with a number, as a formal lithostratigraphic unit, and the term "bed" to identify a sedimentary lithosome bounded by recognizable partings, commonly defining a single flow unit (as in "medium-bedded"). In the Kunyang phosphorite mine, the strata investigated by us range

from Bed 2 to Bed 5 (Fig. 4). Our detailed measuring of sections showed that lithology and bed thicknesses occasionally vary significantly within few 10s of m, requiring the lateral tracing of beds for correlation (Fig. 4).

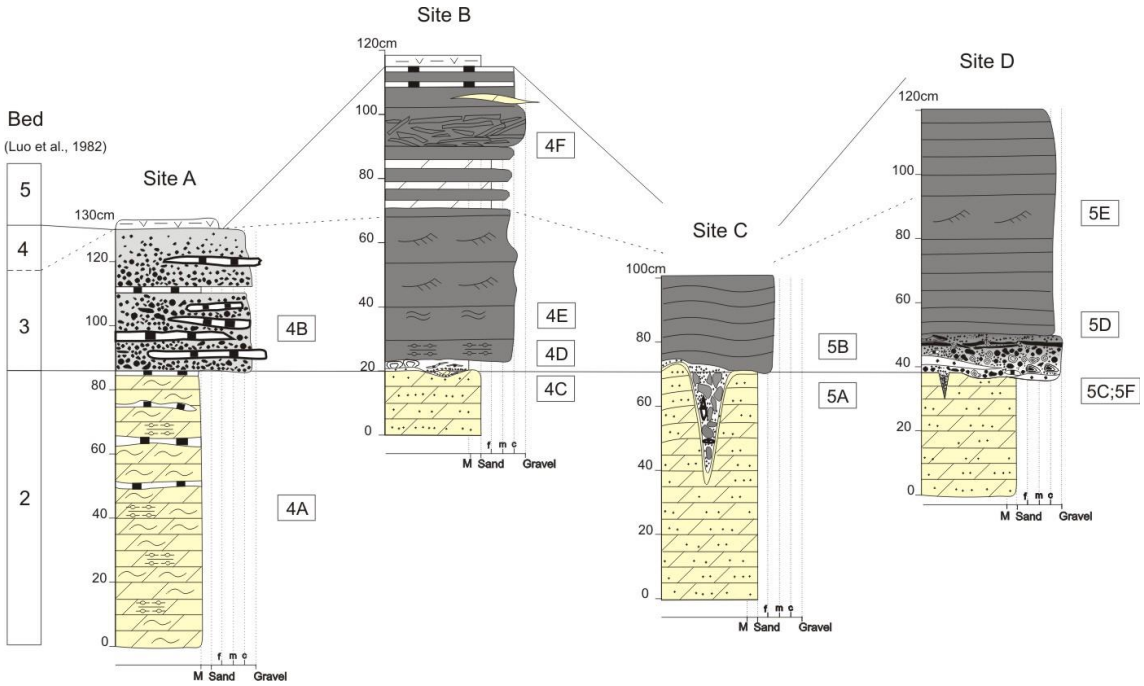

Fig. 4. *Detailed lithostratigraphic columns across the E-C boundary at the four studied sites (A-D) at the Kunyang phosphorite mine near Meishucun. Bed numbers follow Luo et al. (1982). Datum is the top of the Dengying Formation. The volcanic tuff shown at the top of stratigraphic columns at site A and B was dated at 539.4± 2.9 Ma by Compston et al., (2008) and at 535.2± 1.7 Ma by Zhu et al. (2009), respectively. Numbers next to the columns refer to outcrop photographs shown in Figs. 4 and 5. Symbols and patterns are given as in the legend of Fig. 3. Note the considerable lateral variations in lithologies across the different sites despite their distance of only several 100 m from each other.*

Site A (Quarry 4, east; Fig. 1)

Bed 2 is a yellowish, medium-bedded recrystallized dolomudstone (Fig. 5A) with fenestral fabric, in which interbedded chert increases in abundance upwards. It is overlain by Bed 3, consisting of a dark gray phosclast-rudstone, with a sharp and uneven contact. Phosphate clasts are gravel- to sand-size and well rounded. Horizontally aligned flat-pebble chert clasts, which reach tens of cm long and two to five cm thick, float among the phosphate grains (Fig. 5B). Bed 4 is absent. The reworked volcanic tuff (Bed 5) overlies Bed 3 with a sharp and uneven contact.

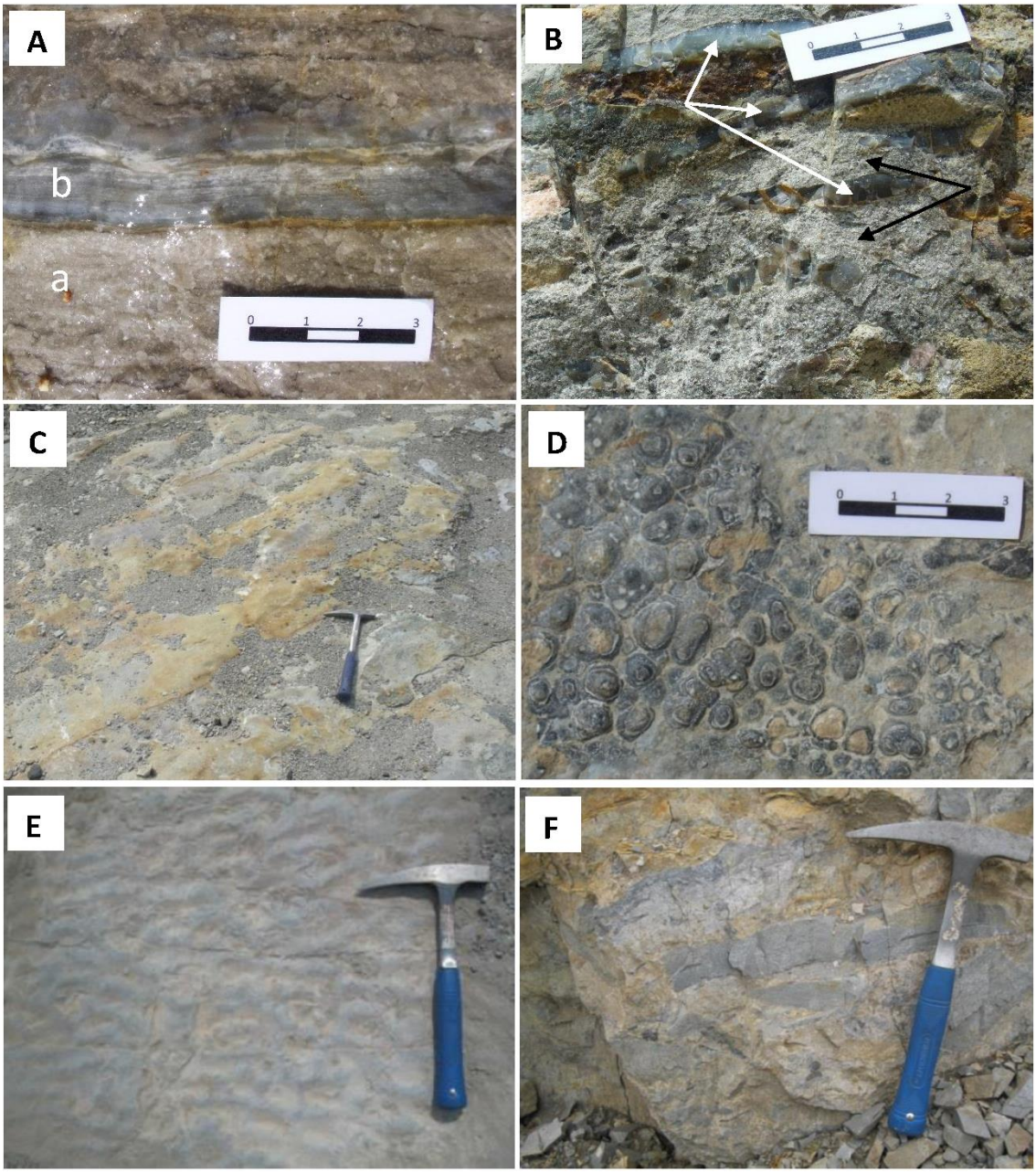

Fig. 5. *Outcrop photographs of exemplary sedimentary structures at sites A and B. A) Recrystallized dolomudstone (a) overlain by laminated chert (b) in Bed 2. B) Phosclast-rudstone of Bed 3, containing angular to shard-like chert clasts (e.g., white arrows) mixed with well-rounded phosphate grains (e.g., black arrows); also see Fig. 8D. C) Oblique view of top-Dengying surface, exposing mega-ripples in sandy dolostone. D) Bedding-plane view of mini-stromatolites on top of Dengying Formation dolostone. E) Interference ripples in phosclast-grainstone. F) Flat-pebble conglomerate within Bed 3. Subhorizontally aligned elongate phosclasts float in a brownish quartzose silt matrix.*

Site B (Quarry 3, west; Fig. 1)

The thickness of the lower phosphorite unit varies strongly within this quarry. At some sites, the lower phosphorite is entirely absent.

Only the topmost 10 to 20 cm of well-sorted and unevenly stratified yellowish sandy dolostone of Bed 2 crop out, but its uneven top surface, undulatory at dm-scale and reaching a relief of up to 50 cm, is widely exposed (Fig. 5C). Bed 2 is overlain by well-sorted phosclast-grainstone of Bed 3 which in places contains chert and dolostone grains. Small phosphatic stromatolites (Figs. 5D, Fig. 9C) are discontinuously distributed on the surface of Bed 2. These stromatolites are not more than 3 cm thick. Thin sections show them to be columnar-branching. Within Bed 3, horizontal and linear-sinusoidal trace fossils about 4 cm long and 1cm in width, wave ripples and interference ripples (Fig. 5E) occur. The contact between the phosclast-grainstone Bed 3 and Bed 4 is difficult to define. According to Luo (1982), Bed 4 is thinly bedded oolitic dolomitic phosphorite; however, we found little lithological difference between Bed 3 and Bed 4 except for an increase in carbonate cement compared to apatite cement. In several locations within this quarry, Beds 3 and 4 are replaced by a laterally discontinuous, ca. 50 cm thick conglomerate composed of grey phosclasts up to several decimeters long (Fig. 5F) in a brownish quartz-silt matrix stained by iron oxide. The reworked volcanic tuff bed (Bed 5) overlies Bed 4 with a sharp planar contact.

Site C (Quarry 2, west; Fig. 1)

The lower phosgrainstone (Beds 3, 4) varies strongly in thickness and is absent in some places. By combining measured sections from several sites within a few 100 m from each other, the following generalized stratigraphy can be constructed:

The basal sandy dolostone (Bed 2) is topped by an uneven surface of up to 50 cm relief, which shows numerous vertical fractures and scallops (Figs. 6A and B). Palaeotopographic depressions are generally filled by a clast-supported, oligomict grey conglomerate assigned to Bed 3 with rounded to subrounded, poorly sorted phosphate clasts and chert clasts up to 60 mm in diameter. Its matrix is composed of quartzose silt, clay and iron oxide. The conglomerate is overlain by grain-supported, medium-sorted apatite- and silica-cemented phosclast-grainstone to rudstone.

Site D (Quarry 2, east; Fig. 1)

The basal section of this quarry exposes the medium-bedded, yellowish sandy dolostone of Bed 2 with faint phosphatic lamina. Vugs and cracks become common towards its surface. This unit is overlain by a black conglomerate about five to ten cm thick which fills topographic depressions and wide fractures in the underlying dolostone (Fig. 6C). The conglomerate is composed of poorly sorted, angular phosphatic mudstone clasts and quartz-rich phosgrainstone clasts (Q-pg in Fig. 6C). The matrix of the conglomerate consists of a mix of mica and clay in microcrystalline quartz. The overlying phosclast-rudstone (Bed 3, Fig. 6D)

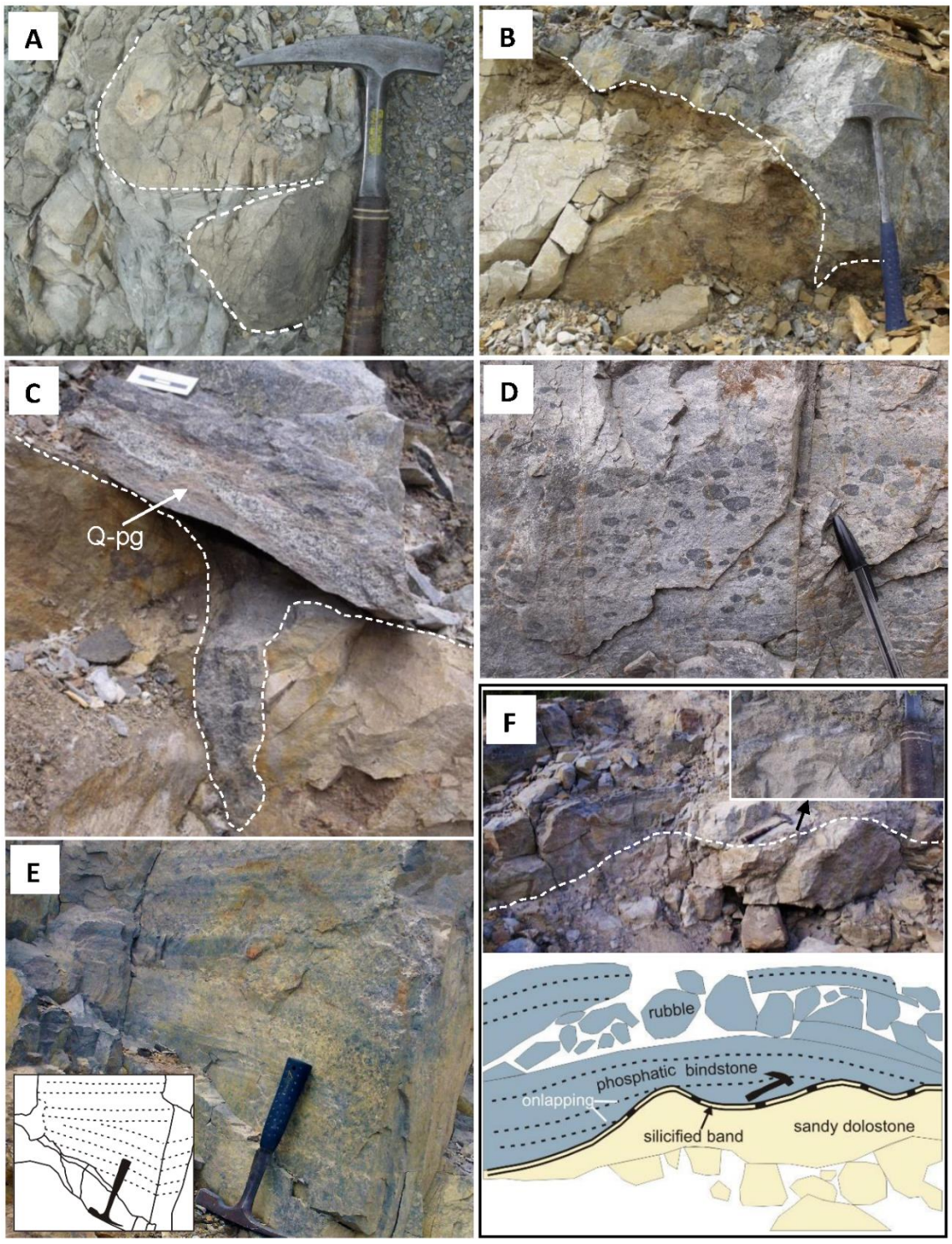

Fig. 6. *Sedimentary structures at sites C and D. A) Top-down view of vertical fracture in sandy dolostone filled with gray phosclast conglomerate. B) Unstratified phosclast conglomerate of basal Cambrian Zhujiajing Fm. overlying the uneven erosional surface above the Ediacaran sandy dolostone of the Dengying Fm. C) Fracture fill in Bed 2: Black phosclast conglomerate fills fracture and is overlain by quartz-rich phosclast-grainstone (Q-pg). D) Poorly sorted phosclast-rudstone. Dark grains are phosphate nodules. E) Cross stratification in phosgrainstone of Bed 3; line drawing in the lower left. F) Stratigraphic onlap of phosphatic bindstone on Dengying Fm. sandy dolostone; hammer for scale. Lower image shows line drawing of facies patterns.*

is composed of phosphatic oncoids, phosphatic intraclasts, phosphate nodules, phosphatic fossil fragments and chert clasts. Its dolomitic cement is partly silicified. A parallel- and cross-stratified phosclast -grainstone overlies silicified phosclast-rudstone with a parallel contact (Fig. 6E). At some locations in Quarry 2, phosphatic bindstone within Bed 3 pinches out and onlaps onto the positive palaeorelief of sandy dolostones of Bed 2 (Fig. 6F). The phosclast-grainstone of Bed 4 shows more dolomitic cement.

4.5.2. Facies analysis and paleoenvironmental interpretation

4.2.1. Dengying Formation: Recrystallized dolomudstone

The medium-bedded recrystallized dolomudstone of the Baiyanshan Member of the Dengying Formation shows common voids lined by subhedral blocky dolomite (drusy mosaic), 200 to 400 µm in size (Fig. 7A). Microcrystalline quartz occurs throughout the dolostone in the form of uneven streaks and isolated clusters (Fig. 7A arrows). Stylolites are common. In some parts of the quarry, galena occurs along bedding planes.

Interpretation

The irregular and roughly circular shape of the voids aligned subparallel to bedding suggests an origin as bird's eye structure. This type of porosity usually forms in water depth of a few cm to dm in (microbial) fine-grained micritic limestones and originates predominantly in inter- to supratidal settings.

4.2.2 Dengying Formation: Sandy dolostone

The sandy dolostone is grain-supported and mainly composed of well sorted, dolomitic and phosphatic peloids, dolomitic ooids and a few muscovite flakes and feldspar grains, which are organized in low-angle crossbeds and herringbone cross bedding**.** Subangular quartz grains (Fig. 7B) account for about 5 to 10% of the total grain count. Dolomitic ooids are mostly "superficial ooids" in which the thickness of the cortex is distinctly less than half of the diameter of the entire ooid. Dolomitic peloids and phosphatic peloids are well rounded. The former show a more blurred internal texture compared to the dolomitic ooids, which show a brownish color under plane-polarized light. The cement is recrystallized to medium- to coarse-grained dolomite so that crystal boundaries cross the internal fabrics of the original grains and the grain-cement boundaries. Stylolites (Fig. 7C), pyrite, other opaque residues and late dolomite concretions are common.

Interpretation

Sedimentary structures, high textural maturity and overall composition indicate an inter- to subtidal environment with medium-strength current or wave energy and near-constant agitation. Given the low proportion, small size and angular shape of quartz and muscovite grains, the terrigenous input was minor and may have been eolian.

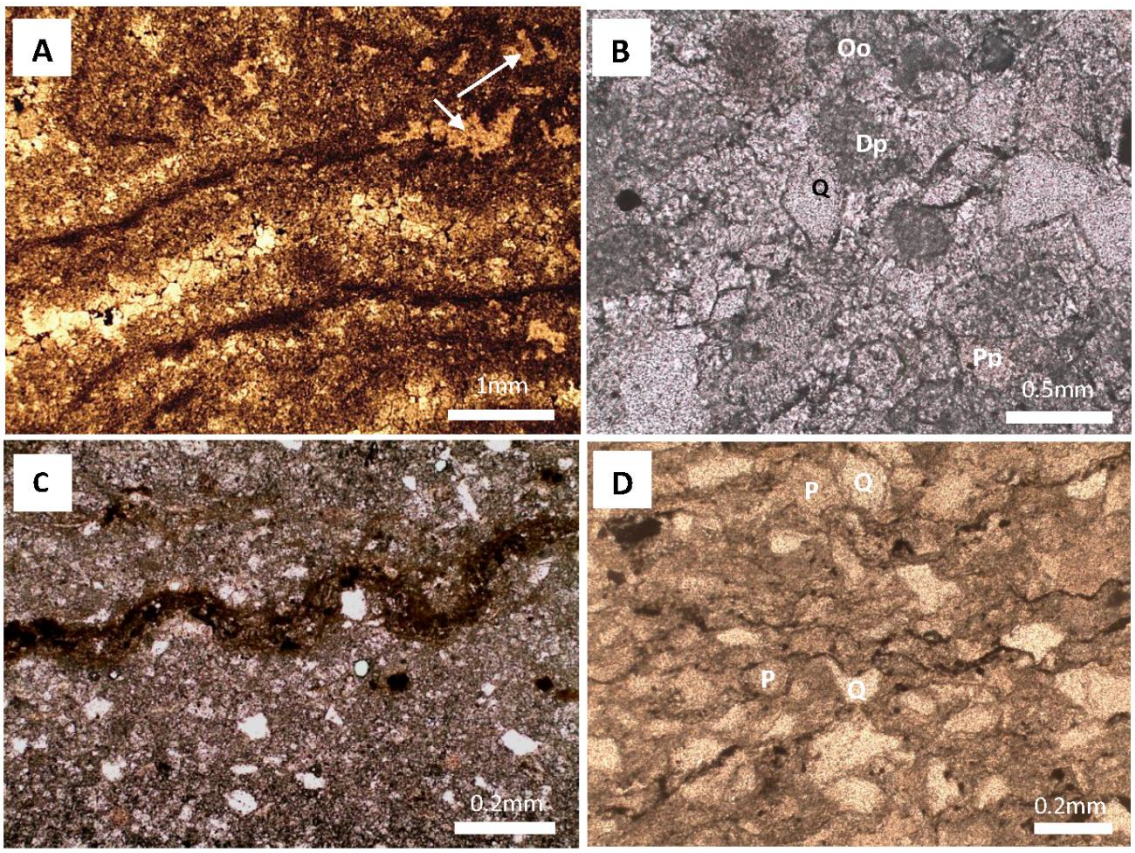

Fig. 7. *Thin-section plane-polarized light petrography of Dengying Formation dolostone (A, B, C) and Zhujiaqing Formation quartz-rich phosclast-grainstone (D) at Kunyang phosphorite mine. A) Partly silicified (arrows) recrystallized dolomudstone (site A, Bed 2); fenestral porosity is filled by subhedral dolomite crystals. B) Grain-supported sandy dolostone (site B, Bed 2). Q - quartz, Dp – dolomitic peloids, Pp - phosphatic peloids, Oo - dolomitic ooids. C) Sandy dolostone (site C, Bed 2). Dark brown stylolite composed of iron oxide and clay minerals across the thin section forms pseudo-bedding plane. D) Densely packed, quartz-rich phosclast-grainstone (site D, Bed 3) composed of (sub-) angular quartz (Q) and subangular phosphate grains (P). Note the sutured grain contacts, indicating extensive compaction and pressure solution.*

4.2.3. Zhujiaqing Formation: Quartz-rich phosclast-grainstone

Subangular, internally structureless phoslithoclasts (80-90%) and fine-grained angular quartz (10-20%) are the main components of this facies and shows a high degree of compaction (Fig. 7D). It fills fractures in the Dengying dolostone and also contributes to the clasts of the conglomerate described below.

Interpretation

The increase in the proportion of angular quartz from the sandy dolostone of the Dengying Fm. to the overlying phosclast-grainstone of the Zhujiaqing Fm. is perhaps explained by an increase of terrestrial influx thus causing the demise of the Dengying Formation carbonate factory. However, this microfacies is only a few cm thick and discontinuous in the Meishucun quarries.

4.2.4. Zhujiaqing Formation: Conglomerate

Two conglomerate varieties can be recognized within the quarries: Type 1 is composed of poorly sorted, subangular clasts of black phosphatic mudstone, soft-sedimentarily deformed quartz-rich phosgrainstone and chert clasts, which range approx. 3 to 20 mm (Fig. 8A) in diameter. These clasts are embedded in a white matrix of microcrystalline quartz with minor proportions of clay- and silt-sized muscovite. Conglomerate Type 2 is similar in texture and distribution, but principally composed of clasts of grey phosphatic bindstone, chert and reworked stromatolite fragments (Fig. 8B). Clast sizes range from 0.5 to 5 cm. Its matrix is composed of quartz sand, clay, dolomite silt and iron oxides.

Both conglomerate types only reach 5 to 50 cm in thickness, immediately overlie the Dengying dolostone and also fill the fractures at its surface; they are therefore highly discontinuous.

Interpretation

The monomict composition, subangular shape and soft-sediment deformed clasts in the Type 1 conglomerate indicates a proximal deposit; clasts probably originated from a nearby phosphatic mud flat. The composition of Type 2 conglomerate clasts resembles that of the overlying sediment. It may therefore represent a transgressive lag.

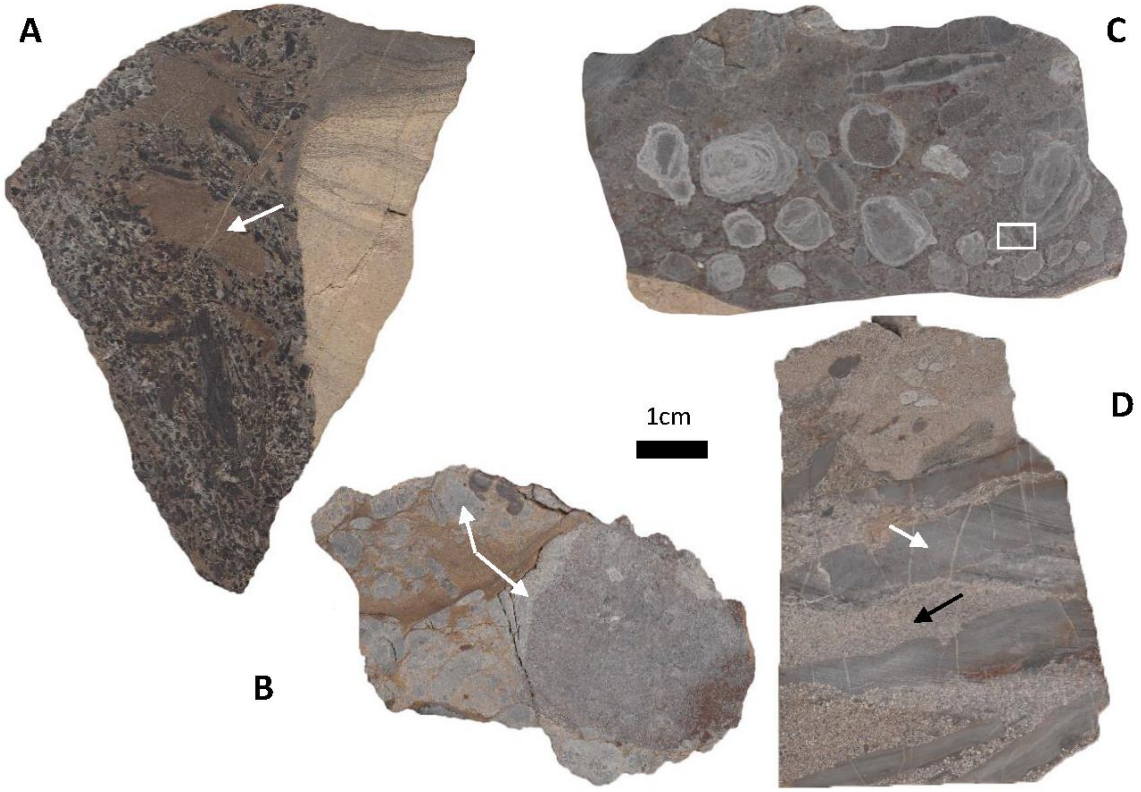

Fig. 8. *Slabbed and polished hand specimens of representative lithologies and sedimentary structures of Zhujiaqing Formation conglomerates and phosclast-rudstones above the E-C contact at Meishucun. A) Type-1 phosclast conglomerate with several dark brown soft-sedimentarily deformed clasts (arrow). This conglomerate forms the typical crack-filling sediment. B) Type-2 conglomerate. Clasts are phosphatic bindstone fragments (e.g., arrows); matrix is composed of quartz sand, clay, dolomite silt and iron oxide. C) Phosclast rudstone rich in asymmetrically grown phosphatic oncoids within silica cement. Framed area is shown in Fig. 9A. D) Phosclast rudstone showing angular, elongate chert clasts (white arrow) and poorly sorted, well rounded phosclasts (black arrow).*

4.2.5. Zhujiaqing Formation: Phosclast-rudstone

In Quarry 2, the phosclast-rudstone is mainly composed of bluish grey, poorly sorted phosphatic oncoids (5 to 15 mm in diameter), phoslithoclasts, and phosphatic fossils within silica cement (Fig. 8C). In Quarry 4, 5 to 10 cm-long chert clasts with internal fine lamination in the phosclast-rudstone account for about 30 - 40% of all clasts (Fig. 8D). The remaining clasts compose light grey, poorly sorted, well-rounded and silica-cemented phosclast-grainstone.

In thin sections, the nuclei of phosphatic oncoids commonly consist of phosphatic bindstone clasts, and the cortexes show uneven and discontinuous laminae. Their shape and the asymmetrical width of laminations suggest stationary growth. The layering of the oncoids is composed of phosphatic micrite and includes some pellets (Fig. 9A). Phosphatic fossils resembling SSF fragments exist in the form of subrounded fragments. Silified cement is widespread in the phosclast-rudstone; phosclasts are also silicified starting from their edge, thus forming rugged grain edges (Fig. 9B).

Interpretation

Oncoids are often used as indicators of a high-energy, low-intertidal to shallow-subtidal environment because it is thought that the growth of oncoids requires frequent overturning and rolling, so that the degree and duration of turbulence will contribute to oncoid shape (Flügel 2009). Lobate growth forms of phosphatic oncoids may indicate less frequent rolling and thus somewhat less energetic, quieter conditions. Laminated chert now represented as clasts derived from silicified, formerly micritic carbonate which was eroded from the underlying sediments. The orientation of the chert clasts locally shows imbrication, which may indicate rapid and shallow flow, such as in tidal channels.

4.2.6. Zhujiaqing Formation: Phosphatic bindstone

Phosphatic bindstone is widespread in the lowermost part of the section. Grains are bound by adhesive microbial films, and microbial laminae may laterally grade into stromatolites. Clusters of small domal stromatolites on top of the Dengying Formation are columnar-branching, up to 3 cm high, exhibit bulbous geometry and are partly phosphatized (Figs. 9C, 9D). The interstices between the stromatolites are filled by well-rounded but poorly sorted quartz grains, phosphate clasts, and grains of various types of diagenetic silica including microcrystalline quartz, chalcedony, and megaquartz. The excellent rounding of the quartz grains indicates long-term abrasion in a high-energy setting. Fibrous apatite around phosclasts formed during early diagenesis (Figs. 9E, 9F), more details about diagenesis will be discussed in section 4.3.

Interpretation

The growth of microbial lamination and stromatolites usually requires a low degree of terrigenous contamination. Judging from the small size, bulbous shape, and the low degree of stromatolite branching, the setting may have been of medium energy. This unit likely formed in a shallow nearshore subtidal setting.

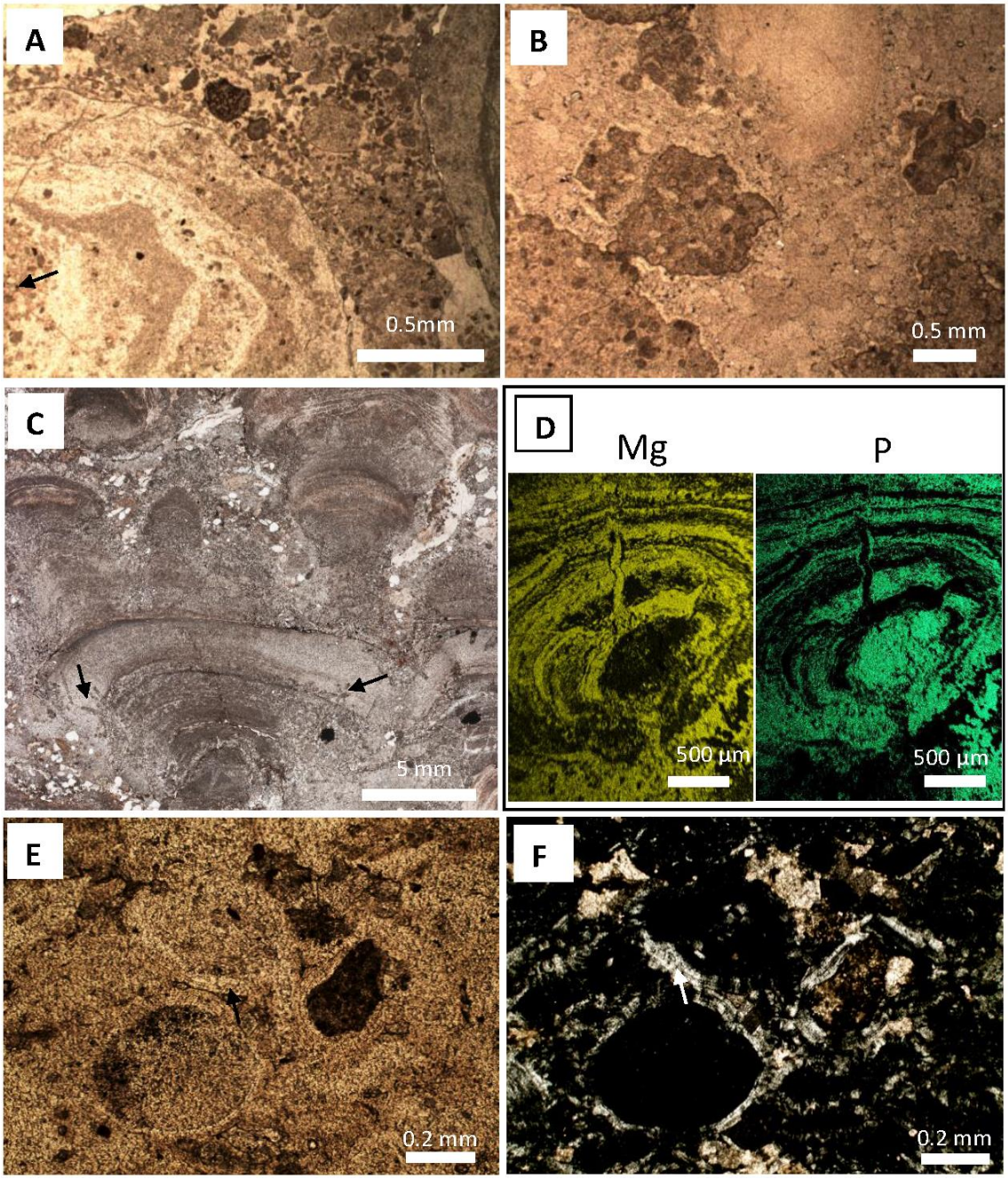

Fig. 9. *Thin-section photomicrographs of phosclast-rudstone and phosphatic bindstones of the Zhujiajing Formation at Meishucun (Bed 3). A) Thin section of part of Figure 8C. The oncoid core is a phos-bindstone clast (arrow). Phosphatic micrite containing phos-peloids form microbial oncoid laminae. B) Phosclast rudstone. Phoslithoclasts float in silica cement. Silicification extends into the clast edges. C) Cross section of stromatolite growing on exposed top-Ediacaran surface. Stromatolitic base (center) branches into three columns (top). Well-rounded quartz and phosphorite grains fill interstices. Random-oriented crystal clusters consist of barite (arrows). D) SEM-backscattered electron (BSE) element maps of Mg and P of a single stromatolite bulb showing alternating phosphate-carbonate composition. E, F) Phosphatic bindstone in plane- (E) and cross-polarized light (F). Laminas around grains represent fibrous apatite cement (arrows). The low degree of compaction indicates early cementation.*

4.2.7. Zhujiaqing Formation: Phosclast-grainstone to packstone

The rock is cemented by patchy dolospar or by silica. Lithoclasts consist of quartz, peloids and phosphatic intraclasts in dolomite-cemented packstone (Figs. 10A, B), and of phosphatic ooids and coated grains in silica-cemented grainstone. Phosphatic ooids are spherical or elliptic superficial ooids with thin coats of radial fibrous laminae; some ooids are compound ooids. Phosphatic oncoids are irregular to spherical. Acicular translucent objects, likely fragments of sponge spicules, are common in the matrix of phosclast-packstone (Fig. 10 C, D). The original matrix was partly phosphatized prior to dolomitization, indicated by small phosphate concretions in the matrix. The phosclast-grainstone shows two generation of cement: An earlier fibrous to microcrystalline isopachous cement is overgrown by a second-generation, pore-filling chalcedony which shows brownish color under polarized light due to impurities, possibly traces of iron oxide (Fig. 10E, F).

Interpretation

Phosphatic ooids and oncoids are commonly related to microbial activity (Siegmund et al., 1994, 1995; Trappe, 1998) and form in the suboxic zone near the water-sediment interface in a restricted, mildly agitated marine low-energy environment. The isopachous silica cement indicates an early diagenetic marine-phreatic origin in which carbonate or phosphate was not available. The lithoclasts, especially the phosphatic intraclasts, were probably transported by storm events into the tidal flats and subsequently cemented by carbonate.

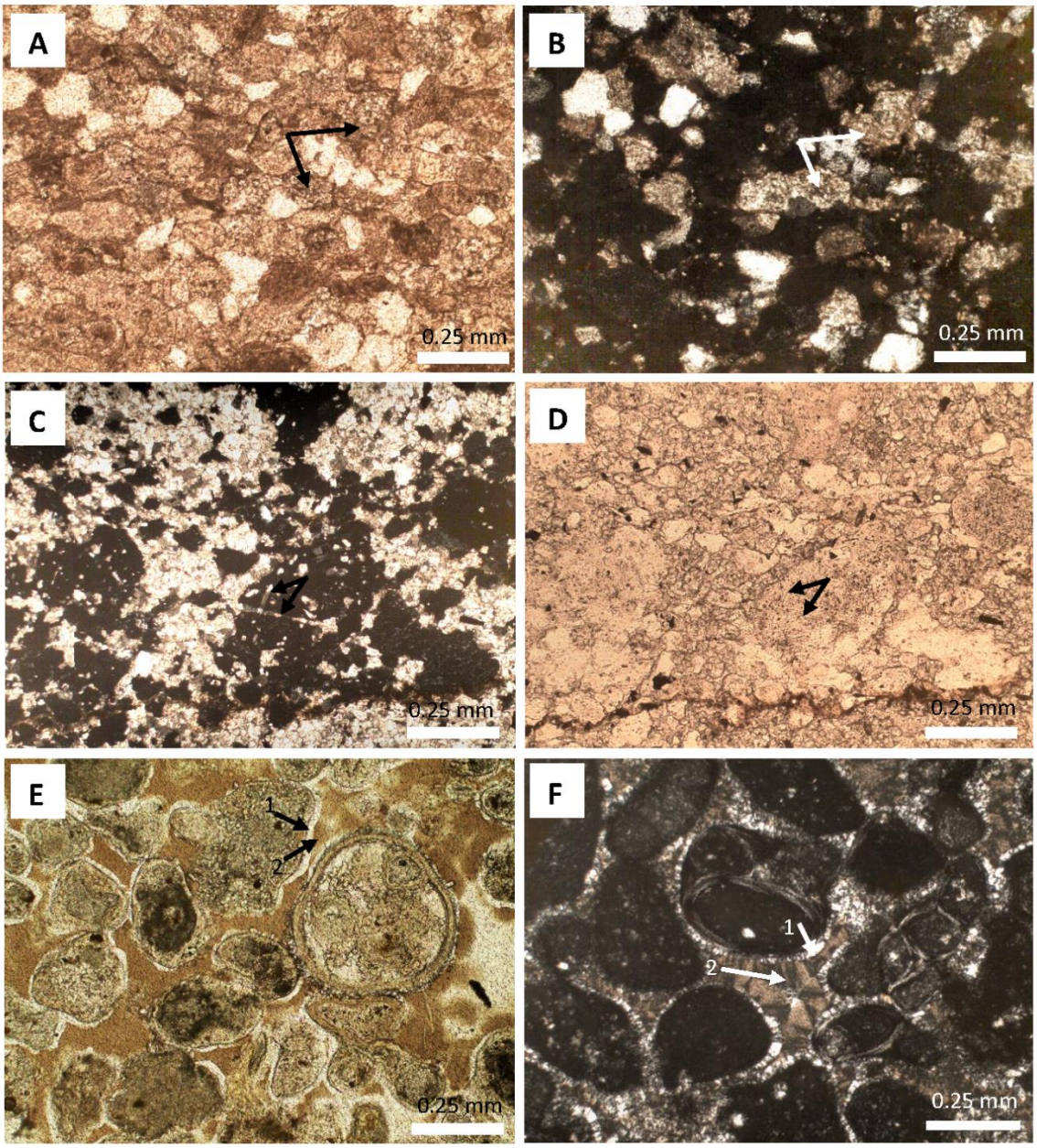

Fig. 10. *Representative thin section photographs of Zhujiaqing Fm. phosclast-grainstone to packstone. A) Phosclast-grainstone in plane-polarized light with poikilitic dolospar cement with cloudy or milky crystal surface (e.g., arrows). B) Same view under cross-polarized light. C, D) Well-rounded but poorly-sorted phosclast-packstone with dolomitized sponge spicule fragments (arrows). Cross-polarized (C), plane-polarized light (D). E, F) Phosclast grainstone in plane-polarized light (E) composed of abundant phosphatic and compound ooids and microbial peloids. Laminae are composed of fibrous apatite. Two phases of silica cement formed around grains and in pore space: The first phase is isopachous, fibrous to microcrystalline (arrow 1); the second is pore-filling chalcedony (arrow 2). Cross-polarized light (F).*

4.5.3. Cementation and diagenesis

The dolostone (Bed 2) and lower phosphorite units (Bed 3 and 4) are cemented by a complex mixture of apatite (A), dolomite (D) and silica (S). Thin-section observation on the geometrical relationship

between the cementing minerals and their fabric allows to derive the following diagenetic processes (Table 1):

(1) An early authigenic, widespread, isopachous radial-fibrous apatite (A1) coated and cemented phosclasts and lithified oncoids in-situ. This type of microcrystalline cement is common in phosphatic bindstone (Figs. 9E, F). Microsphorite apatite (A2) is cryptocrystalline and grows as small nodules in the matrix (Figs. 10C, D) of phosclast-packstone.

(2) In the lower phosphorite (Bed 3 / Bed 4), nonplanar anhedral poikilitic and cloudy coarse grain dolomite (D1) is present in phosclast-packstone (Figs. 10A, B). Neomorphic medium- to coarse-grained clear dolomite crystals (D2) occur in the sandy dolostone of the Dengying Formation (Fig. 7C). This cement luminesces red (Figs. 11 A and B). Planar to subhedral blocky dolomite (D3) is prevalent in recrystallized dolomudstone and fills the voids of stromatolitic bindstone (Figs. 11 C, D); in the latter, it luminesces greenish and red.

(3) Silica cement and replacement: Chalcedony (S1) formed as cement and pore-fill in phosclast-grainstone (Figs. 10E, F). Colorless megaquartz (S2) occurs in the phosclast -rudstone as replacement. The size of the megaquartz crystals increases towards the center of the pore space. Some phosphate grains are completely replaced by quartz (Figs. 11E, F). Microcrystalline quartz (S3) as replacement usually occurs in dolostone, mostly as chert bands 5-10 cm thick and parallel to bedding planes (Fig. 5A) or in irregular shapes (Fig. 7A). This cement type is translucent but slightly brownish under plane light, which is mainly due to abundant fluid inclusions. Length-slow chalcedony (S4) occurs in some phosclast-grainstone samples (Figs. 11G, H) or in the core of oncoids in the phosclast-rudstone.

Interpretation:

The cementation history is complex and involves several generations of apatite (A), dolomite (D), and silica (S).

(1) The phosphatic bindstone shows early in-situ phosphogenesis, which plausibly relates to the microbial activity evidenced by the microbial lamination. Judging from the cement fabric and the low degree of compaction, fibrous apatite cement (A1) formed in a shallow-marine to early burial diagenetic environment. Microsphorite apatite (A2) formed concretions in the dolomitic matrix of the phosclast-packstone. Some concretions coalesce; others grow along the margins of phoslithoclasts, thus gradually enlarging their size. This type of phosphatization usually occurs under conditions of low sedimentation rates, a few centimeters below the water-sediment interface (Southgate, 1986).

(2) The D1 dolomite cement in the lower phosphorite is patchy in Bed 3. Its cloudy surface and poikilitic texture indicates secondary dolomitization of carbonates. Some D1 crystals even replace the early diagenetic phosphate. Crystals of cement generation D2 crosscut grain boundaries (Fig. 6B), which is typical for late-stage recrystallization due to burial diagenesis. Dolomite-cement generation D3 shows straight crystal boundaries, implying long-time growth in open space. Its crystals show well-developed zonal luminescence, perhaps due to different trace element content in the pore waters.

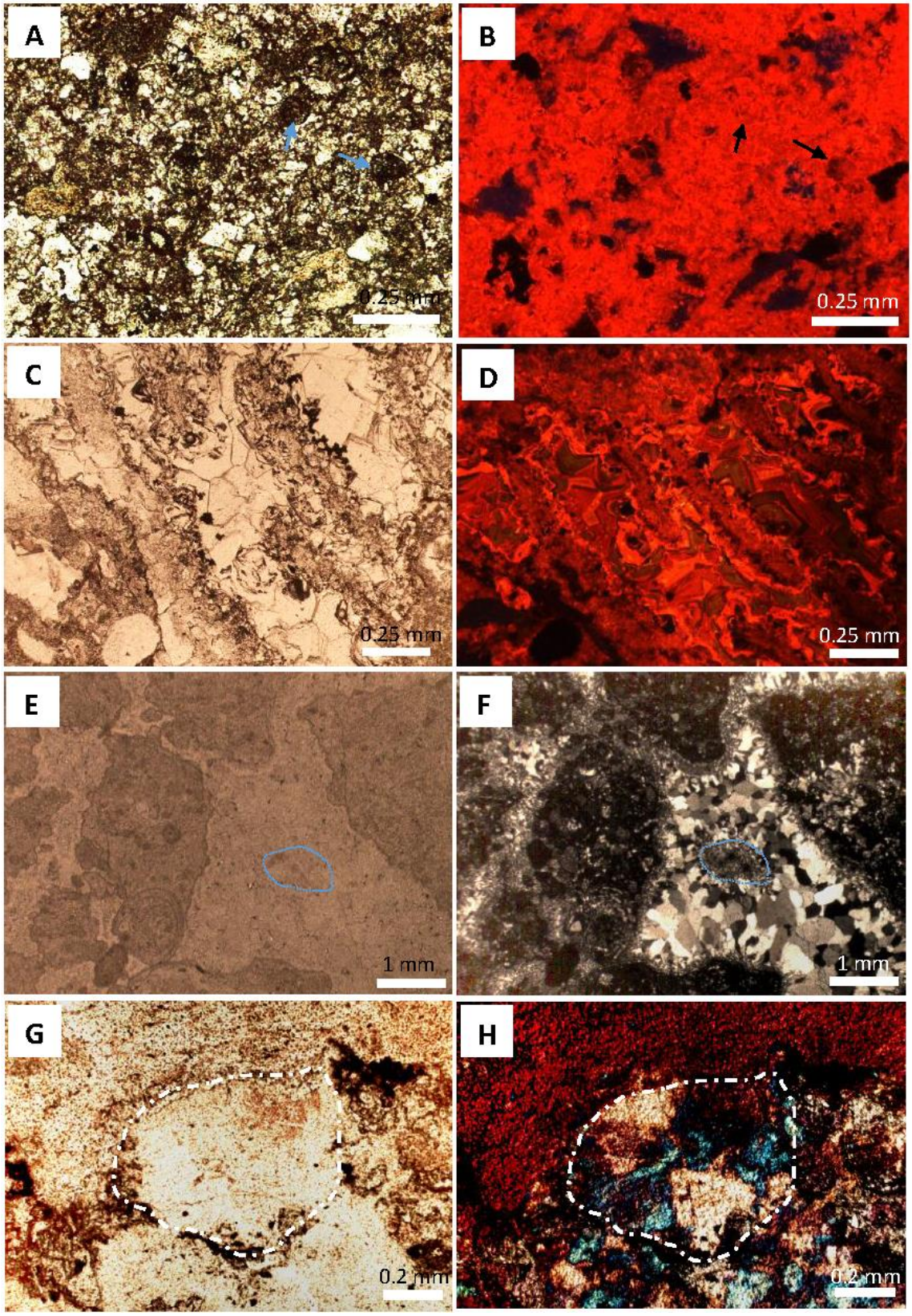

Fig. 11. *Thin-section photomicrographs and cathodoluminescence (CL) images illustrating dolomitization and silicification at Meishucun. A, B) Sandy dolostone of Ediacaran Dengying*

Formation. A: sandy dolostone under plane-polarized light. B: Dominant red luminescence (dolomite crystals). The original texture is shown by contrasting dark and bright luminescence (e.g., arrows show dolomitized ooids), quartz and phosphate grains are non-luminescent. C, D) Recrystallized dolomudstone of Ediacaran Dengying Fm. C: Blocky voids filling under plane-polarized light. D: Luminescence of blocky void filling showing well-developed zoning. E, F) Megaquartz of Zhongyicun Formation phosclast-rudstone (Bed 3). Note that some phosclasts are completely replaced by small sized quartz crystals (e.g., blue circle). The size of megaquartz crystals increases towards the pore center. E) Plane-polarized light, F) Cross polarized light. G) Length-slow chalcedony (white circle) under plane-polarized light in Zhongyicun Formation phosclast grainstone. H) Same view under cross-polarized light with gypsum plate.

(3) The first-generation silica cement S1 commonly consists of two phases: An inner fibrous and an outer botryoidal fabric, both indicating a marine phreatic diagenetic environment. S2 megaquartz fills the pore space and also replaces original lithoclasts during burial diagenesis. S3 silicification was highly selective in recrystallized dolostone, andoccured parallel to bedding planes or along sedimentary structures. S4 is only locally observed in phosclast-grainstone and consists of length-slow chalcedony, which is commonly interpreted as replacement of gypsum (Pittman and Folk, 1971). Liu et al. (1990, 1994) did detailed work on the siliceous components in phosphorite. They interpreted the siliceous component in shallow-water platform phosphorites to be a result of mixing sea water with fresh water, as proposed by Knauth (1979). This process is plausible in the very shallow subtidal environment at Meishucun. Besides, Li et al. (1994), based on a Si isotope study at Meishucun, plausibly suggested a terrestrial silica source.

Extensive chert at the E-C contact is also widespread in Oman (Athel Formation; Ramseyer et al., 2013), the Himalayan Cambrian (Lower Tal Formation; Tiwari, 1999), and southern Kazakhstan (basal Chulaktau Formation; Heubeck et al., 2013); therefore, early diagenetic origin of silica cement generations cannot be ruled out.

In addition, very local, patchy distribution of thick quartz veins and the patchy occurrence of hydothermal galena and barite in Dengying Fm. dolostone at Meishucun demonstrates that minor chert might remobilized during late hydrothermal activity, but this event appears to be a very late stage relates to eruption of Emeishan basalts in the Permian (Bai et al., 2013).

Table 1. *Summary of cement petrography. See text for details and interpretation*

Petrography					Diagenetic environment
Cement type	Mineralogy	Color under polarized light	Response to cathodo-luminescence	Cement fabric	
fibrous	apatite (A1)	pale gray	non-luminescent	isopachous	shallow- marine; early diagenetic
microsphoritic	apatite (A2)	light brown-transparent	non-luminescent	micro-concretionary	shallow burial
nonplanar anhedral	dolomite (D1)	cloudy or milky	not investigated	poikilitic	burial
neomorphic anhedral	dolomite (D2)	colorless	reddish with yellow spots	coarse grained, granular mosaic	burial
blocky subhedral	dolomite (D3)	pale yellow	zoned greenish and reddish	blocky mosaic	burial
fibrous and botryoidal	chalcedony (S1)	colorless to brown	not investigated	isopachous to botryoidal	marine phreatic; early diagenetic
planar subhedral	megaquartz (S2)	colorless to brown		mosaic or drusy mosaic	shallow burial
silicified replacive	micro-crystalline quartz (S3)	slightly brownish		equant mosaic	shallow burial
	length slow chalcedony (S4)	transparent		fibrous botryoidal	shallow burial

4.5.4. Geochemical data

The total REE (∑REE) and Y content of acetic acid leachates of a suite of five sedimentary rocks from the karsted E-C-contact is low and highly variable. It ranges from 0.40 to 12.09 ppm for ∑REE, and from 0.02 to 5.56 for Y (Table 2, Fig. 12). Low REE and Y contents were found for carbonate leachates of the quartz-rich phosclast-grainstone (sample 12-2), the phosphate conglomerate clast (sample 12-3) and the phosclast-grainstone (sample 12-5) whereas the carbonate leachates of the conglomerate matrix (12-4) and the sandy dolostone (12-1) showed REE and Y contents almost 20 times higher due to the leaching method applied. The latter REE contents are similar to dolomitic cements of the Doushantuo Fm. in Weng'an mine (Chen et al., 2003). Samples 12-2 and 12-5 were omitted from further interpretation due to their very low carbonate content and the thus resulting very low REE contents in acetic acid leachates.

The PAAS-normalized REE+Y patterns of the remaining three carbonate leachates are characterized by general LREE and variable HREE depletion, slightly negative Ce/Ce* (0.6 to 0.8), and variable Eu anomalies (Fig. 12). They display seawater-like REE+Y patterns with relative enrichment of HREE over LREE (Pr_N/Yb_N = 0.35 - 0.44) as well as an almost flat PAAS-

Table 2. *Yttrium, barium and rare-earth-element data from acetic-acid carbonate leachates of Ediacaran-Cambrian boundary lithologies at Meishucun, Yunnan (South China). Subscript N means that REE+Y concentrations are normalized to PAAS (McLennan, 1989).Ce/Ce* and Eu/Eu* are calculated according to Bau and Dulski (1996)*

Sample		12-1	12-2	12-3	12-4	12-5
Lithology		Sandy dolostone	Qtz-rich phosclast grainstone	Conglomerate (type 2) clast	Conglomerate matrix	Phosclast grainstone
Strat. Hight	[m]	0.29	0.38	0.5	0.55	0.73
La	[ppm]	2.271	0.088	0.13	3.47	0.057
Ce	[ppm]	2.751	0.11	0.147	4.054	0.093
Pr	[ppm]	0.391	0.016	0.023	0.632	0.014
Nd	[ppm]	1.615	0.087	0.132	2.388	0.073
Sm	[ppm]	0.326	0.017	0.024	0.366	0.015
Eu	[ppm]	0.116	0.029	0.03	0.109	0.037
Gd	[ppm]	0.418	0.028	0.042	0.392	0.023
Tb	[ppm]	0.065	0.004	0.005	0.051	0.003
Dy	[ppm]	0.445	0.025	0.036	0.264	0.022
Ho	[ppm]	0.105	0.006	0.009	0.051	0.005
Er	[ppm]	0.333	0.02	0.026	0.147	0.016
Tm	[ppm]	0.044	0.002	0.003	0.018	0.002
Yb	[ppm]	0.281	0.014	0.018	0.114	0.012
Lu	[ppm]	0.064	0.022	0.023	0.036	0.022
∑ REE	[ppm]	9.225	0.468	0.648	12.092	0.394
Y	[ppm]	5.562	0.112	0.294	2.106	0.029
Ba	[ppm]	175.73	89.88	86.43	66.41	122.10
Ce/Ce*		0.666	0.672	0.617	0.627	0.754
Eu/Eu*		0.984	2.068	1.650	1.170	2.682
Pr_N/Yb_N		0.444890	0.347392	0.396838	1.771465	0.368836
Y_N/Ho_N		1.942717	0.654755	1.241669	1.529607	0.201049

Table 3. *Sr isotopic composition ($^{87}Sr/^{86}Sr$) and Sr and Mn content from acetic acid carbonate leachates of Ediacaran-Cambrian boundary lithologies at Meishucun, Yunnan (South China)*

Sample	**Lithology**	**Strat. Height [m]**	**Sr [ppm]**	**Mn [ppm]**	**Mn/Sr**	**$^{87}Sr/^{86}Sr$**	**2SD**
12-1	Sandy dolostone	0.29	36.9	1967	53.23	0.71106	0.000302
12-2	Quartz-rich phosclast grainstone	0.38	120	51.5	0.43	0.71637	0.000147
12-3	Conglomerate clast	0.5	197	45.4	0.23	0.71307	0.000081
12-4	Conglomerate matrix	0.55	83.3	10.8	0.13	0.71421	0.000112
12-5	Phosclast grainstone	0.73	176	22.9	0.13	0.71267	0.000075

-normalized REE+Y pattern (Pr_N/Yb_N = 1.77). The PAAS-normalized REE pattern of the carbonate-leachate of the sandy dolostone indicates a marine origin with relative enrichment of HREE over LREE (Pr_N/Yb_N = 0.44) and superchondritic Y_N/Ho_N ratios (1.94). A similar pattern was observed for sample 12-3 (i.e., the clast of the Type 2 monomict conglomerate), which also yields a marine signal, with Pr_N/Yb_N = 0.40 and Y_N/Ho_N = 1.24 but with a positive Eu anomaly. However, inter-elemental interferences of BaO with Eu during ICP-MS analysis usually compromise the results (Ba/Sm ratios show positive correlation with Eu/Eu* in our samples). The PAAS-normalized REE+Y pattern of the carbonate leachate of the conglomerate matrix (sample 12-4) is almost flat. This finding may either question a pure marine origin or be a result of a diagenetically induced preferential depletion in HREE (Shields and Stille, 2001). We prefer the former explanation because the carbonate component of sample 12-4 is transported dolomite silt which was deposited as conglomerate matrix.

The strontium isotopic composition ($^{87}Sr/^{86}Sr$) of the carbonate leachates of all samples from the karsted E-C- contact varies highly between 0.70985 and 0.71539 (Table 3 and Fig. 12), with lowest $^{87}Sr/^{86}Sr$ ratios observed for the sandy dolostone (12-1) of the Dengying Fm. and highest $^{87}Sr/^{86}Sr$-ratios for the quartz-rich phosclast-grainstone (12-2) of the Zhujiaqing Fm. All $^{87}Sr/^{86}Sr$-ratios, however, differ significantly from the coeval seawater Sr isotopic composition, which was determined assessing the $^{87}Sr/^{86}Sr$ ratios of terminal Neoproterozoic to lower Cambrian carbonates (0.7080 to 0.7090; Jacobsen and Kaufman, 1999; Veizer et al., 1999). The Sr isotopic composition of the studied samples thus implies that their Sr isotopic composition is likely altered because of post-depositional Sr exchange and/or mobilization.

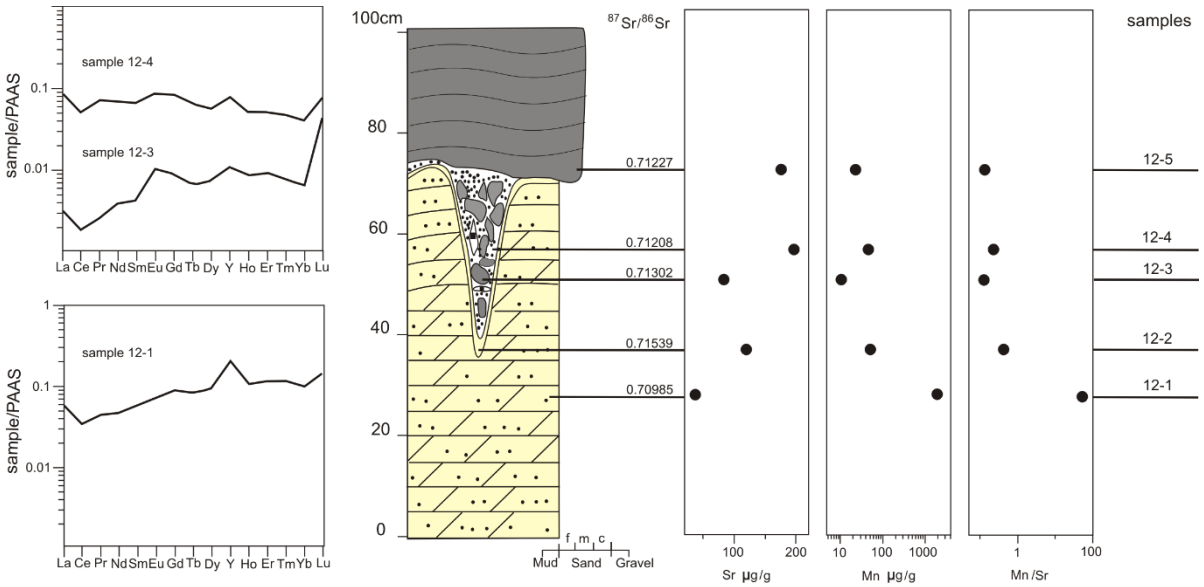

Fig. 12. *Distribution of trace elements (Mn, Sr) and REE+Y patterns (normalized to PAAS (McLennan, 1989)) of acetic acid carbonate leachates of five samples at E-C contact, which are (in ascending order) named 12-1, 12-2, 12-3, 12-4, and 12-5. The $^{87}Sr/^{86}Sr$ isotopic composition of carbonate leachates*

ranges from 0.70985 in the sandy dolostone (12-1) of the Dengying Formation to 0.71539 in quartz-rich phosclast-grainstone (12-2). Elevated $^{87}Sr/^{86}Sr$ (0.70985) values, together with high Mn/Sr ratios (53.2) in sample 12-1 suggest diagenetic alteration of the sample. Carbonate leachates of samples 12-1 and 12-3 show REE+Y patterns similar to seawater with relative enrichment of HREE over LREE (Pr_N/Yb_N = 0.4 - 0.44, Y/Ho =1.24-1.94). Sample 12-4 (conglomerate matrix) shows an almost flat REE+Y pattern (Pr_N/Yb_N = 1.77, Y/Ho =1.53), which likely reflects a modified seawater composition.

4.6. Discussion

4.6.1. Reginal synthesis of facies pattern of the E-C contact

The medium-bedded fenestral micritic dolostone and very-fine-grained, grain-supported sandy dolostone of the topmost Dengying Formation indicate a high-energy coastal, photic-zone, possibly tidal environment. The uneven top surface of this unit, the surficial cavity fills along it, as well as the lateral lithological and thickness changes over short distances in the overlying phosphorite, including wedging and onlap (Fig. 6F), clearly indicate the existence of topographic and bathymetric relief, resulting in a hiatus related to subaerial exposure and karstification (Qian et al., 1996). This hiatus is documented throughout northeastern Yunnan, where it was described by Zeng et al. (1994) as a third-order sequence boundary. Erosion of the Dengying Formation is thought to be more substantial in adjacent northwestern Guizhou and further north in central Sichuan Provinces, but appears to be low or nil in northeastern Yunnan (Zhu et al., 2004; Li et al., 2013). Clearly, the hiatus so well exposed in the Meishucun quarries is not a local phenomenon, but extends throughout the Yangtze platform; it may even be global (Cowie and Brasier, 1989).

At Meishucun, sedimentation resumed in a shallow subtidal, medium-energy environment represented by a cm-thin, discontinuous veneer of sandstone, lenticular microconglomerate and thin patches of desiccated mudstone between subaerially exposed limestone. This depositional environment was initially covered by microbial mats and stromatolites growing in a well-agitated photic zone. Only during the subsequent transgression, accompanied by low sedimentation rate, the local formation and winnowing of granular phosphorites began. These granular phosphorites also record the first mass appearance of small shelly fossils.

The depositional processes across the E-C transition at Meishucun section thus include an initial significant sea-level-lowering event, which produced a karsted surface in the Dengying carbonates. The karsting event was followed by a transgression, during which granular phosphorite deposited along with the mass appearance of small shelly fossils. The phosphorite deposition is interrupted by a deposition of mudstone (Bed 5) typically containing volcanic tuff beds. Because this mudstone unit is not present at the Maotianshan outcrops ca. 30 km east (Sato et al., 2013), its deposition was probably local and occurred in a relatively shallow protected setting, perhaps in a few tens of meters water depth.

4.6.2. Deposition of the basal Cambrian phosphorite at Meishucun

The basal Cambrian phosphorites (commonly, phosphorites are defined as rock contain > 18% P_2O_5) form one of the world's largest phosphate deposits but the processes responsible for their formation

remain debated (Cook and Shergold, 1986; Brasier, 1990b; Donnelly et al., 1990; Cook, 1992; Parnell et al., 2014). Phosphorites of the lower-middle Cambrian, and commonly of similar lithological and facies associations, also occur in the Indian Himalaya (Tal Fm.; Mazumdar and Banerjee, 2001), Tarim (Yurtus Fm.; Yao et al., 2014), Australia (Georgina Basin, Gowers Fm.; Southgate, 2005), and Kazakhstan (Chulaktau Fm.; Heubeck et al., 2013). Elevated P_2O_5 concentrations in E-C boundary sections are recorded nearly worldwide (e.g., Kimura et al. 1997 from Iran; Strauss et al., 1997 from Poland).

Although details and perhaps even major arrangements of the paleogeography are still debated, paleomagnetic data and biostratigraphy indicate that the (micro-) continents India, South China, Australia and Tarim were all located near each other at near-equatorial latitudes along the outer-Gondwana passive margin (Steiner et al., 2007; Li et al., 2008; Santosh et al., 2013). This paleogeographical position would have been ideal for large-scale regional upwelling to occur, making it plausible that – on a regional scale – P was supplied by nutrient-rich oceanic water.

Sato et al. (2013) proposed an alternative scenario for P supply. According to outcrop and drill core studies about 30 km east of Meishucun, these authors suggested that the formation of basal Cambrian phosphorites in Yunnan occurred by primary precipitation of phosphate from seawater that had become enriched in phosphorus derived from alkaline volcanics in restricted embayments along a now-eroded shoreline to the west. Deposition was followed by erosion, reworking and eastward transport of the lithified phosphatic sediments as detrital grains to the current outcrop area of the Zhongyicun Member where they were deposited in a subtidal setting. Aside from the lack of evidence of such volcanism and shorelines, this interpretation also contrasts with the apparently autochthonous nature of phosphatic rinds on the abundant phosphatic ooids and oncoids in the Zhongyicun Member phosclast-grainstones. Any phosphatic ooids, phosphatic oncoids and phosintraclasts which would have formed in hypothetical shallower-water settings further west would have been too fragile to have survived transport which would have exceeded several 10s of km.

We rather suggest that microbial activity influenced local P concentration in the early Cambrian, thus providing the ambient conditions for phosphogenesis. Microbial activity and cyanobacterial blooms are suggested to play an important role in P precipitation (Scopelliti et al., 2009; Goldhammer et al., 2010; She et al., 2013, 2014). She et al. (2013), studying the terminal Proterozoic granular phosphorites of the Doushantuo Formation proposed that the phosphoritic granules had formed by microbially mediated accretionary growth followed by rapid phosphatization at the sediment-water interface. Similarly, the phosphorite microtexture at Meishucun suggest that most phosphorite grains consisted of phosphatic algae and bacteria (Zeng et al., 1993).The subsequent low sedimentation rate allowed for sufficient time to form early diagenetic phosphate rims.

Composition and texture of the base-Cambrian strata clearly demonstrate that the karsted E-C surface provided a substantial bathymetric paleorelief. The Meishucun coast bordered an extensive low-latitude photic-zone carbonate environment in which currents distributed nutrients. During earliest Cambrian,

the Ediacaran-type biomat-dominated habitats were still widespread in shallow marine setting in eastern Yunnan (Weber et al., 2007), the low permeability of fine-grained carbonate, widely covered by microbial films, favored a sharp oxic-anoxic transition near the sediment-water interface where suboxic pore water environments, in which organic matter was degraded and P was enriched could develop quickly (e.g., Krajewski et al., 1994). This shallow and narrow redox transition zone possibly resembled those in many present-day carbonate tidal flats. Phosphoritic sands in the medium-energy setting were subject to periodic gentle reworking which liberated P-rich pore waters from micro-pores and made them available to precipitate in oncoid laminae and – where energy was somewhat higher – as carbonate fluorapatite (CFA) coatings on ooid nuclei. Carbonate and detrital mud, being lighter in weight than CFA, was preferentially washed or winnowed away.

The activity of sulfur-metabolizing microorganisms has been suggested as the major cause of the release of phosphorus and subsequent formation of phosphorites. For example, Schulz and Schulz (2005) demonstrated that the benthic giant sulfur bacteria *Thiomargarita* scavenge enormous amounts of polyphosphate under oxic conditions from seawater and periodically release phosphorus into the pore water when conditions turn anoxic. These phosphorus pulses create temporally and locally restricted pore waters supersaturated with respect to phosphate which make rapid shallow-water CFA deposition possible. Unfortunately, redox-sensitive elements are not enriched enough in the phosphorites at Meishucun, to allow a reliable assessment of the paleo-redox conditions (Xu et al., 2014), and Shield and Stille (2001) caution against the use of REE anomalies of phosphorites as a proxy of paleo-seawater composition.

2.6.3. Depositional gaps in E-C sedimentary sections

Erosion or omission of underlying strata at the Pc-C boundary is globally widespread and expressed by regional unconformities in Siberia (where base-Cambrian strata are also underlain by karstified late Neoproterozoic limestones; Pelechaty et al., 1996) and above late Neoproterozoic rocks in Australia, Canada and England. Many authors (e.g., Peters et al., 2012; Maruyama et al., 2013; Parnell et al., 2014) suggested that the vast terrestrial weathering and denudation at the end of the late Ediacaran washed in abundant nutrients into the ocean, which were re-distributed during the Cambrian transgression. This re-distribution of nutrients subsequently affected the biogeochemistry recorded in marine sections across the E-C boundary.

Aside from the hiatus between the Dengying Formation and Zhujiaqing Formation, significant additional stratigraphic gaps also exist stratigraphically above the Zhujiaqing Formation in the Kunyang phosphorite mine. Li et al. (2013) correlated the Meishucun section with the Laolin and Xiaotan sections in northern Yunnan and pointed out depositional hiati below and above the Zhongyicun Member at Meishucun. Biostratigraphically, the hiatus above the Zhongyicun member at Meishucun omits SSF Zone 3, which is represented mainly by carbonates in the sections of northern Yunnan (Yang et al., 2014). The fact that erosion and weathering was likely more pronounced in southern Yunnan than in

northern Yunnan is also recorded in the comparison of averaged carbon isotope signatures. At Meishucun, the top of the Dengying Fm shows $\delta^{13}C_{carb}$ values of about -2 ‰, while other sections of the top of the Dengying Fm. in northern Yunnan show $\delta^{13}C_{carb}$ values between 0 and 2 ‰ (Li et al., 2013). This finding might either be explained as a surface- to deep-water $\delta^{13}C$ gradient (Jiang et al., 2007) or as a result of pronounced erosion in southern Yunnan accompanied by meteoric diagenesis processes that favored the incorporation of light atmospheric CO_2 in the carbonate (Oehlert and Swart, 2014).

2.6.4. Diagenesis and alteration

Post-depositional alterations have affected the rocks at Meishuncun section and may be caused by meteoric and/or hydrothermal fluid flow, widely obscuring primary sedimentary textures and/or geochemical signatures. Petrography of the complex assemblage of cement generations show an early diagenetic process dominated by phosphate and silica, and a late burial diagenesis affected dolomite.

During exposure, terrestrial input increased. Laminae and thin beds of mica- and quartz-rich sandstone on the exposure surface (subsequently strongly compacted by pressure solution during late burial diagenesis) may relate to this weathering pulse. Phosphorus, which was mainly brought in by marine transgression, formed early-diagenetic apatite cement and thus reduced compaction. Silica cementation, described above in 4.3, is rarely a very-early- or a very-late-stage diagenetic event. Rather, it is a product of early burial diagenesis, and late burial diagenesis further facilitated replacement.

The Mn/Sr ratio is a possible indicator of diagenetic overprint of carbonate rocks because the progressive diagenetic alteration generally increases Mn content while lowering the Sr content within carbonates (Veizer et al., 1999). Mn/Sr-ratios > 10 are thought to indicate late fluid flow alteration. Elevated $^{87}Sr/^{86}Sr$-ratios (0.70985) in sample 12-1 covariate with high Mn/Sr ratios (up to 53) and argue for an alteration of the samples, affecting the mobile element concentration and isotopic compositions and may indicate meteoric diagenesis, consistent with the presented geologic and petrographic data. Even though the spotty galena and barite mineralization in the Meishucun quarries provide evidence for hydrothermal activity, hydrothermalism appears to be late and did not affect the early and burial diagenetic processes at Meishucun.

4.7. Conclusions

A significant terminal Ediacaran sea-level-lowering event exposed an extensive carbonate tidal flat in southern China. Excellent sections exist at Meishucun, southern Yunnan Province, China, where terminal Ediacaran to early Cambrian exposure resulted in moderate karstification of the late Ediacaran Dengying Formation dolostone. When sea level rose again, a lower-intertidal to subtidal, medium- to high-energy phosphorite environment, now represented by the basal Cambrian Zhujiaqing Formation, was established on top of the extensive, uneven and fractured karsted surface which in places had been colonized by stromatolites. Common phoslithoclasts were mixed with abundant phosphatic ooids,

peloids, phos-intraclasts and phosphatic oncoids from open settings and low sedimentation rate. Early diagenetic phosphogenesis became widespread, especially manifested in phosphatic bindstones, and testifies to the important role of microbial activity immediately following the base-Cambrian transgression. The major source of phosphorus was likely related to coastal upwelling and fixation within extensive microbial mats. During early burial, the platform was affected by the mixing of sea water and fresh water, resulting in widespread silicification. The Ediacaran dolostone was likely influenced by meteoric early diagenesis and later by burial diagenesis. Analysis of rare-earth elements indicate that both carbonate cement and the carbonate component of the phosphorite are of marine origins. Depositional gaps of similar character also exist stratigraphically upward in the lower Cambrian of south China. Thus, to further understand the importance of unconformities relating to early Cambrian ecological turnover and associated event chains as well as for strata correlations, a larger stratigraphic interval needs to be considered.

4.8.Acknowledgements

This work was funded by the German Research Foundation (DFG Research Group FOR 736 "*The Precambrian-Cambrian Biosphere (R)evolution: Insights from Chinese Microcontinents*"). We are grateful to Shishan Zhang, Maoyan Zhu, Fangchen Zhao, Michael Steiner and Ben Yang for assistance during fieldwork, Anna Giribaldi (FU Berlin) for thin section preparations, and Kirsten Born (Museum für Naturkunde Berlin) for technical assistance in using the cathodoluminescence microscope. We thank all members of FOR 736 for discussions. XS is grateful for a scholarship from the China Scholarship Council (CSC) and a DAAD Abschlussstipendium.

References

Amthor, J.E., Grotzinger, J.P., Schröder, S., Bowring, S.A., Ramezani, J., Martin, M.W. & Matter, A. 2003. Extinction of *Cloudina* and *Namacalathus* at the Precambrian - Cambrian boundary in Oman. *Geology*, 31, 431-434.

Bai, J., Huang, Z., Zhu, D., Yan, Z. & Zhou, J. 2013. Isotopic Compositions of Sulfur in the Jinshachang Lead-Zinc Deposit, Yunnan, China, and its Implication on the Formation of Sulfur-Bearing Minerals. *ACTA GEOLOGICA SINICA*, 87, 1355-1369:

Bailey, J.V., Corsetti, F.A., Bottjer, D.J. & Marengo, K.N. 2006. Microbially – mediated environmental influence on Metazoan Colonization of matground Ecosystems: Evidence from the Lower Cambrian Harkless Formation. *Palaios*, 21, 215–226.

Brasier, M.D. 1986. Precambrian-Cambrian boundary biotas and events. *Global Bio-events*, 8, 109-116.

Brasier, M.D., Magaritz, M., Corfield, R., Luo, H.-L., Wu, X.-C., Ouyang, L., Jiang, Z.-W., Hamdi, B., He. T.-G. & Fraser, A.G. 1990a. The carbon- and oxygen-isotope record of the Precambrian-Cambrian boundary interval in China and Iran and their correlation. *Geological Magazine*, 127, 319-332.

Brasier, M.D. 1990b. Phosphogenic events and skeletal preservation at the Precambrian-Cambrian boundary interval. *Geological Society, London, Special Publications*, 52, 289-303.

Brasier, M.D., Shields, G., Kuleshov, V.N. & Zhegallo, E.A. 1996. Integrated chemo- and biostratigraphic calibration of early animal evolution; Neoproterozoic—Early Cambrian of Southwest Mongolia. *Geological Magazine*, 133, 445–485.

Charvet, J. 2013. The Neoproterozoic-Early Paleozoic tectonic evolution of the South China Block: An overview. *Journal of Asian Earth Sciences*, 74, 198-209.

Chen, D.F., Dong, W.Q., Qi, L., Chen, G.Q. & Chen, X.P. 2003. Possible REE constraints on the depositional and diagenetic environment of Doushantuo Formation phosphorites containing the earliest metazoan fauna. *Chemical Geology*, 201, 103-118.

Crimes, T.P. & Jiang, Z.W. 1986. Trace fossils from the Precambrian–Cambrian boundary candidate at Meishucun, Jinning, Yunnan, China. *Geological Magazine*, 123, 641-649.

Compston, W., Williams, I.S., Kirschvink, J.L., Zhang, Z. & Ma, G. 1992. Zircon U-Pb ages for the Early Cambrian time scale. *Journal of the Geological Society, London*, 149, 171-184.

Compston, W., Zhang, Z., Cooper, J.A., Ma, G. & Jenkins, R.J.F. 2008. Further SHRIMP geochronology on the early Cambrian of South China. *American Journal of Science*, 308, 399–420.

Cook, P.J. & Shergold, J.H. 1986. *Phosphate Deposits of the World; Volume 1: Proterozoic and Cambrian Phosphorites.* Cambridge University Press, England.

Cook, P.J. 1992, Phosphogenesis around the Proterozoic-Phanerozoic transition. *Journal of the Geological Society, London*, 149, 615-620.

Cowie, J. W. & Brasier, M. D. 1989. *The Precambrian – Cambrian Boundary.* Clarendon Press, Oxford.

Donnelly, T., Shergold, J., Southgate, P. & Barnes, C. 1990. Events leading to global phosphogenesis around the Proterozoic/Cambrian boundary. *Geological Society, London, Special Publications*, 52, 273-287.

Dornbos, S.Q., Bottjer, D.J. & Chen, J.Y. 2004. Evidence for seafloor microbial mats and associated metazoan lifestyles in Lower Cambrian phosphorites of Southwest China. *Lethaia*, 37, 127–137.

Flügel, E. 2009. *Microfacies of Carbonate Rocks: analysis, interpretation and application.* Springer, Berlin; Heidelberg.

Gradstein, F.M., Og, J.G., Schmitz, M.D. & Ogg, J.M. 2012. *The Geological Time Scale 2012.* Elsevier, Amsterdam.

Goldhammer, T., Brüchert, V., Ferdelman, T.G. & Zabel, M. 2010. Microbial sequestration of phosphorus in anoxic upwelling sediments. *Nature Geosciences*, 3, 557-561.

He, T.G. 1989. Classification and correlation of phosphatic sequences of Yuhucun Formation in east Yunnan. *Minerals and rocks*, 9, 1-11. (In Chinese with English Abstr.)

Heubeck, C., Ergaliev, G. & Evseev, S. 2013. Large-scale seismogenic deformation of a carbonate platform straddling the Precambrian-Cambrian boundary, Karatau Range, Kazakhstan. *Journal of Sedimentary Research*, 83, 1004-1024.

Jacobsen, S.B. & Kaufman, A.J. 1999. The Sr, C and O isotopic evolution of Neoproterozoic seawater. *Chemical Geology*, 161, 37-57.

Jenkins, R., Cooper, J.A. & Compston, W. 2002. Age and biostratigaphy of Early Cambrian tuffs from SE Australia and southern China. *Journal of Geological Society, London*, 159, 645-658.

Jiang, G.Q., Kaufman, A.J., Christie-Blick, N., Zhang, S.H. & Wu, H.C. 2007. Carbon isotope variability across the Ediacaran Yangtze platform in South China: Implications for a large surface-to-deep ocean delta C-13 gradient. *Earth and Planetary Science Letters*, 261, 303–320.

Kaufman, A.J., Knoll, A.H., Semikhatov, M.A., Grotzinger, J.P., Jacobsen, S.B. & Adams, W. 1996. Integrated chronostratigraphy of Proterozoic–Cambrian boundary beds in the western Anabar region, northern Siberia. *Geological Magazine*, 133, 509–533.

Kimura, H., Matsumoto, R., Kakuwa, Y., Hamdi, B. & Zibaseresht, H. 1997. The Vendian–Cambrian $\delta^{13}C$ record, North Iran: Evidence for overturning of the ocean before the Cambrian explosion. *Earth and Planetary Science Letters*, 147, E1–E7.

Knauth, L.P. 1979. A model for the origin of chert in limestone. *Geology*, 7, 274-277.

Krajewski, K.P., Vancappellen, P., Trichet, J., Kuhn, O., Lucas, J., Martinalgarra, A., Prevot, L., Tewari, V.C., Gaspar, L. & Knight, R.I. 1994. Biological processes and apatite formation in sedimentary environments. *Eclogae Geologicae Helvetiae*, 87, 701-745.

Landing, E., Geyer, G., Brasier, M.D. & Bowring, S.A. 2013. Cambrian evolutionary radiation: Context, correlation, and chronostratigraphy - overcoming deficiencies of the first appearance datum (FAD) concept. *Earth-Science Reviews*, 123, 133-172.

Lawrence, M.G. & Kamber, B.S. 2006. The behavior of the rare earth elements during estuarine mixing-revisited. *Marine Chemistry*, 100, 147-161.

Li, D., Ling, H.F., Jiang, S.Y., Pan, J.Y., Chen, Y.Q., Cai, Y.F. & Feng, H.Z. 2009. New Carbon isotope stratigraphy of the Ediacaran-Cambrian boundary interval from SW China: implication for global correlation. *Geological Magazine*, 146, 465-484.

Li, D., Ling, H.F., Shields-Zhou, G.A., Chen, X., Cremonese, L., Och, L., Thirlwall, M. & Manning, C.J. 2013. Carbon and strontium isotope evolution of seawater across the Ediacaran-Cambrian transition: Evidence from the Xiaotan section, NE Yunnan, South China. *Precambrian Research*, 225, 128-147.

Li, Y.H., Wan, D.F. & Jiang, S.Y. 1994. Silicon Isotope study on the Meishucun Precambrian-Cambrian boundary section, Yunnan Province. *Acta Geoscientica Sinica*, 1-2, 75-84. (In Chinese with English Abstr.)

Li, Z.X., Bogdanova, S.V, Collins, A. S., Davidson, A., De Waele, B., Ernst, R.E., Fitysimons, I.C.W., Fuck, R.A., Gladkochub, D.P., Jacobs, J., Karlstrom, K.E., Lu, S., Natapov, L.M., Pease, V., Pisarevsky, S.A., Thrane, K. & Vernikovsky, V. 2008. Assembly, configuration, and break-up history of Rodinia: A synthesis. *Precambrian Research*, 160, 179-210.

Li, Y.Y. 1986. Proterozoic and Cambrian phosphorites – regional review: China. *In:* Cook, P.J. & Shergold, J.H. (ed.) *Phosphate Deposits of the World; Volume 1: Proterozoic and Cambrian Phosphorites*. Cambridge University Press, Cambridge, 42-61.

Liu, B.J., Xu, X.S. & Xu, Q. 1995. Sequence and stratigraphy and basin dynamics of the southeastern margin of the Yangtze plate in south China during the late Proterozoic to early Palaeozoic. *Sedimentary Facies and Palaeogeography*, 5, 1-16.

Liu, K., Chen, Q. & Han, A. 1990. Siliceous component and siliceous rock in phosphorite strata. *Acta Petrologica Sinica*, 1, 46-57. (In Chinese with English Abstr.)

Liu, K. & Chen, Q. 1994. Cementation process of phosphorites. *Scientia Geologica Sinia*, 29, 62-70. (In Chinese with English Abstr.)

Luo, H., Jiang, Z.W., Xu, C., Song, X. & Xue, X. 1980. On the Sinian-Cambrian boundary of Meishucun and Wangjiawan, Jining County, Yunnan. *Acta Geologica Sinica*, 54, 95-111.

Luo, H., Jiang, Z., Wu, X., Song, X. & Ou, Y. 1982. The Sinian-Cambrian Boundary in Eastern Yunnan. Yunnan People's Publishing House, P.R. China.

Luo, H., Jiang, Z., Wu, X., Song, X., Ou, Y., Xing, Y., Liu, G., Zhang, S. & Tao, Y. 1984. Sinian–Cambrian boundary stratotype section at Meishucun, Jinning, Yunnan, China. People's Publishing House, P.R. China.

Luo, H., Jiang, Z., Wu, X., Song, X. & Ou, L. 1990. The global biostratigraphical correlation of the Meishucunian Stage and the Precambrian-Cambrian boundary. *Science China Chemistry*, 34, 377-384.

Luo, H., Wu, X. & Ou, L. 1991. Facies changes and transverse correlation of the Sinian-Cambrian boundary strata in eastern Yunnan. *Sedimentary Geology and Tethyan Geology*, 65, 27-35.

Luo, H.L, Jiang, Z.W, Wu, X.C, Ou, L., Song, X.L. & Xue, X.F. 1992. A further research on the Precambrian–Cambrian boundary at Meishucun Section of Jinning, Yunnan, China. *Acta Geologica Sinica*, 5, 197–206.

Mazumdar, A. & Banerjee, D.M. 2001. Regional variations in the carbon isotopic composition of phosphorite from the Early Cambrian Lower Tal Formation, Mussoorie Hills, India. *Chemical Geology*, 175, 5-15.

Marshall, C.R. 2006. Explaining the Cambrian "Explosion" of Animals. *Annual Review of Earth and Planetary Sciences*, 34, 355-384.

Maruyama, S., Sawaki, Y., Ebisuzaki, T., Ikoma, M., Omori, S. & Komabayashi, T. 2013. Initiation of leaking Earth: An ultimate trigger of the Cambrian explosion. *Gondwana Research*, 25, 910-944.

McBride, E.F. & Folk, R.L. 1977. The Caballos Novaculite revisited, Part 2: Chert and shale members and synthesis. *Journal of Sedimentary Petrography*, 4, 1261-1286.

McLennan, S.M. 1989. Rare earth elements in sedimentary rocks: Influence of provenance and sedimentary processes. *Geochemistry and Mineralogy of Rare Earth Elements*, 21, 169-200.

Na, L. & Kiessling, W. 2015. Diversity partitioning during the Cambrian radiation. *Proceedings of the National Academy of Sciences of United States of America*, 112, 4702-4706.

Nier, A. 1938. The Isotopic Constitution of Strontium, Barium, Bismuth, Thallium and Mercury. *Physical Review*, 54, 275-278.

Oehlert, AM. & Swart, P.K. 2014. Interpreting carbonate and organic carbon isotope covariance in the sedimentary record. *Nature Communications*, 5, 1-7.

Parkhaev, P.Y. & Demidenko, Y.E. 2010. Zooproblematica and Mollusca from the Lower Cambrian Meishucun section (Yunnan, China) and taxonomy and systematics of the Cambrian small shelly fossils of China. *Paleontological Journal*, 44, 883–1161.

Parnell, J., Mark, D.F., Frei, R., Fallick, A.E. & Ellam, R.M. 2014. $^{40}Ar/^{39}Ar$ dating of exceptional concentration of metals by weathering of Precambrian rocks at the Precambrian–Cambrian boundary. *Precambrian Research*, 246, 54-63.

Pelechaty, S.M., Grotzinger, J.P., Kashirtsev, V.A. & Zhernovsky, V.P. 1996. Chemostratigraphic and sequence stratigraphic constraints on Vendian-Cambrian basin dynamics, northeast Siberian craton. *Journal of Geology*, 104, 543–563.

Peters. S.E. & Gaines, R.R. 2012. Formation of the 'Great Unconformity' as a trigger for the Cambrian explosion. *Nature*, 484, 363-366.

Planavsky, N., Rouxel, O., Bekker, A., Lalonde, S., Konhauser, K., Reinhard, C. & Lyons, T. 2010. The evolution of the marine phosphate reservoir. *Nature*, 467, 1088-1090.

Pittman, J.S. & Folk, R.L. 1971. Length-slow Chalcedony after Sulphate Evaporite Minerals in Sedimentary Rocks. *Nature Physical Science*, 230, 64-65.

Qian, Y. 1989. Early Cambrian Small Shelly Fossils of China with Special Reference to the Precambrian–Cambrian Boundary. Stratigraphy and palaeontology of systemic boundaries in China, Precambrian-Cambrian boundary. Nanjing University Publishing House, P.R. China.

Qian, Y. & Bengtson, S. 1989. Palaeontology and biostratigraphy of the Early Cambrian Meishucunian Stage in Yunnan Province, South China. *Fossils Strata*, 24, 1–156.

Qian, Y., Zhu, M.Y., He, T.G. & Jiang, Z.W. 1996. New investigation of Precambrian-Cambrian boundary sections in eastern Yunnan. *Acta Micropalaeontologica Sinica*, 13, 225-240.

Ramseyer, K., Amthor, J.E., Matter, A., Pettke, T., Wille, M. & Fallick, A. F. 2013. Primary silica precipitate at the Precambrian/Cambrian boundary in the South Oman Salt Basin, Sultanate of Oman. *Marine and Petroleum Geology*, 39, 187-197.

Santosh, M., Maruyana, S., Sawaki, Y. & Meert, J.G. 2013. The Cambrian Explosion: Plume-driven birth of the second ecosystem on Earth. *Gondwana Research*, 25, 945-965.

Sato, T., Isozaki, Y., Hitachi, T. & Shu, D. 2013. A unique condition for early diversification of small shelly fossils in the lowermost Cambrian in Chengjiang, South China: Enrichment of phosphorus in restricted embayments. *Gondwana Research*, 25, 1139-1152.

Sawaki, Y., Nishizawa, M., Suo, T., Komiya, T., Hirata, T., Takahata, N., Sano, Y., Han, J., Kon, Y. & Maruyama, S. 2008. Internal structures and U-Pb ages of zircons from a tuff layer in the Meishucunian formation, Yunnan Province, South China. *Gondwana Research*, 14, 148-158.

Schulz, H.N. & Schulz, H.D. 2005. Large sulfur bacteria and the formation of phosphorite. *Science*, 307, 416-418.

Scopelliti, G., Bellanca, A., Neri, R. & Sabatino, N. 2010. Phosphogenesis in the Bonarelli Level from northwestern Sicily, Italy: petrographic evidence of microbial mediation and related REE behavior. *Cretaceous Research*, 31, 237-248.

Seilacher, A., Buatois, L.A. & Mángano, M. G. 2005. Trace fossils in the Ediacaran-Cambrian transition: Behavioral diversification, ecological turnover and environmental shift. *Palaeogeography, Palaeoclimatology, Palaeoecology*, 227, 323-356.

She, Z.B., Strother, P., McMahon, G., Nittler, L.R., Wang, J.H., Zhang, J.H., Sang, L.K., Ma, C.Q. & Papineau, D. 2013. Terminal Proterozoic cyanobacterial blooms and phosphogenesis documented by the Doushantuo granular phosphorites I: In situ micro-analysis of textures and composition. *Precambrian Research*, 235, 20-35.

She, Z.B., Strother, P. & Papineau, D. 2014. Terminal Proterozoic cyanobacterial blooms and phosphogenesis documented by the Doushantuo granular phosphorites II: Microbial diversity and C isotopes. *Precambrian Research*, 251, 62-79.

Shields, G., Strauss, H., Stephen S. Howe, S.S. & Siegmund, H. 1999. Sulphur isotope Compositions of sedimentary phosphorites from the basal Cambrian of China: implications for Neoproterozoic-Cambrian biogeochemical cycling. *Journal of Geological Society, London*, 156, 943-955.

Shields, G. & Stille, P. 2001. Diagenetic constraints on the use of cerium anomalies as palaeo-seawater redox proxies: an isotopic and REE study of Cambrian phosphorites. *Chemical Geology*, 175, 29-48.

Siegmund, H. 1994. Microfacies, geochemistry and genetic aspects of lowermost Cambrian phosphorites of south China. *Bulletin of National Museum of Natural Science*, 10, 143-159.

Siegmund, H. 1995. Fazies und Genese unterkambrischer Phosphorite und mariner Sedimente der Yangtze-Platform, Südchina. Berliner geowissenschaftliche Abhandlungen, A173, Berlin.

Steiner, M., Li, G.X., Qian, Y., Zhu, M.Y. & Erdtmann, B.D. 2007. Neoproterozoic to early Cambrian small shelly fossil assemblages and a revised biostratigraphic correlation of the Yangtze Platform (China). *Palaeogeography, Palaeoclimatology, Palaeoecology*, 254, 67-99.

Strauss, H., Vidal, G., Moczydlowska, M. & Paczesna, J. 1997. Carbon isotope geochemistry and palaeontology of Neoproterozoic to early Cambrian siliciclastic successions in the East European Platform, Poland. *Geological Magazine*, 134, 1–16.

Southgate, P.N. 1986. Proterozoic and Cambrian phosphorites-specialist studies: Middle Cambrian phosphatic hardgrouds, phoscrete profiles and stromatolites and their implications for phosphogenesis. *In:* Cook, P.J. & Shergold, J.H. (ed.) *Phosphate Deposits of the World; Volume 1: Proterozoic and Cambrian Phosphorites.* Cambridge University Press, Cambridge, 327-351.

Trappe, J. 1998. *Phanerozoic Phosphorite Depositional Systems.* Springer, Berlin ; Heidelberg.

Tiwari, M. 1999. Organic-walled microfossils from the Chert-phosphorite Member, Tal Formation, Precambrian-Cambrian Boundary, India. *Precambrian Research*, 97, 99-113.

Veizer, J., Ala, D., Azmy, K., Bruckschen, P., Buhl, D., Bruhn, F., Carden, G.A.F., Diener, A., Ebneth, S., Godderis, Y., Jasper, T., Korte, C., Pawellek, F., Podlaha, O.G. & Strauss, H. 1999. Sr-87/Sr-86, delta C-13 and delta O-18 evolution of Phanerozoic seawater. *Chemical Geology*, 161, 59-88.

Wang, J. & Li, Z.X. 2003. History of Neoproterozoic rift basins in South China: implications for Rodinia break-up. *Precambrian Research*, 122, 141-158.

Weber, B. & Zhu, M.Y. 2004. Arthropod trace fossils from the Zhujiaqing Formation (Meishucunian, Yunnan) and their paleobiological implications. *Progress in Natural Science*, 13, 25-30.

Weber, B., Steiner, M. & Zhu, M.Y. 2007. Precambrian-Cambrian trace fossils from the Yangtze Platform (South China) and the early evolution of bilaterian lifestyles. *Palaeogeography, Palaeoclimatology, Palaeoecology*, 254, 328-349.

Xue, Y.S. & Zhou, C.M. 2006. Resedimentation of the early Cambrian phosphatized small shell fossils and correlation of the Sinian-Cambrian boundary strata in the Yangtze region, Southern China. *Journal of Stratigraphy*, 30, 64-75. (In Chinese with English Abstr.)

Xu, L.G., Lehmann, B., Zhang, X.G., Zheng, W. & Meng, Q.T. 2014, Trace element distribution in black shales from the Kunyang phosphorite deposit and its geological significances. Acta Petrologic Sinica, 30, 1817-1827. (In Chinese with English Abstr.)

Yang, B., Steiner, M., Li, G.X. & Keupp, H. 2014. Terreneuvian small shelly faunas of east Yunnan (South China) and their biostratigraphic implications. *Palaeogeography, Palaeoclimatology, Palaeoecology*, 398, 28-58.

Yao, C.Y., Ding, H.F., Ma, D.S. & Li, G.X. 2014. Carbon Isotope Features of the Sugetbrak Section in the Aksu-Wushi Area, Northwest China: Implication for the Precambrian/Cambrian Stratigraphic Correlations. *ACTA GEOLOGICA SINIA*, 88, 1535-1546.

Yeh, L., Sun, S., Chen, Q. & Guo, S. 1986. Proterozoic and Cambrian phosphorite deposits: Kunyang, Yunnan, China. *In:* Cook, P. J. & Shergold, J.H. (ed.) *Phosphate Deposits of the World; Volume 1: Proterozoic and Cambrian Phosphorites*. Cambridge University Press, Cambridge, 149-154.

Yin, G.Z. 1996. Division and correlation of Cambrian in Guizhou. *Guizhou Geology*, 13, 115-128. (in Chinese with English Abstr.)

Zeng, Y.F., He, T.G., Shen, L.J., Xie, Y.S. 1993. Mechanism of the formation of lower Cambrian biophosphorites in eastern Yunnan. *Journal of Mineralogy and Petrology*, 6, 49-56

Zeng, Y.F., Shen, L.J. & He, T.G. 1994. Preliminary analysis of the outcrop sequence stratigraphy for phosphatic series of early Cambrian in eastern Yunnan. *Journal of Mineralogy and Petrology*, 3, 43-53.

Zhang, J.M., Li, G.X. & Zhou, C.M. 1997. Deposits of the volcanic eruption event from the basal Lower Cambrian phosphatic sequence in eastern Yunnan and their significance. *Journal of stratigraphy*, 21, 91-100. (In Chinese with English Abstr.)

Zhu, M.Y., Li, G.-X. & Zhang, J.M. 2001. Early Cambrian stratigraphy of east Yunnan, southwestern China: A synthesis. *Acta Palaeontologica Sinica*, 40, 4-39.

Zhu, M.Y., Babcock, L.E. & Peng, S.C. 2006. Advances in Cambrian stratigraphy and paleontology: Integrating correlation techniques, paleobiology, taphonomy and paleoenvironmental reconstruction. *Palaeoworld*, 15, 217-222.

Zhu, M.Y., Strauss, H. & Shields, G.A. 2007. From snowball earth to the Cambrian bioradiation: Calibration of Ediacaran-Cambrian earth history in South China. *Palaeogeography, Palaeoclimatology, Palaeoecology*, 254, 1-6.

Zhu, R.X., Li, X.H., Hou, X.G., Pan, Y.X., Deng, C.L. & He, H.Y., 2009. SIMS U-Pb zircon age of a tuff layer in the Meishucun section, Yunnan, southwest China: Constraint on the age of the Precambrian-Cambrian boundary. *Science in China Series D: Earth Sciences*, 52, 1385-1392.

Zhou, C.M., Zhang, J.M., Li, G.X. & Yu, Z.Z. 1997. Carbon and oxygen isotopic record of the early Cambrian from the Xiaotan Section, Yunnan, South China. *Scientia Geologica Sinica*, 32, 201-211.

CHAPTER V

Conclusions and outlook

Conclusions and Outlook

The results can be summarized as follows:

1). The earliest-Cambrian Zhujiaqing Formation on the southwest Yangtze platform in eastern Yunnan shows, despite its highly variable thickness, only minor changes in relative water depth of deposition, ranging between tidal and shallow epi-continental platform facies. Its deposition thus appears to be controlled by differential subsidence. Subsidence rates were highest in the northern study area where a quite complete stratigraphic record, such as at Laolin section, is preserved. The relatively constant shallow water depth and low to moderate terrestrial input provided a rather stable physical setting to accommodate the onset of the metazoan bioradiation.

2). Distinct lithologic changes, recognized through the definition of twelve lithofacies, reflect dramatic changes in water chemistry throughout the Zhujiaqing Formation. Three lithofacies-association end members in a stratigraphic-upward sequence include (1) siliceous-phosphatic sand-dominated subtidal, (2) phosphatic-dolomitic mud-dominated peritidal, and (3) dolomitic-calcareous mud-dominated subtidal. The rapidly evolving shallow-water benthic metazoans of that time may have been forced to adapt to the rapidly changing bottom-water and pore-water chemistry.

3). The Ediacaran-to-Cambrian stratigraphic interval studied here shows a significant sea level drop at the end of the Ediacaran which exposed extensive tidal flat surfaces, resulting in karstification of the late-Ediacaran Dengying Formation. Subsequent transgression-related upwelling supplied large amounts of phosphorus to medium- and high-energy subtidal and lower-intertidal environments, allowing microbially mediated syndepositional and early diagenetic phosphatization. Basal Cambrian phosphorites are best represented by the thick mineable phosphates of the Zhujiaqing Formation in the Meishucun area of southern Yunnan. PAAS-normalized REE patterns of carbonate leachates of the Meishucun phosphorites indicate their marine origin.

4). The sequence of multiple diagenetic events studied at the Ediacaran to Cambrian boundary interval in Meishucun suggests that carbonate platform silicification occurred during early burial and was possibly related to the phreatic mixing-zone environment, while dolomitization was likely influenced by meteoric and burial diagenesis. ´

Future challenges:

The Zhujiaqing Formation will be a rewarding unit to study the progress of the “agronomic” or substrate revolution and trace fossil systematics in detail which would contribute to the reconstruction of early metazoan ecological niches. The earliest-Phanerozoic hardgrounds documented in the geological record widely occur in phosphorites and phosphatic dolostone in the upper Zhongyicun Member, predating

those described by Lee et al. (2015) from the Cambrian Series 3, Stage 5. Because hardgrounds are widespread during calcite seas such as the Ordovician, Jurassic and Cretaceous but are rare at aragonite sea times (such as the Permian and Triassic), Lee et al. (2015) interpret their Cambrian occurrence as indicating the onset of a calcite sea period. However, because global and regional environmental parameters fluctuated significantly and rapidly throughout the Cambrian, multi-proxy analyses should be undertaken to constrain the environmental diagenetic and processes contributing to the formation of these surfaces (Christ et al., 2012).

The sedimentology and geochemistry of the Dahai Member should be studied quantitatively, especially to test whether its paleosalinity could be globally representative. Petrographic observations of thin sections indicate that the original micrite recrystallized to sparite; thus, geochemical studies are needed to infer its original composition from diagenetic overprint.

It would also be meaningful to place the sedimentary evolution of the Zhujiaqing Formation in a worldwide context by investigating whether the change from phosphorite- to carbonate-dominated deposition is observable worldwide and would possibly be related to changes in global oceanic circulation patterns. Do time-equivalent and similar stratigraphic sequences exist outside the Yangtze platform, such as in eastern Siberia and Western North America?

References

Lee, J.-H., Chen, J. & Woo, J. (2015). The earliest Phanerozoic carbonate hardground (Cambrian Stage 5, Series 3): Implications to the paleoseawater chemistry and early adaptation of hardground fauna. *Palaeogeography, Palaeoclimatology, Palaeoecology* 440, 172–179.

Nicolas Christ, N., Immenhauser, A., Amour, F., Mutti, M., Tomás, S., Agar, S. M. & Kabiri, L. (2012). Characterization and interpretation of discontinuity surfaces in a Jurassic ramp setting (High Atlas, Morocco). *Sedimentology* 59, 249–290.

APPENDIXES

A1. Field areas and investigated sections

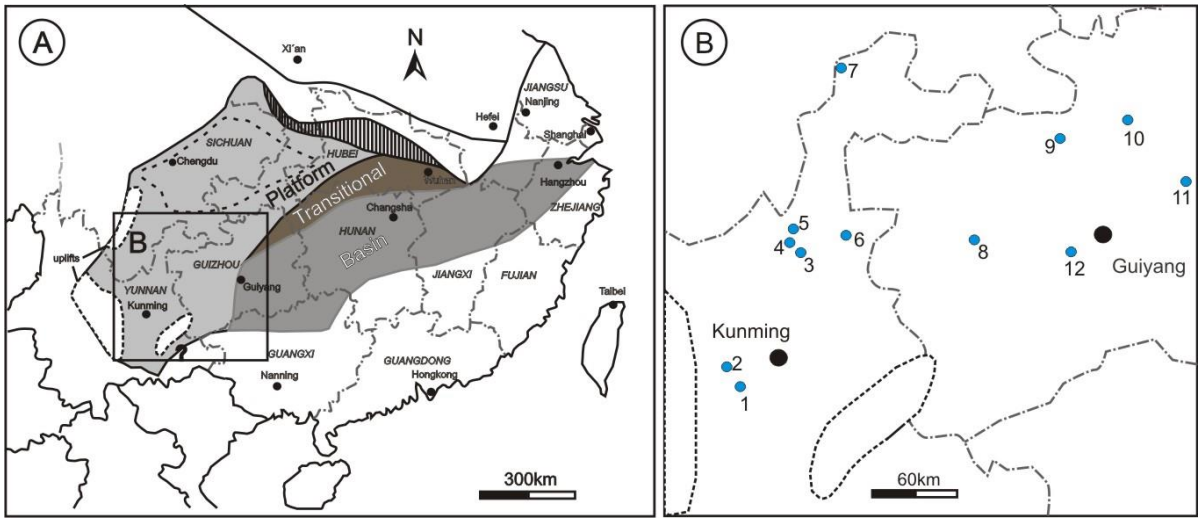

Fig. A1.1. *A) Generalized paleogeographic reconstruction of the Yangtze microcontinent during the early Cambrian. B) Geographic locations of the investigated sections in eastern Yunnan and western Guizhou Provinces.*

Table. A1.1. *Visited sections and investigated formations. DY = Dengying; ZJQ = Zhujiangqing; SYT = Shiyantou; GZW = Gezhongwu; NTT = Niutitang; TZC = Taozichong*

Section	Coordinates	Formations
1 - Meishucun	N24^0 50′35.25″, E 102^0 23′02.62″	DY, ZJQ, SYT
2 - Mingyihe	N24^0 46′7.14″, E 102^0 28′30.30″	DY, ZJQ
3 - Laolin	N26^0 16′44.1″, E 103^0 13′25.1″	DY, ZJQ, SYT
4 - Zhujiaqing	N26^0 18′18.87″, E 103^0 13′16.07″	ZJQ
5 - Lishuping	N26^0 22′38.1″, E 103^0 12′51.7″	DY, ZJQ
6 - Yulu	N26^0 21′51.47″, E 103^0 35′01.93″	DY, ZJQ
7 - Xiaotan	N28^0 15′10.61″, E 103^0 36′36.04″	ZJQ
8 - Gezhongwu	N26^0 38′52″, E 105^0 51′17″	DY, GZW
9 - Zhaishang	N27^0 33′17.62″, E 106^0 14′13.65″	DY, NTT
10 - Heishapo	N27^0 41′19.55″, E 106^0 40′43.23″	DY, NTT
11 - Longshancun	N27^0 3′25.24″, E 107^0 35′38.60″	DY, NTT
12 - Taozichong	N26^0 39′06.16″, E 106^0 27′44.68″	DY, TZC

A2. Detailed partial stratigraphic columns at selected sites

2.1 Xiaotan Section

Fig. A2.1. *Detailed stratigraphic column of Xiaotan section of Yunnan province at the top Zhujiaqing Formation where* $\delta^{13}C_{carb}$ *increases prominently from -6 to around 0. Within this 7m-thick interval, hardgrounds are abundant and bioturbation intensity increased greatly upwards. To be continued. Yellow stars refer to corresponding photographs.*

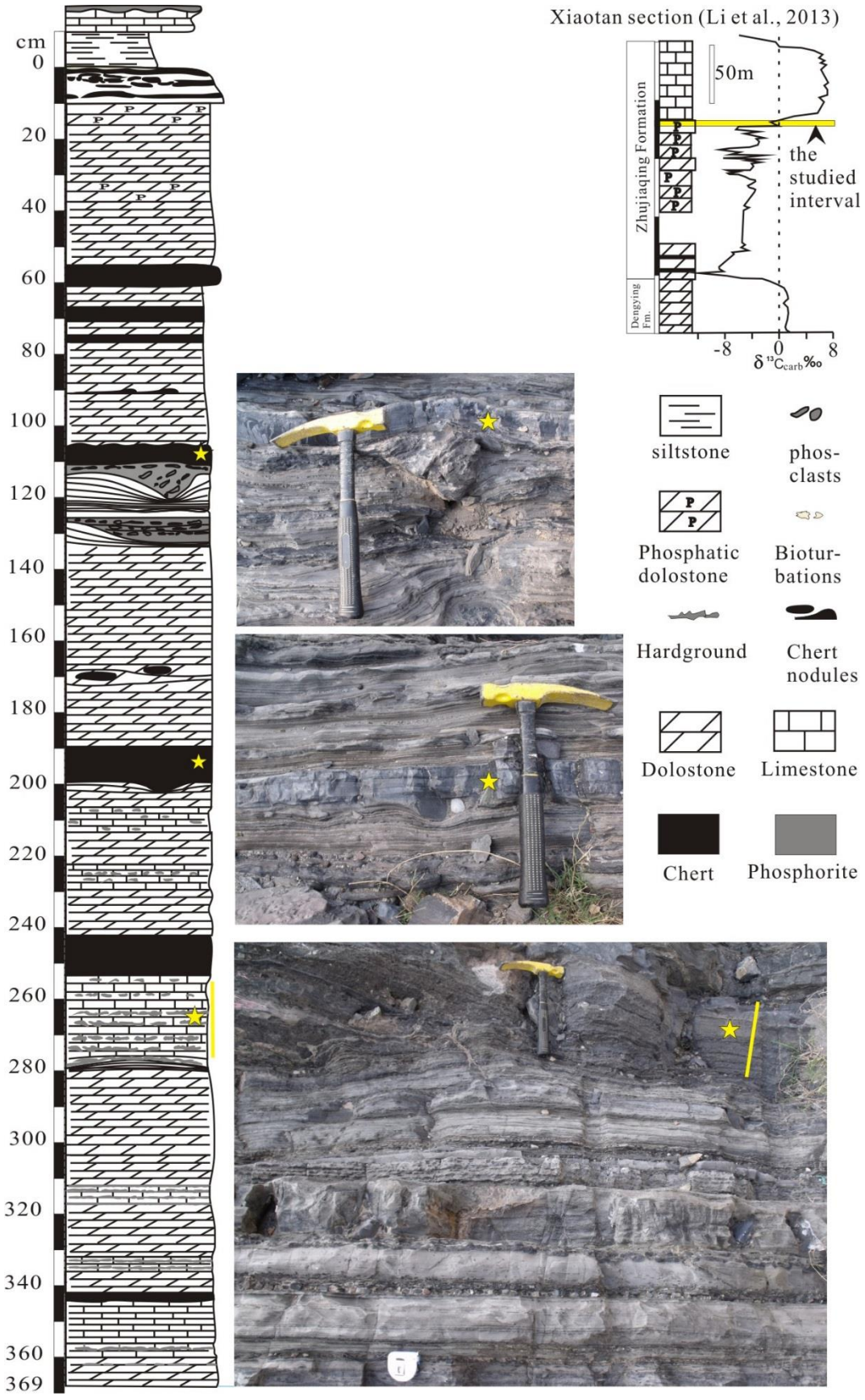

Stratigraphic-downward continuation of the bottom of Fig. A2.1

2.2 Stratigraphic sections measured in western Guizhou Province.

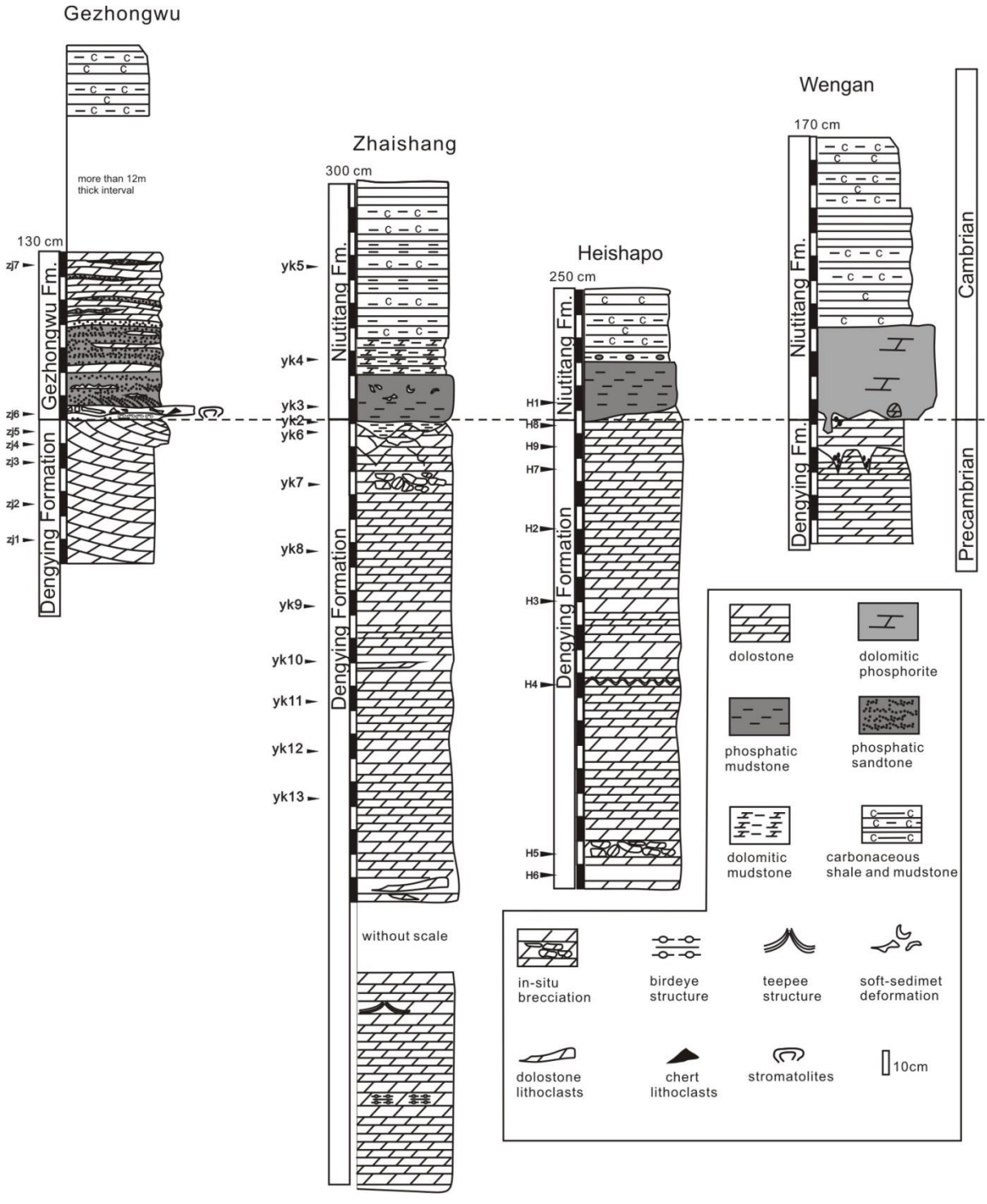

Fig. A2.2. *Detailed stratigraphic columns of sections in western Guizhou Province across the Precambrian to Cambrian boundary interval. A prominent paleokarst surface is present in all sections at the top of the latest Ediacaran Dengying Formation and is taken as stratigraphic datum. Abbreviations to the left mark petrographic thin sections. Refer to Figs. 1.1 and 1.2 for locations.*